JOURNAL OF APPLIED PHYSICS

MARCH
1939
Vol. 10 No. 3

Measurement of
Arc
Characteristics
C. F. [illegible]

JOURNAL OF APPLIED
PHYSICS

MARCH, 1939 Vol. 10, No. 3

In This Issue

Page

The Egg or the Chick 141

Electrical Discharges in Air at Atmospheric Pressure. The Nature of the Positive and Negative Point-to-Plane Coronas and the Mechanism of Spark Propagation LEONARD B. LOEB AND ARTHUR F. KIP 142

Physics of Rubber. I. Its Observed Elastic and Thermoelastic Behavior EUGENE GUTH 161

Operational Calculus. I LOUIS A. PIPES 172

Resumés of Recent Research 181

Temperature Symposium 184

Contributed Original Research

On Resonators Suitable for Klystron Oscillators W. W. HANSEN AND R. D. RICHTMYER 189

Note on the Quantitative Spectrographic Analysis of Small Amounts of Rubidium and Potassium in Biological Materials WILLI M. COHN 200

Measurement of Some Arc Characteristics at 1000 Atmospheres Pressure C. G. SUITS 203

In Every Issue

New Books 186
Contributors to this Issue 187
Here and There 188
Recent Booklets on Instruments and Materials x
Advertising Index xiv

BOARD OF EDITORS

ELMER HUTCHISSON, *Editor*

Associate Editors

F. BITTER
W. E. FORSYTHE
L. A. JONES
W. F. MEGGERS
B. E. WARREN
J. B. WHITEHEAD
V. K. ZWORYKIN

Publication of the
American Institute of Physics

ADMINISTRATIVE STAFF

HENRY A. BARTON, *Director*

MADELINE M. MITCHELL, *Publications Manager*

WILLIAM C. COPP, *Advertising Manager*

GOVERNING BOARD

JOHN T. TATE, *Chairman*
KARL T. COMPTON
E. C. CRITTENDEN
WHEELER P. DAVEY
HOMER L. DODGE
HARVEY FLETCHER
ARTHUR C. HARDY
VERN O. KNUDSEN
MELVIN MOONEY
FREDERIC PALMER, JR.
R. L. PEEK, JR.
GEORGE B. PEGRAM
W. B. RAYTON
F. K. RICHTMYER
WALLACE WATERFALL

THE JOURNAL OF APPLIED PHYSICS, published monthly at Prince and Lemon Sts., Lancaster, Pa., is devoted to physics in its role as the science basic to other natural sciences and to the arts and industries. Previous to 1937 this publication was known as PHYSICS. It aims to be of service not only in physical laboratories, but also in the laboratories of industrial, chemical, geological, geophysical, meteorological, radio, and similar concerns. THE JOURNAL OF APPLIED PHYSICS publishes editorials, news of physicists and reviews, as well as technical papers of applied physics.

SUBSCRIPTION PRICE

	U. S., POSS. AND CANADA	FOREIGN
To members of scientific societies	$5.00	$5.70
To all others	7.00	7.70

Manuscripts should be submitted to Elmer Hutchisson, Editor, University of Pittsburgh, Pittsburgh, Pennsylvania.

Changes of address, proofs, and complaints of failure to receive the JOURNAL OF APPLIED PHYSICS should be addressed to the Publications Manager. New copies can be sent free only if notice of nondelivery is received within three months of date of issue.

Subscriptions and orders for back numbers should be addressed to Prince and Lemon Streets, Lancaster, Pa. or to the American Institute of Physics, 175 Fifth Avenue, New York, N. Y.

Advertising rates supplied on request. Orders, advertising copy and cuts should be sent to the American Institute of Physics.

Entered as second class matter at the Post Office at Lancaster, Pennsylvania, under the Act of March 3, 1897. Accepted for mailing at the special rate of postage provided for in the Act of February 28, 1925, authorized May 2, 1932.

Copyright 1939, by the American Institute of Physics.

THERMIONIC AMPLIFIER

For Adapting Your Present Potentiometer To Glass Electrode Measurements

Glass electrode potentials can now be measured with ordinary potentiometers by simply adding to the circuit this Thermionic Amplifier. It magnifies potentiometer unbalance to such an extent that, in spite of the high electrode resistance, high accuracy and sensitivity are obtained. The Thermionic Amplifier is simple to operate and is frequently used for routine testing.

The amplifier and potentiometer can also be used to measure potential in other high resistance circuits without drawing an appreciable current.

We will be glad to discuss the application of this amplifier to any specific problem you may have in mind.

Catalog E-00A gives general information.

7673 THERMIONIC AMPLIFIER $155.00

Practical limit of sensitivity, 0.0001 volt. Control (electrode) current adjustable to less than 10^{-14} ampere at balance. Error due to this current is less than 0.0001 volt per 10,000 megohms.

LEEDS & NORTHRUP COMPANY, 4978 STENTON AVE., PHILA., PA.

LEEDS & NORTHRUP

MEASURING INSTRUMENTS · TELEMETERS · AUTOMATIC CONTROLS · HEAT-TREATING FURNACES

Jrl A E-00A(1)

Contributions to the Mechanics of Solids

A VOLUME OF 29 ARTICLES BY MEN OUTSTANDING IN THE FIELD OF APPLIED MECHANICS, PUBLISHED IN HONOR OF THE SIXTIETH BIRTHDAY OF STEPHEN TIMOSHENKO

This volume contains much interesting and valuable material on current problems in applied mechanics and their solution, on new applications of theory, or extension of theory. There are, for instance, the article by Ludwig Prandtl dealing with a mechanical explanation of the phenomenon of hysteresis of plasticity in metals, von Karman's article on the application of the method of orthogonal functions to various problems in structural mechanics, G. I. Taylor's discussion of stresses and strains in certain crystals, and the article on certain characteristics of stress distribution in a plane field by von Mises. $5.00.

PROBLEMS IN MECHANICS

By G. B. Karelitz, J. Ormondroyd, and J. M. Garrelts

This new book contains nearly 800 problems on the application of the principles and theorems of mechanics to practical engineering. The famous collection of problems by I. V. Mestchersky is the basis of this book, but these original problems have been transposed to suit American practice and supplemented by more than 300 new problems. The problems are outstanding for their practical value and for the comprehensive range of topics they cover. They can be used with any textbook on mechanics. *To be published in April.*

MACMILLAN • NEW YORK

Please mention this journal when writing to advertisers

CAMBRIDGE PHYSICAL TRACTS

This new series provides authoritative accounts of subjects of topical physical interest written by those actively engaged in research. An individualist outlook is held to be important, much as it would be in a course of lectures; and "completeness" is not aimed at in the sense of recording the full width of related work by others. The tracts are, in fact, personal interim reports of important work in progress, and if rapid advances make it desirable, the issue of new editions or revisions is provided for. About a dozen tracts are in preparation.

Published

NEGATIVE IONS, *by H. S. W. Massey.* $1.75

An account of recent research, employing the methods of quantum theory, into the nature and properties of negative ions.

THE MOBILITY OF POSITIVE IONS IN GASES, *by A. M. Tyndall.* $1.75

Results of investigations dealing with ions of one gas in another; source of ions, measurement of ions, and other aspects.

SUPERCONDUCTIVITY, *by D. Shoenberg.* $1.75

A coherent statement of what the theory of the phenomenological aspect of Superconductivity has to explain.

In the Press

ELECTRON OPTICS, *by O. Klemperer.*

This will be of importance to research workers in television.

CONDUCTION IN METALS, *by A. H. Wilson.*

An introduction to the theory of metals, and a clarification of the physical principle on which the theory is based.

Cambridge University Press

The Macmillan Company

60 Fifth Ave., New York

PRINCIPLES OF ELECTROCHEMISTRY

DUNCAN A. MACINNES

Rockefeller Institute, New York
Past President, The Electrochemical Society

This entirely new treatise, 15 years in preparation, is both a readable and an extremely painstaking account of the science of electrochemistry as it is today. Careful arrangement of the subject matter and logical development of the concepts involved make it particularly desirable for use as a textbook. The basic principles are discussed and critically evaluated; and the foundation thus laid is used as a basis for the introduction of more recent ideas, such as the extension of the DeBye-Hückel theory, the application of the interionic attraction theory to electrolytic conductance, and the use of the glass electrode.

It contains an excellent introduction to the thermodynamics of electrochemistry and a comprehensive treatment of electrode potentials. It gives the modern theoretical status of the basic principles of electrochemistry, with emphasis on the interionic attraction theory. An unusual feature, one not possessed by any other text in the field, is its critical evaluation of experimental data. It is a mine of experimental values, not merely abstracted from the literature, but critically presented, and where necessary, recomputed. On the experimental side there is a very complete presentation of transference numbers and a good account of the much discussed theory and practice of electrophoresis.

An idea of the scope of the book is given by the table of contents as follows:

Introduction
Faraday's Law and Coulometers
Electrolytic Conductance and the "classical" Theories of Dissociation
Electrical Transference
The Principles of Thermodynamics and the Galvanic Cell
Chemical Potential, Activity, and Related Quantities
The Debye-Hückel Method for the Theoretical Calculation of Activity Coefficients
Concentration Cells and the Validity of the Debye-Hückel Theory
The Effects of Gravity and Centrifugal Force on the Electromotive Force of Galvanic Cells
Standard Electrode Potentials from Galvanic Cells without Liquid Junctions
Thermodynamic Ionization Constants from the Potentials of Cells without Liquid Junctions
Thermodynamic Studies of Non-Aqueous Solutions
Galvanic Cells with Liquid Junction Potentials
Standard Potential Determinations of the Elements Involving Cells with Liquid Junctions, or Equilibrium Measurements
The Determination and Meaning of pH Valves
The Standard Potentials of Electrode Reactions
"Oxidation-Reduction" Potentials
Potentiometric Filtrations
The Interionic Attraction Theory of Conductance of Aqueous Solutions of Electrolytes
The Conductance of Electrolytes
The Conductance of Electrolytes in Non-Aqueous and Mixed Solvents
The Use of Conductance Measurements in Various Physico-Chemical Investigations
The Effect of Structure and Substitution on the Ionization Constants of Organic Acids and Bases
The Dielectric Constants of Liquids and the Dipole Moments of Molecules
Electrokinetic Phenomena
Electro-osmosis, Electrophoresis and Streaming Potentials
Irreversible Phenomena, Passivity and Overvoltage
Indexes

512 Pages Profusely Illustrated, 24 Chapters $6.00

REINHOLD PUBLISHING CORPORATION
330 West 42 Street New York, N. Y.

EPPLEY THERMOPILES *for* RADIANT ENERGY MEASUREMENTS

Manufacturing Eppley thermopiles. Due to the fineness of the wire used, most of the manufacturing process must be performed under the microscope.

We are prepared to furnish thermopiles of either bismuth-silver or copper-constantan, mounted in vacuum or air type cases. We also furnish thermopiles and mountings especially designed to meet individual needs. A card will bring you our Bulletin R–3 which contains illustrations, sample curves, complete descriptive matter, prices, references, etc., with regard to Eppley thermopiles.

EPLAB
THE EPPLEY LABORATORY, INC.
SCIENTIFIC INSTRUMENTS
NEWPORT, R.I.
U.S.A.

BUILT FOR *Lasting Accuracy*

The B & L Laboratory Wavelength Spectrometer is of the simplified constant deviation prism type and is built to give enduring service with uniform accuracy in routine laboratory work. All optical surfaces and moving parts are completely enclosed to protect them against dust and corrosion. The constant deviation prism is of the Pellin-Broca type and is made of a single piece of flint glass of high dispersion. Wavelength drum can be read directly from the eyepiece position. Telescope and collimator are permanently aligned at right angles to each other. Slit width is controlled by a micrometer screw, and slit length by a V-slide operating close to the face of the slit jaws. Eyepiece holder is equipped with cross hairs and a shutter. Write for Catalog D-221 describing B & L Spectrometric Equipment. Bausch & Lomb Optical Co., 670 St. Paul St., Rochester, N. Y.

BAUSCH & LOMB

....WE MAKE OUR OWN GLASS TO INSURE STANDARDIZED PRODUCTION

FOR YOUR GLASSES INSIST ON B & L ORTHOGON LENSES AND B & L FRAMES...

PRECISION INSTRUMENTS FOR MEASUREMENT AND CONTROL

GM

Portable D'Arsonval Galvanometers

You are sure of close accuracy plus ruggedness when you choose a G-M designed taut-suspension galvanometer.

High angular sensitivity is combined with a large scale-angle to allow close accuracy both in measuring current and voltage, and for null point indicating in bridge and potentiometer circuits. The coil is sufficiently damped to give minimum reading time. It is also well balanced to give uniform scale accuracy. No special care is needed in leveling the instrument.

Mirror Type Shown at left is the G-M mirror type galvanometer. It is equipped with a mirror on the moving coil, plus a 6 volt lamp and lens system. A sharp black index line in an illuminated field is projected on the translucent scale. One model requires an extra power source. Another has an enclosed transformer. Both models have removable bottoms. Sensitivity ranges available run from 0.02 to 0.20 microampere per millimeter scale-division.

Pointer Type Shown at lower left is the G-M pointer type. The design of the magnetic circuit provides uniform flux density over the entire scale range. Sensitivity ranges available run from 0.10 to 1.00 microamperes per millimeter scale-division.

Write for the G-M Catalog giving specifications and prices on these galvanometers, as well as the complete line of G-M instruments.

Pointer Type This galvanometer is rugged enough to withstand severe handling in portable use.

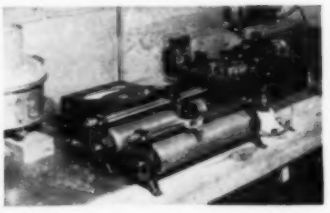

At Missouri This pair of G-M slide wire rheostats is representative of the G-M equipment being used at the University of Missouri. Other G-M instruments available for laboratory work are: suspended coil galvanometers, electric thermometers, photoelectric cells, demonstration photoelectric relays.

G-M LABORATORIES INC.

DEPT. B. 1731 BELMONT — CHICAGO, U. S. A.

HARVARD COLLEGE
MAR · 1 1939
LIBRARY

Journal of Applied

Physics

Volume 10 March, 1939 Number 3

The Egg or the Chick?

PHYSICISTS are sometimes guilty of being a little conceited when comparing engineering and physics. They feel that progress in engineering is limited by the work of the physicist and that they, therefore, are the important cogs in the wheel. Actually engineering and physics have always advanced together, physics leading with new knowledge; engineering with the application of this knowledge to human needs; and physics advancing again through new developments in engineering.

The importance of engineering in the development of modern physics is especially clear in the field of electronics. While it is true that the physicist developed some of the basic relations for the emission of electrons from heated filaments still there is hardly a single research in this field which does not make use of multi-electrode vacuum tubes, cathode-ray oscillographs or other products of modern engineering.

One might think that in optics for instance, there would be little need for engineering. Yet consider the new 200-inch telescope. Can anyone deny that it is essentially an engineering problem rather than a physical one? Again, consider a large spectrograph. Its rigid base needs careful engineering design. Commercial motors are used for feeding its arcs and cooling, and standard photo-cells and amplifiers are used in making records. Or if we consider a photoelastic bench for stress analysis, we find that the engineer has come to the aid of the physicist in providing dial gauges, fine materials for samples and, recently, even large-sized Polaroid sheets for producing polarized light.

Most striking of all recent applications of engineering to the progress of physics is in the field of nuclear structure. The enormous tanks needed to house electrostatic generators or the large magnets for cyclotrons could not be built without the aid of the engineer.

A physicist who has at his command electrical power to carry out almost any experiment he can devise, is apt to forget how handicapped he would be without the advantages of modern engineering. Thus the physicist uses engineering to advance physics and the engineer uses physics to advance engineering. Neither has the right to feel "cocky" except for the great work that they have carried forward together.

For Months to Come

In an effort to provide useful and informative survey articles of the highest quality a new editorial policy will be followed in several of the coming issues of this journal. It is planned in each of these issues to emphasize a particular subject in which considerable progress has been made in the past few years. A leader in each field has been appointed who will act as guest editor or advisor. He will assist in preparing a program of outstanding papers in his own field. We hope in this way to provide our readers with authoritative and up-to-the-minute accounts of what is happening in each branch of applied physics.

In the April issue, a plan somewhat similar to that mentioned above will be followed. A fine group of papers giving the background, technique and recent developments in photoelasticity will be published. This issue will be illustrated by excellent photographs of all the photoelastic laboratories in the country.

Electrical Discharges in Air at Atmospheric Pressure

The Nature of the Positive and Negative Point-to-Plane Coronas and the Mechanism of Spark Propagation

BY LEONARD B. LOEB AND ARTHUR F. KIP

University of California, Berkeley, California

NEARLY forty years ago Townsend deduced his famous theory of sparking by assuming ionization by positive ions in a gas.[1] Today, while we know that this particular mechanism is definitely impossible, yet a theory involving equations similar to Townsend's but ascribable to one of several different secondary mechanisms may be invoked to explain sparking.[2] The most frequent equation for the discharge current i in vogue today takes the form

$$i=i_0\frac{e^{\alpha x}}{1-\gamma(e^{\alpha x}-1)}.$$

Here i_0 is the current caused by the initial electrons in the air. α (called the first Townsend coefficient) represents the number of new electrons formed by each of the initial electrons in advancing 1 cm in the direction of the field in the gas and x is the length of the gap. The quantity γ, which is called the second Townsend coefficient, represents the number of secondary electrons liberated at the cathode per positive ion formed in the gap by positive ion impact. It could as well represent the secondary electrons created by photoelectric action at the cathode per positive ion created in the gap, thus assuming parallelism between positive ion and photon production. It is seen in analogy to Townsend's original equation that i becomes indefinitely large irrespective of i_0 when the denominator $1-\gamma(e^{\alpha x}-1)$ approaches zero, or roughly when $1/\gamma=e^{\alpha x}$. This was interpreted by Townsend and many after him as being the condition leading to a spark. In fact, on rough quantitative test, since α/p and γ are functions of the ratio of field strength X to pressure p, i.e., X/p, it has been possible approximately to calculate the sparking potential $V_s=X_s\delta$ from these constants over a *limited* range of $p\delta$ of low value.[2] Here δ is the sparking distance at V_s. Strictly mathematically interpreted, such an equation is quite indeterminate. It can *only represent a condition of instability* dependent on i_0 which ultimately leads to a spark. Under most circumstances the observed V_s is independent of i_0. The agreement with observed sparking values is, therefore, more or less purely fortuitous and results from the rapid increase in current with X/p and x in the neighborhood of this region giving the illusion of a threshold. For example, in air near sparking $\alpha/p=Ae^{BX/p}$ so that $1/\gamma=e^{Apxe^{BX/p}}$, whence the condition changes very rapidly with X/p.

There is, however, a real significance to the relation $1/\gamma=e^{\alpha x}$ which is the *physical* criterion for the stable state of a self-sustaining discharge. For it insures that for each electron in the gap there will be created through some cathode mechanism taken together with cumulative ionization enough new electrons to *maintain* the current in its existing state.[3] This interpretation has been confused with the sparking condition although it is *applicable only to a stable regime occurring after the unstable regime of the spark has passed*. It is clear, however, that for any gap if $\gamma e^{\alpha\delta}>1$ there will be an increase of the current and charges in transit. This results in a building up of space charges and a *possible rearrangement* of such charges in the gap culminating in the passage of a greater current for the same poten-

tial or else in an extinction of the current because of space charge accumulation. That is, the condition $\gamma e^{\alpha\delta} > 1$ represents some sort of an instability which will alter a steady-state current. Now since Townsend's pioneer work we define a *spark* as *an unstable discontinuous process marking the transition from one stable state of current in a gas to another stable state*. Hence, where the increase of charge produces an increase of current through a transition resulting from a rearrangement of space charges we can set the condition $\gamma e^{\alpha\delta} = 1$ as the *threshold or lower limit below which a spark cannot pass*. Thus the condition for instability while it does not insure a spark sets a *lower limit* for the sparking potential V_s. Accordingly the conventionally measured sparking potential V_s is clearly an indefinite quantity occurring according to circumstances somewhere in the region $\gamma e^{\alpha\delta} > 1$, and *appearing* to be more sharply defined in virtue of the exceedingly rapid variation of $\gamma e^{\alpha\delta}$ with V_s. Hence, where $\gamma e^{\alpha\delta}$ may have to be much greater than unity to cause a spark with observable frequency, the observed value of V_s may not be *seriously different* from the threshold value.

Though the condition above is independent of any photocurrent it is clear that once we are in the region $\gamma e^{\alpha\delta} > 1$ *at least one electron* must appear in the gap to start the discharge. The achievement of a spark by the action of one electron under these conditions, however, depends on the further conditions (1) that it creates a conducting path between the electrodes and (2) that this path terminates in a space charge distribution at the cathode ensuring maintenance of the *newly* established current path such that at least the electricity stored on the electrodes can be discharged. Whether under any circumstances the electron will succeed in initiating a spark or not depends very much on conditions such as pressure, gap geometry and length, gas nature, the character of the cathode surface and the *amount by which* $\gamma e^{\alpha\delta}$ *exceeds unity*. If the excess is small the chance is probably vanishingly small. In that case one must await the advent of one fortunately situated turn of events started by one of countless electrons which fail. As potential increases, more and more of the electrons succeed in causing a spark, until at some potential sparks occur with sufficient frequency to warrant the investigator with his circuit in accepting this value as the minimum sparking potential, hereafter termed the conventional sparking potential, V_s. Experimentally we measure as the sparking potential the value of V_s at which in some arbitrary time, say five seconds, one of the electrons in the photocurrent sets off a spark say in 50 percent or 90 percent of the cases tried. This as is seen is a purely arbitrary value and corresponds to the passage of a spark for some possible 10^6 electrons in the gap. In some cases it may take an externally produced proper sequence of *several* electrons in time and space to achieve a spark; that is, the spark passage may depend on the externally stimulated photoelectric current i_0 from the cathode. Usually this is not the case and one electron suffices.

In accord with the original Townsend concept of gap breakdown and consistent with the view above, it had been believed that when $\gamma e^{\alpha\delta}$ exceeded unity very slightly and an initial electron was liberated at the cathode the electron multiplication in the progress of the electrons across the gap and the movement of the positive ions across the gap would produce the space charge distortions leading to a spark. On this basis, Loeb[4] and Rogowski[5] and later Franck and von Hippel,[6] Schumann,[7] Sämmer[8] and Kapzov[9] calculated the conditions leading to a spark. However the researches of Pedersen[10] with Lichtenberg figures, Tamm,[11] Rogowski[12] and Strigel[13] with oscillographs, Beams,[14] Dunnington,[15] von Hamos,[16] White,[17] Wilson[18] with Kerr cell shutter, Newman[41] with electrical waves, and Flegler and Raether[19] with C. T. R. Wilson cloud chamber have shown that these mechanisms are definitely impossible at much above 100 mm pressure and gaps more than three mm for the following reason. Both White[17] and Raether[20] have measured the velocity of advance of the electron avalanche tip and found that the observed velocities were of the order of 10^7 cm/sec. in agreement with those to be expected from the theory of electron mobilities. Hence, the time of gap breakdown did one electron and its progeny as an avalanche have to cross a gap of one cm would be of the order of 10^{-7} second. Their own observations as well as the others indicated that by all the criteria used for defining breakdown, the breakdown times for the gaps

observed were of the order of one-fifth that to be expected for the single electron avalanche to cross the gap. With slightly overvolted gaps (~5 percent) this breakdown, furthermore, did not propagate as an avalanche from the cathode but as a mid-gap or anode streamer, traveling *towards the cathode* with *velocities* in excess of that of electron travel.[17–19] While the hypothesis of Loeb[21] that such times could be accounted for by a continuous chain of electron avalanches across the gap where each electron covered only mm instead of cm sufficed, the mechanism for such an occurrence was obscure. With Cravath's[22] and later Dechene's[23] discovery that photo-ionization was caused by the radiation from the positive corona discharge, the solution was near. It led at once to Cravath and Loeb's[24] suggestion that the high velocity of propagation could be accounted for by photo-ionization in the distorted field region in advance of an avalanche channel such that nearly simultaneous avalanches could extend across the gap. This furnished the needed mechanism for the chain of avalanche breakdown. A similar conclusion as to the mechanism was arrived at later somewhat more clearly by Flegler and Raether[19] from cloud track studies. It was not until the recent studies of the positive and negative point-to-plane coronas by Kip[25, 26] and Trichel[27, 28] in the senior author's laboratory, however, that a clear and complete picture of the mechanism of spark breakdown as commonly observed in gaps above three mm and pressures above 100 mm could be achieved. It is, therefore, not unfitting that a summary of these phenomena which are now clearly explained should precede attempts further to discuss the sparking condition.

The reason why the coronas should furnish the basis for such an understanding lies in the fact that discharge propagation results in and also from inhomogeneities in electrical fields produced by cumulative ionization and the difference between electron and positive ion mobilities. Unfortunately the inhomogeneities of such fields are not open to calculation or study by experimental methods. It is for this reason that no material progress in the new direction has resulted from the countless researches using plane parallel gaps. Since, however, the inhomogeneous electrical fields *before* discharge in the neighborhood of conducting metal points are capable of evaluation with more or less accuracy such fields make possible investigations of phenomena otherwise inaccessible to the experimenter.

Returning now to the point-to-plane gap, both theory and experiment agree in assigning to the geometry and field *about the point* the predominating role, and relatively little importance to the plane electrode, provided the gap is long. While hemispherically-capped cylindrical electrodes permit field calculations such calculations are tedious and the results are not very accurate. Accurate solutions can be carried out for the fields in the case of confocal paraboloid electrodes. Experimental studies were carried out both with hemispherical and confocal paraboloid arrangements by Kip[25] and the results indicated that estimates made from the hemispherical points, assuming confocal paraboloid geometry, would serve under most circumstances for longer gaps. The form of the value of the ratio of field strength to pressure in the gap near the point as a function of distance from the point is computed and shown in Fig. 1 for 0.03- and 4.7-mm diameter points for a 6-cm gap at the starting potentials of fields for the positive point corona in air at atmospheric pressure. The reason for the use of the ratio instead of field strength is that this permits at once of the evaluation of Townsend's first coefficient at each point. On this basis it is possible from Sanders'[29] and Masch's[30] data for α/p as a function of X/p to calculate the values of α as a function of distance x from these various points. For the positive point this gives some chance to calculate the number of ions formed per electron approaching the point, since one may neglect the inhibiting action of the space charge. For the negative point as we shall see the decreasing field as x increases from the point makes the space charge distortion such that calculations are not very significant except for low ionization. In Fig. 1, the values of Townsend's function α are also plotted as a function of x at the existing fields. The areas under these curves for positive corona at onset placed into the exponent for αx of the expression $n=e^{\alpha x}$ give the number of electrons in a single electron avalanche proceeding from outside to a positive point. This for the points used rises continuously from some 10 electrons for the largest point to 10,000 for the

smallest point and is the same for negative as well as positive points where space charges do not inhibit. We will here designate as an *electron avalanche* an electron and all the other electrons it creates in the field in its path to or from an electrode. With this background we may now turn to the consideration of the negative point corona in air.

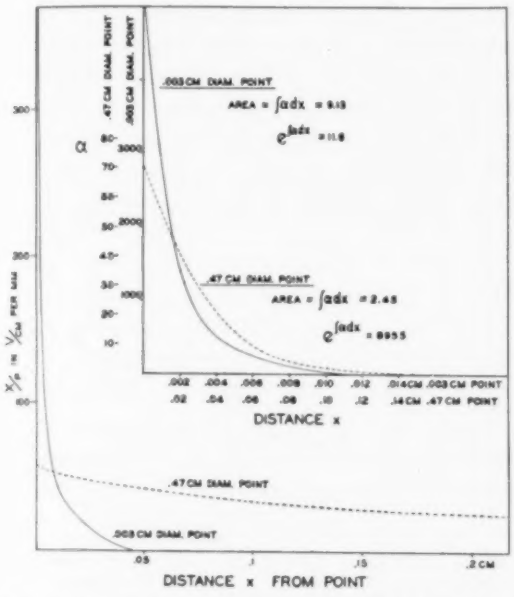
.003 CM DIAM. POINT
.47 CM DIAM. POINT
AREA = ∫αdx = 9.13
$e^{\int \alpha dx}$ = 11.9
AREA = ∫αdx = 2.45
$e^{\int \alpha dx}$ = 8955
DISTANCE x
DISTANCE x FROM POINT

FIG. 1. X/p *vs.* distance from parabolic points of 0.003- and 0.47-cm diameters, computed for a 6-cm gap at starting potentials, and Townsend's α *vs.* distance for the same geometries. Areas under the latter curves give $\int \alpha dx$.

Negative Point Corona

As soon as the field at some spot on the negative point reaches such a value that an incoming positive ion is likely to generate a secondary electron at the cathode (negative point) surface on impact, that electron proceeds outward and ionizes the gas by collision, producing an electron avalanche. In the strong field near the point it will quickly ionize, but the cumulative effect of the avalanche does not become appreciable until the electrons produced have traversed several ionizing free paths away from the point; that is, $n = e^{\alpha x}$ and, thus, depends on x as well as α. As the avalanche recedes the fields causing the electrons to ionize weaken for two reasons. First, due to the rapid decline of the field X as distance x increases and, secondly, since the electrons in moving away leave behind them relatively immobile positive ions whose space charge reduces the field. Hence, the electrons recede from the point leaving a cloud of positive ions behind whose density rises nearly exponentially as one recedes from the point and then declines more gradually. Retarded by this space charge, the electrons slow down and attach to molecules of O_2 to make slow negative ions which eventually drift to the positive plate. The field set up between the point surface and the positive space charge increases the field acting on electrons near the point. Positive ions reach the cathode and more electrons are liberated and so new avalanches form. These increase the ionization and the space charge near the cathode, decreasing ionization strongly beyond the positive space charge. Meanwhile the positive space charge is slowly moving towards the cathode surface.

Accompanying the ionization a considerable number of atoms are excited to radiation by the electrons. With the high fields some molecules are simultaneously ionized and excited. This is indicated by the presence of the spark spectrum of N_2 and air near the cathode. Such excited atoms emit radiations which are capable of ionizing the gas photoelectrically. Hence with the first avalanche photons causing ionization are emitted in all directions by the discharge. This photoelectric ionization has been directly observed and measured by Greiner,[31] Cravath[22] and Dechene[23] in corona while Raether[19, 20, 47] and Gorrill[32] have similar evidence from cloud-chamber studies. The ions start new avalanches at neighboring spots until the whole region of the point which is capable of emitting electrons by positive ion impact is carrying out the process noted above. What the magnitude of the field required is depends on the following considerations. The chance of electron liberation must be such that for the positive ions created in a given avalanche, *one* of these must liberate a secondary electron at the cathode to perpetuate the avalanches. This with constantly changing fields is thus a rather ill-defined quantity. However it depends on the work function for secondary electron emission on positive ion bombardment and on the kinetic energy of the positive ions as well as their ionization potential. It varies from

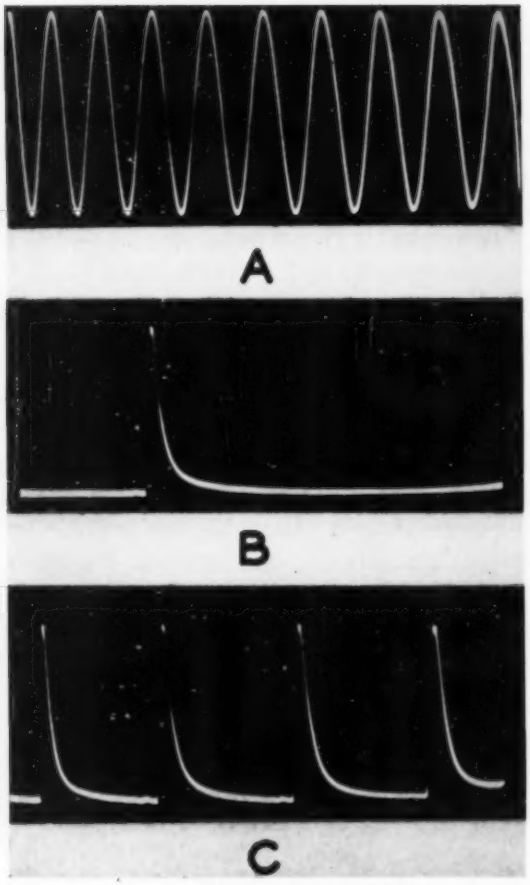

FIG. 2. Negative point corona oscillograms, for a 0.5-mm diameter point and 3-cm gap. (A), 1000 c.p.s. calibration; (B), single pulse, 0.1 μA; (C), repeating pulses at 0.7 μA.

spot to spot on the surface and is lower (secondary emission γ higher) for a gas-coated surface than for an outgassed surface. It is exceedingly capricious, and so far it has been nearly impossible to control and reproduce the values of this quantity. H_2 enhances the effect in some cases such as with Pt, Cu, Fe and Ni electrodes; CO, SO_2 and H_2S destroy it.[33] The extent of the spread of the avalanches over the surface depends on the extent of the active surface where adequate fields exist. For needle points of 0.03 mm diameter, the whole point is doubtless covered. For larger points the spots vary in size to about 0.2 mm.[27] The spot on a given electrode varies very little in size as the field increases and the current varies. It is not possible to fix the velocity with which the avalanches spread over the point and build up the space charge until it chokes off the further growth by accumulation of space charge. Oscillograms to be shown and the time sequence of events show that it is very rapid. An avalanche of the size inferred above probably takes some 2 to 3×10^{-9} sec. The lateral spread and the building up of successive avalanches must therefore take on the order of some 10^{-8} to 10^{-7} sec. In this time the advance of the positive space charge has allowed it to reach the cathode giving the current pulse shown in the oscillograms of Fig. 2 taken from the work of Trichel.[27] Ionization has practically ceased during this time. The space charge then clears by being swept into the cathode and the current declines probably much as shown in the current oscillogram. When the field has been increased sufficiently by the removal of positive ions, the last ions start new electron avalanches and the process repeats. It is seen that depending on the strength of the clearing field and the rate of removal of the ions, the potential remaining constant, the process will repeat itself periodically. Thus one can expect to observe the regular current pulses shown in the oscillograms which resemble closely those of a relaxation oscillator. The periodic discharges have been observed down to values as low as 5000 per second. At applied potentials giving frequencies

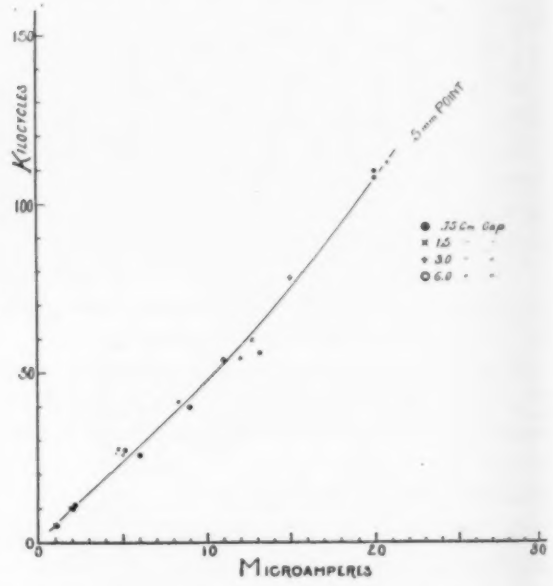

FIG. 3. Frequency of periodic pulses from negative point corona *vs.* current for various gap distances.

somewhat below this value, the pulses become sporadic and irregular owing to the fields decreasing to such magnitudes that repetition of the pulses periodically is not insured by secondary electron emission by positive ion bombardment. As the field is gradually increased, the clearing fields speed up the process. With constant spot size the frequency, and hence the current, rise regularly with the potential. These give the linear increase of frequency with current shown in Figs. 3 and 4. It is seen that gap length does not increase the frequency for a given current while the point size does. This is to be expected since at the starting potential, fields at the point vary very little with gap length while the smaller points, having smaller active areas, shorter ionizing distance, x, and higher fields, give the same currents by increasing the frequency.

As fields increase for the same spot the currents then rise linearly and the oscillograms show that this is accomplished by having the new current impulses start at higher points on the decaying positive ion space charge currents. How far up in frequency the regular impulses occur could not be ascertained as the resolving power of the oscillo-

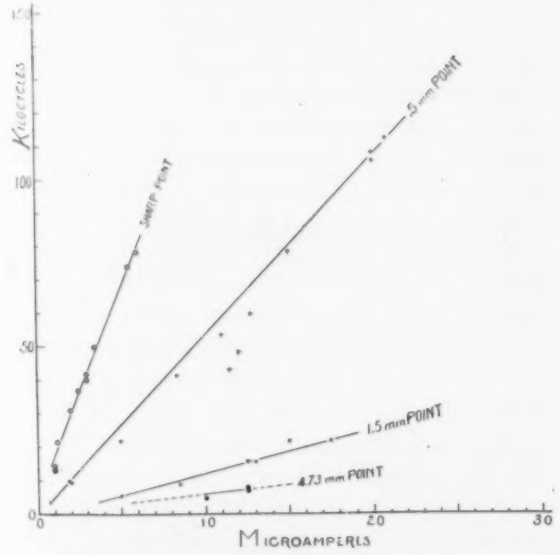

FIG. 4. Frequency of periodic pulses from negative point corona *vs.* current for various sizes of points.

graph at 200,000 impulses begins to be defective. It may continue until it approaches the time for the lateral spread of the discharge, or what is more likely it will continue until, with increasing potentials, a second active spot appears. This spot will, in general, take up the discharge, being a new point where low work function and high field now permit the process to occur, giving the surface of the first spot, denuded of its gas film by

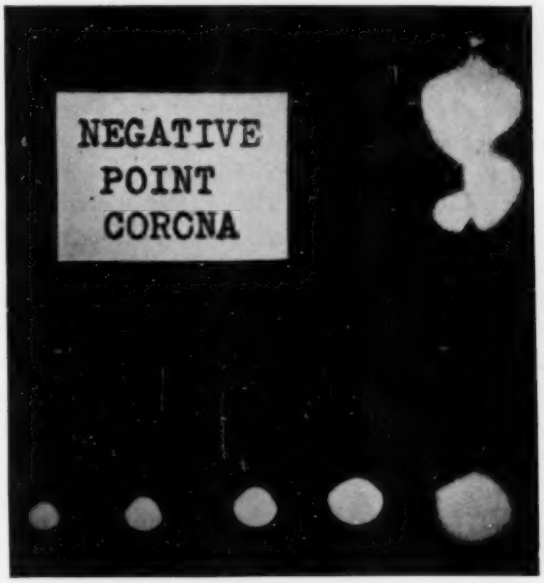

FIG. 5. Glow at end of negative point, showing increased extension of glow as voltage increases from left to right.

the positive ion bombardment, time to recover.[33] Once it has recovered, the first spot takes on its function and the second spot goes out and so alternation continues. Later several spots may appear. This is seen in Fig. 5 where one sees the glow extending into the gap further and further as the field increases to the last point where two or three new spots appear at active regions on the needle shank. These phenomena are all confirmed by the visual observation of the point in discharge by telemicroscope. Such pictures are shown in Fig. 6. There one can see the fine dark space which appears as a dark ring at the cathode, akin to a Crookes dark space in glow discharge, due to lack of ionization and excitation in the first few free paths. Beyond this is the bright electric blue glow of the ionization by the avalanches. Still further out in the region where electrons are slowing up, one sees a larger dark space of no appreciable ionization. Beyond this again where the attaching electrons build up a heavy negative space charge one sees the faint purplish haze (arc spectrum of N_2 and NO) due

to a second weakly ionizing region produced by this accumulation. At higher fields this extends well into the gap and takes on the characteristic mushroom shape shown which may vary with

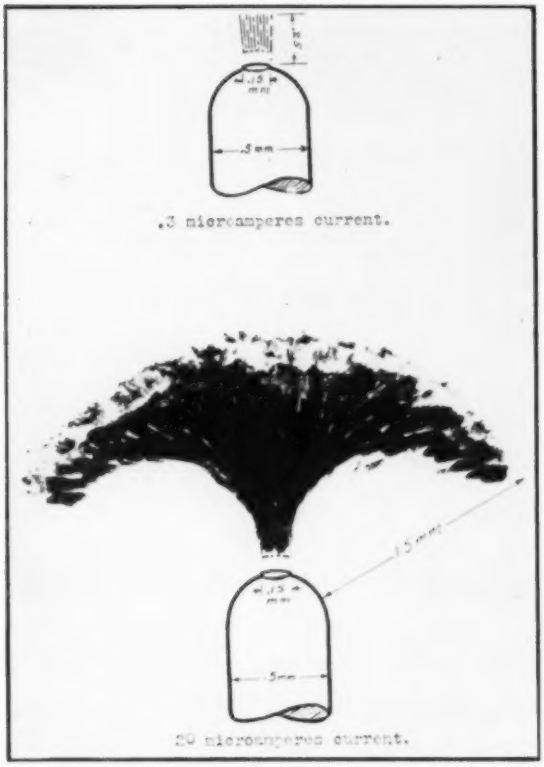

FIG. 6. Visual appearance of negative point corona, as observed through telemicroscope.

external conditions and point size. From the scale of the drawing one sees, however, that this is only a small fraction of the 3- to 6-cm gap used. The succession of events just after ionization and during the last of the clearing of the positive space charge is seen in Fig. 7 which schematically shows the density of ions above the axis and the field distortions below. It also shows the appearance of the correlated visual phenomena.

In the rest of the gap the weak fields allow of a considerable accumulation of slowly moving negative ions. The field here is only a few hundred volts per cm. At the plate, however, this space charge produces a sharp gradient which as current increases becomes more and more pronounced.

Now it must be clear from all that has preceded that the negative point discharge is a self-extinguishing phenomenon due to field concentration and positive space charge accumulation. A breakdown to a spark cannot propagate from the cathode through the space charge cloud. Since at appropriate fields the negative point corona *does cause breakdown to a spark*, it appears that spark propagation *cannot have proceeded outward from the point*. When the positive corona is studied it will be seen that on the other hand the positive space charge can build out or propagate as a streamer toward the cathode. Hence, it is clear that when the space charge at the positive plane electrode due to the negative ions reaches an appropriate value the spark will break by a positive discharge from the anode. This will be discussed at a later point.

Positive Point Corona

One may now turn to the positive point-to-plane corona in air. When one places a positive potential on the point and measures the current as a function of the potential one at first gets practically no current unless outside ions from a radioactive source or from the plate cathode are liberated in the gap. Under these conditions one gets a weak current proportional to the strength of the outside ionization which is larger than the ion saturation current i_0.[25] It is termed a *field intensified ionization current* and represents merely a multiplication of the electrons in the field near the point due to ionization by electron impact. While Townsend's α has values in regions where the field strength to pressure ratio X/p is greater than 20 in air, the current above does not increase until the ratio X/p at some ionizing paths from the point reaches a value $X/p=90$. For experiments by Loeb[34] have shown that it is not until negative ions encounter such fields that the negative ion sheds its electron so that it is free to ionize. Experimentally the starting potentials for such coronas are observed only when fields are such that $X/p=90$ extends out some tenths of a mm from the point. The current then increases asymptotically with a given i_0 from low values and increases smoothly. This is shown in Part A of the curve of Fig. 8. Above a certain minimum value one reaches a sudden increase of current of considerable magnitude.[25] On the oscillograph this increase is characterized by the appearance of pulses of

current lasting perhaps as much as 10^{-3} sec. which then go out.[26] These when examined with sufficient amplification were shown by Trichel to be composed of many small and partially resolved bursts of current involving up to about 10^7 ions and occurring at frequencies of the order of 10^5 per second or more. The region in which these phenomena occur are indicated on Part B of Fig. 8. For very fine needle points these increase in number until at what we term the *onset potential* the corona proceeds as a continuous self-sustaining *burst corona*.[28] At this point external ionization is no longer needed. The value of the onset potential V_s can be accurately located only by raising the potential above V_s and then reducing the potential until the current ceases. This "*offset potential*" corresponds to the value of V_s at which the pulses of burst corona become self-sustaining as seen in the oscillograph and thus the onset potential can be determined by the offset potential. The onset potential might be found by using an external ion source and noting at what potential the pulses change to a steady burst corona. The regime beginning with the first pulses of the burst corona and extending to the onset potential is the regime of *intermittent corona* and is termed the *Geiger-counter regime*. It is the region in which each ion created in the gap when sufficiently spaced in time produces a burst pulse which lasts for some time and goes out. As the burst pulse current is of the order of tenths of a microampere it can be used to count the advent of ions in the gap, and thus can be utilized to count the number of ionizing particles in the active volume. Geiger[35] and others[36] found that by placing a high resistance R in series with the point, the iR drop due to the burst pulse current lowers the potential of the point below the value of V_s so that if the burst pulses are cut off quickly the device can be used to count α- and β-particles and γ- or cosmic rays by the ions created by them in the gap, *if they do not come at too high a frequency*. The effect of the resistance is merely to extend the narrow counting plateau in voltage so that cut-off becomes more certain and is not limited to the inconveniently small potential range between the beginning of burst pulses and V_s. With all but the very finest needle points, slightly above the voltage at which the intermittent burst pulse corona starts, but well below the onset of the steady burst corona at V_s, there appear on the oscillograph *inductive kicks* of much larger magnitude than those characterizing burst corona.[26] These may be observed by the arrangement shown in Fig. 9B, which is also used for detecting intermittent burst pulses. In some cases isolated kicks of this type may appear alone. In other cases these kicks initiate the burst corona. *After a burst starts one never observes the kicks*. The oscillograms of the burst corona pulse are shown in Fig. 10,

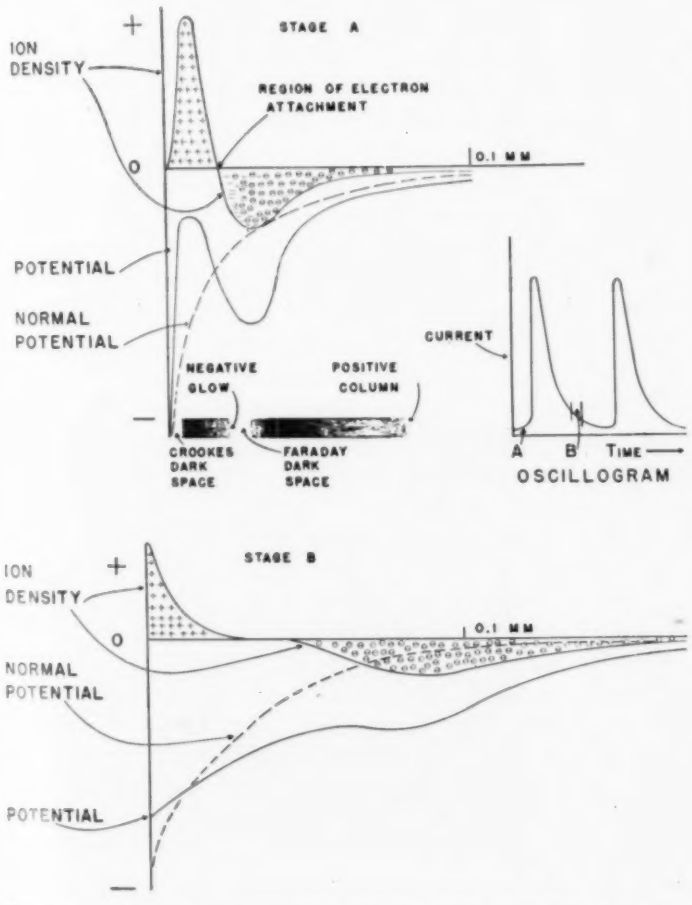

Fig. 7. Negative point corona space charge distribution just after ionization and during the last of the clearing of the positive space charge.

while Fig. 11 shows an inductive kick initiating a burst pulse corona, which later cuts itself off due to space charge weakening of the field. By

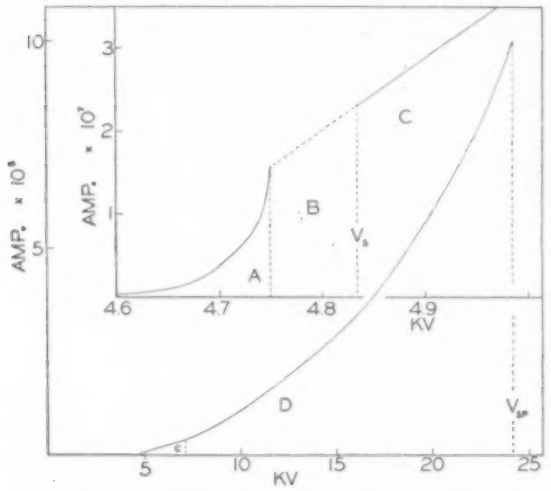

FIG. 8. Current-voltage curve for a positive point to plane corona, with enlarged curve of onset region. 0.5-mm diameter point, 2-cm gap. Region A is the field intensified ion current region, B is the region of intermittant bursts and streamers (giving Geiger-counter action), C is the linear current-voltage region. V_s is the onset potential, and V_{sp} is the breakdown potential.

the proper arrangement of gap geometry and voltage, and the judicious use of electrons from γ-ray ionization, or by the use of a gauze over the plate with an appropriate field between it and the plate to regulate the passage of negative ions into the gap as shown in Fig. 12, the inductive kicks can be made to repeat themselves without leading to a burst corona. The frequency of these kicks can be in a measure controlled by the field applied between gauze and plate. High resistance in series with the point will also cause repeated kicks without burst corona. If one attempts to increase the frequency of the inductive kicks beyond a certain value, depending on gap geometry and applied voltage, by increasing the strength of the external ionization, the kicks go over to more or less continuous burst corona. In general, it may be stated that if enough external ionization is provided, the burst corona process occurs at all voltages above A, while if no external ionization exists, V_s marks the beginning of stable burst corona. At voltages approaching V_s and above it, the burst corona process is always initiated by an inductive kick. In addition, the kicks never occur during the burst corona process.[26, 28]

By shielding the plate with a gauze as shown in Fig. 12, the current to the plate is not characterized by either the irregular burst pulse or the kick. All that is observed is a smooth pulse of the ion current due to the burst pulse or to the kick. Hence both the fluctuations in the burst corona and the kick registered in the case of the unscreened plate are *inductive effects* due to sudden changes of charge distribution about the point and in the gap.[44] The method shown in Fig. 9B thus measures both the inductive effect and the ion current to the plate. By using a plate placed near to the gap and shielded from ions by a cardboard screen, as shown in Fig. 9A, the

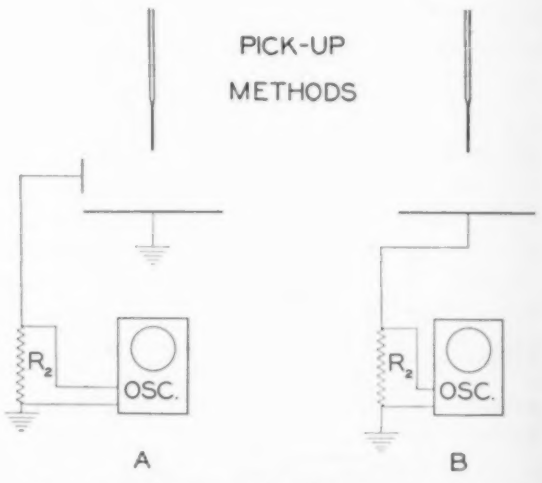

FIG. 9. A. Inductive method for detecting electrostatic pulses from corona with oscillograph. B. Method for detecting ion current and electrostatic pulses from corona with oscillograph.

inductive pulses only, due to either a burst pulse or kick, may be observed.[26]

Figure 13 shows the small inductive kick with pick-up as shown in Fig. 12 but with only partial screening of the plate. Here the ion current reaching the plate and inductive kick on the plate are both registered. Complete shielding would eliminate the inductive kick, but leave the ion current pulse. From the time elapsed between the kick and the advent of the center of the current pulse, the time of transit of the ions in the kick from point to plate can be measured. Calibration of the oscillograph deflection and the magnitude and duration of the current pulse

FIG. 10. Oscillogram of burst pulses from positive point corona using pick-up method shown in Fig. 9B.

enable the number of ions producing the kick to be measured. This number varies from 10^9 to 10^{10} ions.

Visual observation of the point with the microscope and with camera reveals at once the difference between burst pulses and the large kick-producing phenomena. The burst corona is always manifested by a brilliant blue glow covering the point and lying very close to it with maximum intensity at the point surface. The kicks are always characterized by streamers from 3 mm to 2 cm in length radiating from the point, and in many cases moving straight towards the plate. These are fine lines of a bright blue color that extend outward from the point and will hereafter be called *streamers*. Fig. 14(a) shows a photograph of the burst corona, while Fig. 14(b) shows streamers superposed on the bursts. The camera being sensitive to the near ultraviolet reveals on longer exposure much more in extent than the eye sees. On the other hand, no less than 50 streamers can be revealed by the camera while the eye sees individual streamers. The camera indicates a lateral spreading or branching of streamers. The eye does not see this in individual streamers, except in the case of large points, where the light intensity of a streamer is greatest, and where the branching is at greater angles. Cloud-track pictures made by Gorrill[32] of the pre-onset streamers definitely indicate them to be branched, accounting for the apparent bulging of the streamers of Fig. 14(b).

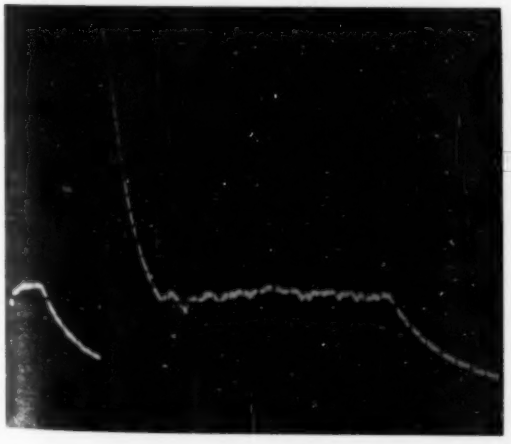

FIG. 11. Oscillogram of positive point inductive kick accompanying streamers, using pick-up method shown in Fig. 9B. Plateau is due to burst corona initiated by and immediately following streamer.

As the potential increases *above onset*, as previously stated, streamers disappear and *only*

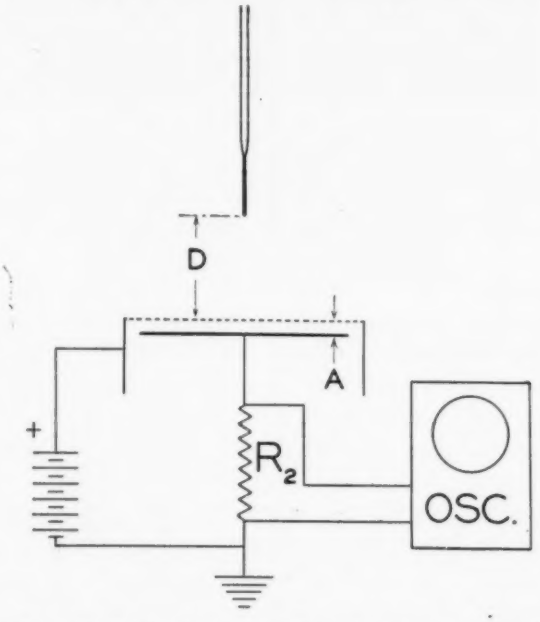

FIG. 12. Shielded plate for detecting ion current pulses with oscillograph. This arrangement is also used to produce repeating streamers.

the fluctuating burst corona is observed. Above onset the current-potential curve rises *linearly* with a slope which is greater the shorter the gap.[25] If the gap is very short the corona does not occur and a *spark breaks at once without corona*.[25] The gap length at which corona is no longer observed corresponds to the length of the pre-onset streamers observed with that point as predicted by us in Kip's first paper.[26] The ratio of potential to current in the linear region corresponds to the *space charge gap resistance R*.[25, 36] This resistance R multiplied by the current gives a potential which is equal to the value of the space charge potential set up by the positive ions crossing the gap. Its value at onset is nearly equal to the width of the Geiger-counter region B of Fig. 8. Hence the Geiger-counter region and its attend-

ant phenomena are in part to be ascribed to the effect of the positive ion space charge which the burst pulses set up and which obviously inhibit and at lower voltages choke off the burst corona in this region. As the potential is increased beyond onset the glow on the point spreads continuously over larger areas of the point quite in contrast to the glow on the negative point

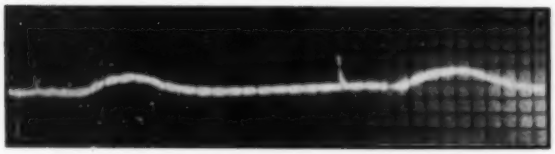

FIG. 13. Oscillogram taken by method shown in Fig. 12, with screen moved aside to allow recording of small electrostatic pulse at time of streamer propagation, followed by ion current at plate. Time interval between vertical line and center of pulse to the right is about 0.004 sec.

corona.[27] With increasing potentials the linear relation between current and potential ceases and current increases rapidly with applied potential.[25] Eventually the current and potential reach such a value that a *spark* ensues. Before this point is reached oscillograph, visual and camera observations again show the presence of streamers.[26] For small points these streamers can be observed to lengthen with increasing potential and shortly thereafter the spark occurs.[26] With large points the reappearance of streamers is followed so quickly by the spark that these streamers can only be observed by placing a high resistance in series with the point. The increase in length of the streamers from six mm to one cm as a function of potential has been measured. In a 6-cm gap with 0.05-mm point the breakdown followed after the streamers had reached a length of 1.1 cm. The visual observation of breakdown at this stage indicates that breakdown occurs when one decaying streamer path is reached by a new streamer before it is extinct. The successive streamers follow down old streamer channels. If on striking the cathode such streamers make an efficient cathode spot a rearrangement of space charges at once results in a spark. That the old extinct streamer channels are thus utilized is indicated if one shoots a stream of air parallel to the plate.[28] The extinct channels move sufficiently slowly near the plate to be diverted by an air blast. As the rapidly propagating new streamers reignite an old deflected path the revived path shows the deflection of the old channel. The *streamers* are not visibly deflected by air blasts. Observation of the point in air enclosed in a Pyrex glass tube in the dark shows that as the potential rises a great deal of ultraviolet light is present. The glass glows brilliantly as does the cathode surface. Studies with the screen over the plate show a considerable photoelectric emission from the cathode plate *if the gap is not too large.* There is some diffuse general photo-ionization of the gas but this is far less than the photo-emission of the plate for a three-cm gap. Fig. 8 shows the characteristic course of a current-potential curve. Region A is that of the field intensified ionization current, while B represents the Geiger-counter regime and V_o the onset potential. Region C represents the linear region of the current potential curve while region D is the region where Ohm's law ceases to hold and V_{sp} is the sparking potential. With this description we are able to analyze the mechanism active in the light of our analysis of the field at the points at onset.

At low fields all one observes is the avalanche formation and ion multiplication by factors of

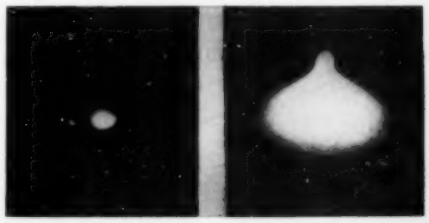

FIG. 14. (a) Photograph of burst corona glow surrounding 2.0-mm diameter positive point. (b) Photograph of many pre-onset streamers from 2.0-mm diameter poistive point, superposed on burst corona glow.

the order of 10 in the region near the point at which X/p exceeds 90 resulting from electrons detached from ions. As the field increases and the avalanches become greater the electrons formed are quickly drawn into the point leaving the positive space charge behind. Once this has occurred the photoelectrons produced in the gas outward from the point by the first avalanche send electrons into the point. Since the field distortion produced by the space charge of the first avalanche has an axis normal to the point

the maximum field distortion will lie along such an axis. The field at the tip of the avalanche will be increased above that at the point surface. The photoelectrons coming in along the axis will be favored by the axial field where α is higher. The ionization produced by the next electron moving into the point along its axis gives a second avalanche. The electrons from this avalanche rapidly move up the space charge channel to the point. This action can readily be demonstrated by the potential changes induced on the electrode in Fig. 9A in streamer formation when a high resistance is in series with the point and the pick-up electrode is placed level with the point; for they reduce the point potential to a value where the field reverses at the pick-up electrode. As a result of the second avalanche the space charge along the axis of the first avalanche is increased and extended radially from the point. The field at the tip of the space charge is still further increased. Hence, the ionization proceeds outward from the tip at the velocity of electron travel *or higher* increasing the field and producing more space charge along the axis. This succession of avalanches along an axis constitutes a *burst* or an incipient streamer. In a uniform potential gradient or field of sufficient magnitude this process would continue right across the gap. In the radial field of the point, however, the field strength rapidly decreases and presently the tip of the burst or streamer finds itself in a region where the potential gradient is so low that even with its enhanced field it can no longer propagate; that is, a burst or streamer can form and proceed only as long as the potential gradient is adequate. To *start* a burst or a streamer probably requires *a much higher field* than to *continue the propagation of a well-developed burst or streamer*. Hence the occurrence and length of bursts and streamers depend on the field distribution about the point.

Into a clear gap the length of the streamer varies with the applied potential, as one might expect. If the field is reduced by the diffused positive space charge of a preceding streamer near but ahead of the point, bursts *cannot develop into streamers*. The propagation of bursts or streamers is also inhibited by other effects. First self-repulsion and diffusion of the positive ions tend to broaden the streamer channel and weaken the space charge. This movement is slow since positive ions have a low mobility. Thus in the 10^{-8} sec. of streamer formation the movement of the ions is negligible. In addition the positive ion channel as a whole tends to move radially from the point towards the plate with a velocity of 10^{5} cm/sec. near the point down to a velocity

FIG. 15. Cloud-chamber picture of pre-onset streamer taken by Gorrill, showing branching. Point is 2.0 mm in diameter.

of 10^{3} cm per sec. near the plate. There is also some broadening of the channel due to the lateral diffusions of the electrons with high thermal energies. The average breadth is $\bar{y}=(2Dt)^{\frac{1}{2}}$, where D is the coefficient of diffusion and t is the time of travel. In the short travel and high fields at points t is short and broadening is small. This accounts for the strongly directive character of the streamer axis. The electrons of later avalanches moving up the space charge probably do not diffuse much owing to the conservative action of the positive space charge channel. Again the photoelectrons are produced in the gas all about the axis of the streamer in diminishing numbers as one recedes from the axis. Near the tip of the burst or streamer the number is greatest but many electrons are produced at points such that lines drawn from them to the tip make an angle with the axis. This can lead to the formation of a crooked streamer if only one electron is produced. If more are produced and are equally successful in ionizing, then the streamer branches. If the fields are high enough such branches may develop for a considerable distance. Since, however, they expand the tip at the beginning, they tend to shorten the length of the branched streamer, especially early in the

branching process. Hence, it is not strange to find branching taking place *conspicuously only in high field regions* such as in overvolted plane parallel gaps and *near the point* in point-to-plane gaps. Where, as in a plane parallel gap, the field is highly directive, branches in general trend towards the cathode. In the corona this tendency is less noticeable. Hence, aside from propagation into low field regions streamer propagation is inhibited by electron and ion diffusion, divergence of incoming avalanches and actual branching. Fig. 15 shows branching in a cloud-track picture of a streamer taken by Gorrill.[32]

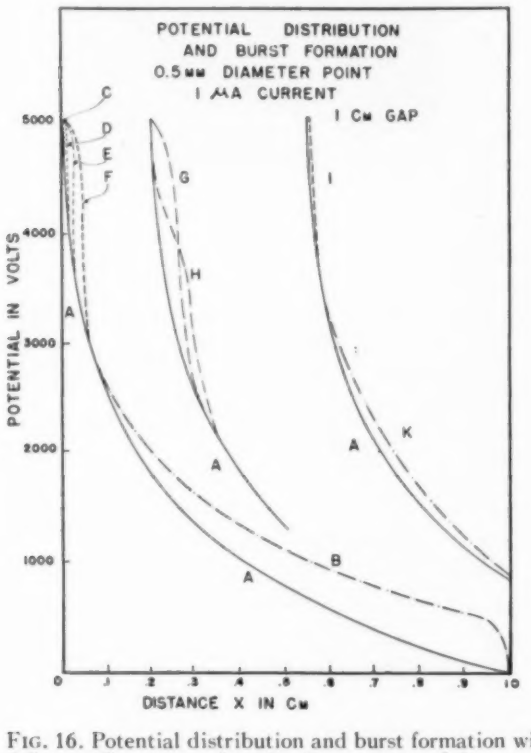

FIG. 16. Potential distribution and burst formation with a 0.5-mm diameter point, 1 μA current, and 1-cm gap. Curve A is the undistorted potential in each case. Curve B shows the space charge distortion near the cathode due to extinct bursts. Curves C, D, E and F show successively the approximate potentials after the first, second, fifth and tenth avalanches in burst formation. Curves G and H show later stages of a burst where diffusion and movement in the field occur. Curves I and K show a new burst starting as the old one recedes. At higher fields this may overtake the old burst, forming a streamer.

The diagram of Fig. 16 shows the potential distribution in a gap and the effect of space charge on the development of bursts or streamers schematically. From the character of this action we at once understand the positive point-to-plane corona mechanism. Given an adequate field the first ion starts an avalanche which quickly develops into a burst. At low fields this propagates only to the extent of creating a *burst* streamer of some 10^6 to 10^7 electrons. This takes some 10^{-8} to 10^{-7} sec. It then ceases and its micro area of electrode is inhibited from starting a new burst for some 10^{-5} sec. or more while the space charge is being swept away from the point. In the meanwhile photoelectrons created to each side of the axis of the burst as far away as 10^{-2} mm crash into the positive point at clear places giving other avalanches that propagate new bursts. These in 10^{-5} to 10^{-3} sec. spread all over the regions of the point surface where the field is adequate. Before the 10^{-3} sec. needed for clearing out the first burst has elapsed the many offspring bursts ranging in size from avalanches of 10^2 to bursts of 10^7 ions have built up a positive space charge outward in the gap. This is large enough to *lower the field at the point surface to such a value that bursts can no longer form*. Thus the *burst pulse* in the Geiger regime *below onset* is merely a series of bursts extinguished by their own space charge.

In 10^{-3} sec. or more the gap is clear of all positive space charge and a *new* burst pulse can start. The duration of the pulses is irregular; some are long and others short. The appearance of burst pulses depends on the presence of initiating negative ions or electrons in the gap which reach the point. There can thus be no regularity as regards size or frequency of such burst pulses, and we have the intermittent burst pulse corona of the Geiger regime. For small points the fields are so confined that the avalanches can only lead to burst formation, and bursts never can develop into long streamers.

As the potential on the points is increased the space charge accumulation must be larger and larger in order to choke off the bursts and to give the burst pulses. Eventually a potential V_s is reached where the space charge no longer suffices to choke off the bursts and we have merely the fluctuating burst corona of Trichel.[28] This is composed of bursts and avalanches random in time, space and size, occurring in the order of 10^5 to 10^6 or more per second and comprising from 10^2 to 10^8 ions. As the field increases still further these bursts extend over larger areas of

surface and extend farther out into the gap as seen in Fig. 17. Eventually the fields become so high (300 to 500 percent above onset) that space charges in the gap *cease to inhibit* streamer growth and adequate fields even for fine points extend so much farther into the gap that the bursts can develop into streamers.

The careful measurement of the potential of the first appearance of bursts with confocal paraboloid electrodes permits of an evaluation of the minimum fields for burst formation at the electrode. If the space charges are measured for a given corona current one could at once, then, predict the value of V_s and the width of the Geiger regime.

With larger points the high fields extend farther into the gap. Under these conditions the growth of bursts out into the gap is to be expected and streamers will form. Streamers propagate farther into the gap, the larger the radius of the point and the higher the potential applied. Data at present are not sufficiently complete to permit us to determine the minimum field for the development of a burst and its propagation as a streamer. It is possible that this will be found shortly. It is clear, however, that once a streamer or burst pulse has propagated with its 10^9 to 10^{10} ions, the gap is fouled by a space charge of positive ions. In its propagation the streamer may have initiated a burst pulse such as shown in Fig. 10. In general it will do so. It is possible that the space charge distortion of a streamer may even be great enough to choke off a burst and, in fact, at the *onset of streamer propagation*, but few of these initiate bursts. If the burst pulse is short-lived it may not appear against the background of the inductive disturbances set up by the streamer. If after the streamer has died out and its space charge is removed from the gap a timely ion or secondary electron from a γ-ray or elsewhere arrives at the point a new streamer may start out. By choosing a gap length such that after each streamer the space charge is removed a *series* of streamer kicks or pulses can be obtained. This can be accomplished by judicious γ-ray ionization, by getting photoelectric ions from the plate by use of a screen and auxiliary field, or by the use of a *high* resistance in series with the point which so reduces the potential of the point that the new streamer or burst corona cannot start before the gap is cleared. By varying the field between screen and plate so that the photoelectric ions

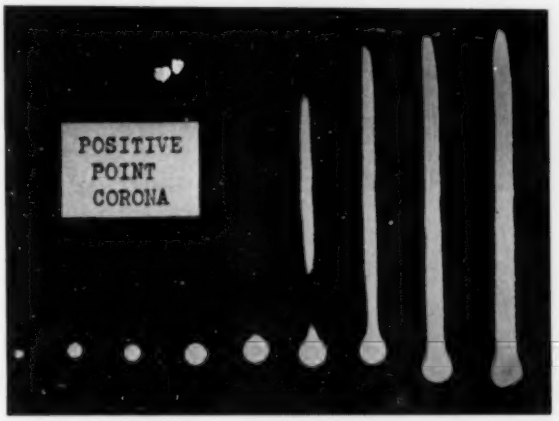

FIG. 17. Photographs of glow covering positive point during burst corona, showing increase in extension of glow into gap and increase in area covered as voltage is increased from left to right.

arrive at the point in shorter and shorter time intervals the time between streamers can be reduced until the interval begins to be less than that to clear the field. At this stage the streamers cease to repeat. If the γ-ray source is made so intense that there is not time enough for space charge clearance between streamers, the streamers go over to burst corona.

As the potential increases beyond the streamer potential threshold the burst corona pulses are more likely to follow a streamer, and they increase relative to the streamers, ending finally in continuous burst corona. Thus *the potential range of pre-onset streamer production is quite limited*. This fact coupled with the late introduction of the oscillograph into corona studies is primarily responsible for the very recent discovery of streamers.*

For a 0.5-mm point and a 4-cm gap, burst pulses begin at some 4900 volts. By 5100 volts one has already passed through the region of Geiger-counter action, streamers and burst pulses and into the continuous fluctuating burst corona. An increase of some 3900 more volts takes one past the linear space charge controlled burst

* Many years ago M. Toepler (reference 38) and J. Zeleny (reference 37) in a study of a corona actually observed streamers. The streamers were thereafter designated as brush discharge.

FIG. 18. Photograph of glow around positive point showing incipient streamers.

corona. In this region the field at the point is kept nearly constant owing to the effect of the positive ions from the burst corona. Hence, bursts do not propagate far outward and current increases only by the lateral areal spread of the bursts over the point surface. It is this condition which permits of the constant resistance of the gap. As potential increases the current increases in direct proportion. The resistance for confocal paraboloids where fields are known is then a linear function of the gap length as Kip showed.[25]

On further increase of potential, the space charge is swept out more and more rapidly. There is far less space charge about the point and the resistance decreases with increasing potential. Hence, the current increases more rapidly than linearly with the potential. This increase continues for a very long range of potentials from 10,000 volts up to nearly 30,000 volts. Where this takes place the burst corona glow extends farther and farther into the gap as shown in the photographs of Fig. 17. Eventually the field is high enough at some distance from the point so that the bursts suddenly begin to grow into streamers. Incipient streamers are shown in Fig. 18 just beyond the glow. Then in a very short range of potentials, streamers begin to propagate across the gap. For one needle point of 0.05-mm diameter with a 6-cm gap the streamers were 6 mm long at 23 kv and 11 mm long at 30 kv. Thereafter, with little potential increase, they began to cross the gap. Visually this crossing *appears* to result from new streamers that catch up with old streamer channels and so revive them and propagate across the gap. Fig. 19 shows a number of such streamers taken with camera using an exposure time of 5 sec. When one of these streamers succeeds in creating a good source of secondary electrons at the cathode plate a spark or an arc results.

The breakdown or sparking mechanism in the positive point-to-plane corona discharge is easily seen in the case of spark breakdown at the potential of streamer production *below* burst corona *onset* when the gap is short. If for instance in a long gap a given point at a certain potential gives a 1-cm streamer then in a 1-cm gap at about that potential there is no corona. The gap at once breaks down in the form of a spark and corona is not observed. In this case the *pre-onset streamers cross the gap* and, striking the cathode, start the breakdown mechanism. Here the cleared gap field is *high enough across the whole gap to allow streamers* to propagate across, once the point potential is high enough to initiate a streamer. It is seen that in this instance we are approaching closely to the conditions existing in a plane parallel plate gap. This analysis, then, it is seen brings us nearer to an understanding of the case of ordinary spark breakdown at atmospheric pressure.

Before beginning to discuss that problem it is necessary to draw some general conclusions from what has gone before. It was seen that in the intense field gradients varying rapidly with distance from the *negative* point, the ionization in electron avalanches acts in such a fashion as to build up space charges that *inhibit or choke off the discharge*. In the case of the positive point, on the contrary, the space charges build up in such a fashion as to enhance breakdown away from the electrode and along a direction primarily set by the lines of force in the field. Thus, while in high fields the negative avalanche tends to impede its own progress by space charge formation, the positive space charge propagates itself towards the cathode once adequate initiating and sustaining fields exist. It furthermore does this along an axis parallel to the field in an exceedingly limited area of cross section. The mechanism of the streamer formation is now qualitatively rather clear although quantitatively and mathematically it is little understood. With the recognition of this situation one may

accordingly consider the spark between plane parallel electrodes.

Sparking Mechanism Between Plane Parallel Electrodes

Bearing in mind the inhibiting action of the positive space charge on the electron avalanche advance and the accelerative action of the same on the advance of the positive end in streamer formation, stimulating breakdown, one may consider conditions in the plane parallel gap. The starting values of X/p for both types of point-to-plane corona in *air* are in excess of 90 since in the large volumes of low field strength region the initiatory electrons all attach to form ions which must be re-ionized above $X/p=90$. In a plane parallel gap filled with air at 760 mm pressure the value of X/p at the conventional sparking potential V_s for a gap about 1 cm long is only 40; but in contrast to the point-to-plane gap the field is quite uniform. Under these conditions Raether[20] shows that the energy of agitation of the electrons is of the order of 6 volts. Attachment of photoelectrons from the cathode to molecules to give ions is therefore unlikely. Hence, we do not require the high value of X/p to produce the initiatory electrons. It is only when potentials are suddenly applied to a gap where no photoelectrons are liberated that we would need to depend on a high field for producing electrons.

There is, however, an even more important difference to be noted. The high values of X/p at the corona points are required because of the very restricted regions of adequate field strength. In the plane parallel gap the smaller fields can cause the same cumulative ionization over immensely longer stretches. With the whole gap in a condition to retain free electrons and with the high uniform fields existing we have, as was seen in corona studies, ideal conditions for streamer propagation. Thus the immediate question to be raised is whether under these circumstances electron avalanche formation can lead to the formation of breakdown streamers. This question can only be answered by quantitative considerations for which thanks to Raether[20] we now have the necessary data.

Consider for example the plane parallel air gap at 760 mm with $\delta=1$ cm at the conventional sparking potential V_s of 30,400 volts. Under these conditions $X/p=40$, $\gamma\sim 2\times 10^{-6}$ and $\alpha=13$ as given by Sander's data.[29] As a result it takes on the average 0.053 cm advance in the field direction to double the number of electrons. At the end of the path 1 cm long the electron avalanche will consist of about 4×10^5 electrons, and in the last 0.053 cm there were created 2×10^5 positive ions which are left behind as the electrons are drawn into the anode. Now Raether has shown that the electron avalanche near these fields will have spread axially an average distance $\bar{y}$ given by $\bar{y}^2=2Dt$. Here D is the coefficient of diffusion of electrons at $X/p=40$, which can be determined from the electron mobility, and t is the time taken to cross the 1 cm which is $\sim 10^{-7}$ sec. For the present case $\bar{y}\sim 0.01$ cm. The number of positive ions in the last ionizing path $l=0.053$ cm that lie within a cylinder of approximately 0.01-cm radius is $n=2\times 10^5$. This gives the charge density ρ of positive ions as $\rho=ne/\pi\bar{y}^2l$, where e is the electron. This density of charge will produce a field strength X_ρ, due to space charge of $X_\rho=4\pi\rho$, or roughly 12,000 volts per cm in our case. Hence, near the conventional sparking potential V_s after 1-cm travel the electron avalanche will be exerting an inhibitory effect on the avalanche movement in the applied field X of 30,400 volts per cm. If the potential had been raised five percent so that $X/p=42$, α would have been 17 and at the end of 1 cm the number of positive ions $n=1.2\times 10^7$. Hence,

FIG. 19. Photograph of positive point breakdown streamers traversing completely across the gap. Exposure time is five seconds.

the electron avalanche could have progressed only 0.75 of a cm for the same degree of inhibition. Actually long before $X_p = 12{,}000$ the rear end of the electron avalanche is being retarded while the electrons in advance are being pushed forward by the negative electron space charge at the anode end of the avalanche in an enhanced field. It is quite clear that at the conventional sparking potential we are already close to if not beyond the field strengths where inhibition and positive streamer formation can occur. The impossibility of applying with certainty data, such as Sander's taken in gas of one purity, to the case of the gases used in spark studies makes it difficult to fix accurately the relations more closely: for traces of impurity can change α by 20 percent. It is, however, not unreasonable to expect to observe spark breakdown by streamer formation in the neighborhood of the conventional sparking potential in air for gaps of the order of, or in excess of, 1-cm length. In such breakdown owing to the photo-ionization in advance of the tip we can expect times of breakdown to be distinctly less than those for electron avalanche propagation across the gap. Now it has been observed by Torock,[39] Dunnington,[15] Holzer,[40] von Hamos,[16] White,[17] Wilson[18] and Flegler and Raether[19] that practically *all breakdowns using longer gaps and/or overvolted gaps* proceeded from the midgap region or from the anode as *positive streamers towards the cathode and not as electron avalanches from the cathode.* It was only in the last stages of the breakdown that weak avalanche advance from the cathode was observed. It was furthermore observed by Rogowski[12] and Strigel[13] as well as White,[17] Wilson[18] and others[41] that it was in the overvolted gaps that the really short formative time lags occurred. These were the shorter the higher the overvoltage. In fact it was early pointed out by White[17] and later more clearly by Flegler and Raether[19] that under these conditions the high positive space charges inhibited the advance of the electron avalanche towards the anode and stimulated rapid streamer propagation towards the cathode. It was not, however, until the controlled study of streamer formation in positive corona and the study of the negative corona gave more data, that the exact mechanisms active in this form of breakdown were understood.

Forgetting for the present what takes place near and perhaps above the conventional sparking potential, one may turn to the region of fields lying between threshold $\gamma e^{\alpha\delta} = 1$ and V_s. Here on theory sparks *may take place* but occur so infrequently that, except just at V_s or slightly above, neither time lag, Kerr-cell studies or photographs of cloud tracks have been made. Raether[20] has observed avalanches below V_s emanating from the illuminated cathode traversing the gap of about 1-cm length at 250-mm pressure in a uniform and orderly fashion at velocities of $\sim 10^7$ cm/sec. which exhibit the broadening at the tip consistent with diffusion. These have *not* led to a spark. The sparks passing just above or at V_s observed by Dunnington, and Flegler and Raether, and White, however, appear *to emanate from near the cathode and progress as electron avalanches* at about 10^7 cm/sec. across the gap. Near the end of the path in almost all cases of gaps above 3 mm in length and above 100-mm pressure the anode streamer is seen to form and move towards the advancing avalanche tip. This course of events together with the total time of $\sim 2 \times 10^{-8}$ sec. of gap breakdown point clearly to the mechanism active.

The first electron proceeds from the cathode and in about 0.053 cm forms its first ion. It has also formed some photons which start new avalanches in the gas and from the neighboring regions of the cathode. As the first avalanche advances it builds up by cumulative ionization an axial field distorting positive space charge near mid-gap, which enhances ionization directively near the cathode. In the front portion of the electron avalanche tip the negative space charge axially enhances the field and produces new photoelectrons on the anode side which prolong that end of the advancing tip. Finally about the time that positive ion production from the avalanches is beginning to slow down the advance, the electrons from later avalanches at the cathode end proceeding up the space charge channel at exceedingly high velocities reduce the inhibiting action.[42, 43] This inhibiting action may account for the stepping of leader strokes in lightning as indicated by Schonland.[43] By this

time a space charge streamer has begun to propagate from the anode and the spark quickly results.

The great fall of potential observed in these short time intervals is, as Slepian[44] has pointed out, an inductive or displacement current such as observed by Kip in his streamer propagation.[26] The visible light production in the streamers can come from the photons accompanying the 10^{10} ions formed per cm length in the streamer channel as observed by Kip. Owing to the incipient inhibiting action and the slower development of avalanches in the early stages of the advance of the first avalanche from the cathode, the formative time lag of breakdown will in general be longer than with overvolted gaps in conformity with the observations of all the workers including Flegler and Raether.

It must be noted, however, that even near V_s the passage of the spark is a rare occurrence; for it is only one in 10^5 to 10^7 of the initiating photoelectrons starting from the cathode which permit breakdown. It can be seen then that the combination of secondary electron production by photo-ionization from a primary electron avalanche which results in the breakdowns observed by Dunnington and White *at* V_s is an exceedingly rare occurrence. Thus while the criterion $\gamma e^{\alpha\delta}=1$ sets a threshold, even at potentials considerably above the value set by this condition of instability, the *realization* of a spark below V_s is rare indeed and seems to be conditioned by a sequence of electronic avalanche events that is most infrequent.

One may then ask why it is, when $\gamma e^{\alpha\delta}>1$, leading to an accumulation of space charge, that the breakdown at higher pressures does not *eventually* follow, albeit rather slowly. This question probably should be left unanswered until more data are at hand. One can, however, make certain observations. When in a clear gap, $\gamma e^{\alpha\delta}>1$, the secondary electrons create more new avalanches than sufficient to maintain the current. Hence, with constant i_0 the ions must be expected to cumulatively increase in the gap, building up a space charge over a considerable interval of time. This space charge accumulation would be expected to eventually rearrange itself in such a way as to cause breakdown. Aside from the dissipative and destructive action on the charges built up resulting from lateral electron and positive ion diffusion in long time intervals, with consequent loss from the gap and possible recombination, it is probable that another action prevents the slow type of breakdown at higher pressures. For it was noted that *the active agents in breakdown at the higher pressures were due to localized or concentrated space charges*. In the longer time required for gradual building up *all such localization disappears* and the space charges take on a general diffusive character. Such space charges it was noted *inhibit streamer formation* in corona. It is, therefore, not unlikely that under these conditions the cleared gap criterion for a threshold $\gamma e^{\alpha\delta}=1$ is no longer applicable and new values of the quantities γ and α at a higher X/p are required. Hence, it is only with a rare sequence of events that can concentrate the charges along an axis, which may occur only above $\gamma e^{\alpha\delta}=1$, that a spark will occur. These are rarer and the process of breakdown is indubitably slower the nearer one is to the threshold.

There is one condition, however, where the process of breakdown can occur nearer to $\gamma e^{\alpha\delta}=1$. This lies in the regime of low pressures. When, for a 1-cm gap, the pressure lies between 0.1 mm and 10 mm, the value of X/p for a spark is markedly higher in all gases than at NTP for it lies in the neighborhood of 100 to 60. Here the values of α are much greater. The photoelectric ionization produced by an avalanche extends over very large distances as absorption is less. The avalanche spreads by diffusion over large areas and the efficiency and tempo of the processes is considerably increased. Under these conditions it would not be surprising to see the whole gap nearly simultaneously break into a glow discharge as a result of the rearrangement and building up of space charge as calculated by Franck and von Hipple, Schumann, Sämmer and Kapzov and as suggested by Steenbeck.[46] In this case the values of V_s observed should approach more and more closely to those calculated from the values of γ and α from Townsend's criterion, as they are observed to do. The formative time lags in this case will be much longer and what evidence there is at hand from the work of Allibone and

Meek[45] seems to bear this out. For very short gaps again the mechanism will doubtless be very different.

From this it will be seen that the mechanism of spark breakdown in air is not a unique mechanism even in the limited range of pressures usually encountered. It is not even approximately predicted by Townsend's criterion in some of the commonly observed cases at higher pressure. Thus *one criterion* for a spark breakdown cannot be and *should never have been universally applied to all conditions*. In particular it is, however, seen that the corona mechanisms have led us to a fairly clear understanding of the spark breakdown at atmospheric pressure while so far the other mechanisms are quite obscure.

Bibliography

1. J. S. Townsend, Nature **62**, 340 (1900); Phil. Mag. **1**, 198 (1901).
2. L. B. Loeb, Rev. Mod. Phys. **8**, 267 (1936).
3. G. Holst and E. Oosterhuis, Phil. Mag. **46**, 1117 (1923).
4. L. B. Loeb, J. Frank. Inst. **205**, 305 (1928).
5. W. Rogowski, Archiv. f. Elektrotechnik **20**, 99 (1928).
6. J. Franck and A. von Hippel, Zeits. f. Physik **57**, 696 (1929).
7. W. Schumann, Zeits. f. tech. Physik **11**, 58, 132, 195 (1930).
8. J. J. Sämmer, Zeits. f. Physik **81**, 490 (1933).
9. N. Kapzov, Physik. Zeits. Sowjetunion **6**, 82 (1934).
10. P. O. Pedersen, Ann. d. Physik **71**, 371 (1923).
11. I. Tamm, Archiv f. Elektrotechnik **20**, (1928).
12. W. Rogowski, Archiv f. Elektrotechnik **20**, 99 (1928).
13. R. Strigel, Wiss. Veroffent. aus dem Siemens-Konzern **11**, 52 (1931).
14. J. W. Beams, J. Frank. Inst. **206**, 809 (1926).
15. F. G. Dunnington, Phys. Rev. **38**, 1535 (1931); E. O. Lawrence and F. G. Dunnington, Phys. Rev. **35**, 396 (1930).
16. L. Von Hamos, Ann. d. Physik **7**, 857 (1930).
17. H. J. White, Phys. Rev. **46**, 99 (1934).
18. R. R. Wilson, Phys. Rev. **49**, 1082 (1936).
19. E. Flegler and H. Raether, Zeits. f. Physik **99**, 635 (1936); **103** 315 (1936); H. Raether, Zeits. f. Physik **96**, 567 (1935).
20. H. Raether, Zeits. f. Physik **107**, 91 (1937).
21. L. B. Loeb, Science **69**, 509 (1929).
22. A. M. Cravath, Phys. Rev. **47**, 254(A), (1935); with L. B. Loeb, *ibid* **47**, 259(A), (1935).
23. C. Dechene, J. de phys. et rad. **7**, 533 (1936).
24. A. M. Cravath and L. B. Loeb, Physics **6**, 125 (1935).
25. A. F. Kip, Phys. Rev. **54**, 139 (1938).
26. A. F. Kip, Phys. Rev. to be published.
27. G. W. Trichel, Phys. Rev. **54**, 1078 (1938).
28. G. W. Trichel, Phys. Rev. **55**, 382 (1939).
29. F. G. Sanders, Phys. Rev. **44**, 1020 (1933).
30. K. Masch, Archiv. f. Elektrotechnik **26**, 589 (1932).
31. E. Greiner, Zeits. f. Physik **81**, 543 (1933).
32. S. Gorrill, Thesis in preparation, University of California (1939).
33. L. F. Curtiss, Phys. Rev. **31**, 1060, 1127 (1928).
34. L. B. Loeb, Phys. Rev. **48**, 684 (1935).
35. H. Geiger and H. Mueller, Physik. Zeits. **29**, 839 (1928).
36. Sven Werner, Zeits. f. Physik **90**, 384 (1934); **92**, 705 (1934).
37. J. Zeleny, J. Frank. Inst. **218**, 685 (1934); **218**, 685 (1934).
38. M. Toepler, Ann. d. Physik **2**, 50 (1900).
39. J. J. Torock, Trans. A. I. E. E. **47**, 177 (1928); **48**, 46 (1930).
40. W. Holzer, Zeits. f. Physik **77**, 676 (1932).
41. Morris Newman, Phys. Rev. **52**, 652 (1937).
42. L. B. Snoddy, J. R. Dieterich and J. W. Beams, Phys. Rev. **52**, 739 (1937).
43. B. F. J. Schonland, Proc. Roy. Soc. **A164**, 132 (1938).
44. J. Slepian, Electrical World **91**, 768 (1928).
45. T. E. Allibone and J. M. Meek, Proc. Roy. Soc. **A168**, 97 (1938).
46. M. Steenbeck, Wiss. Veröff. aus dem Siemens-Werken **15**, 32 (1936).
47. H. Raether, Zeits. f. Physik **110**, 611 (1938).

The Physics of Rubber

I. Its Observed Elastic and Thermoelastic Behavior

EUGENE GUTH

Department of Physics, University of Notre Dame, Notre Dame, Indiana

Introduction

THE physics of rubber is investigated today principally because of the many uses of rubber in daily life. These uses arise because of its baffling *physical* behavior. Therefore, physical tests are used generally in the rubber industry to test the properties of the rubber goods produced. However, the physics of rubber is of importance not only because of its relation to daily life and industry[1] but because of its purely scientific interest. Three main reasons for the physicists' interest in rubber are:

(1) Rubber has properties intermediate between a fluid and a solid. For instance, it is incompressible like a fluid and yet has a shape like a solid. It has a melting point below which it is amorphous and above which it is crystalline. The melting of rubber can be called an unsharp phase change belonging to the order-disorder transition so much discussed recently in connection with alloys.

(2) Rubber bears an important analogy to biological substances, such as muscle. In fact, considerable light can be thrown on the mechanism of muscular action, especially retraction, from the theory of the elasticity of rubber. This fact will be indicated later.

(3) Rubber can be used conveniently for the testing of certain theories where other substances fail. For instance, the theory of hardness by H. Hertz neglects plasticity and can, to a certain extent, be demonstrated better with rubber than with a metal because rubber is reversibly elastic over a longer range.

Phenomenologically and historically we can distinguish between two phases of the physics of rubber. The first phase consisted of the discovery of the properties of rubber and its description in terms of thermodynamics, theory of elasticity, etc., i.e., in terms of classical physics Among others, physicists of the rank of Joule, Kelvin and Roentgen have participated in this development. The application of thermodynamics and the theory of elasticity has brought order to a wealth of seemingly unconnected facts.

The second phase attempts to determine the microscopic behavior—the molecular structure of rubber—and to derive from it the macroscopic behavior of rubber. This work was begun only recently and is a chapter of modern physics. Its object is to relate the macroscopic properties of rubber with the form and size of its molecules and their inner mobility as well as with the inter- and intra-molecular forces. The time seems opportune for such an attempt because, on the one hand, recently the problem of the inter- and intra-molecular statistics of long chain molecules (which also is of importance for the behavior of such molecules in solution) has been introduced and partly developed.[2] On the other hand, our knowledge concerning molecular forces has now a more certain foundation through quantum mechanics.

The present review considers particularly the discussion of the elastic and thermal behavior of rubber from a theoretical point of view. The actual application of thermodynamics is carried through further than in any earlier discussion. A few remarks will be made, also on experimental technique employed in the stress-strain work at the University of Notre Dame.

In the older investigations on rubber, unfortunately, the samples were not defined precisely enough chemically to establish their identity sufficiently. The same criticism holds for the experimental technique applied. In spite of this, however, it is interesting that the older results show the same general trend as the newer ones. Finally, it shall be seen that no data existed

in the literature hitherto which would allow the application of thermodynamics with certainty.

The present installment considers (1) the stress-strain relations of rubber, (2) Poisson's ratio and (3) the thermoelasticity of rubber. Succeeding installments will treat (4) thermodynamics of stressed rubber, (5) internal energy and entropy of stressed rubber from experiment,

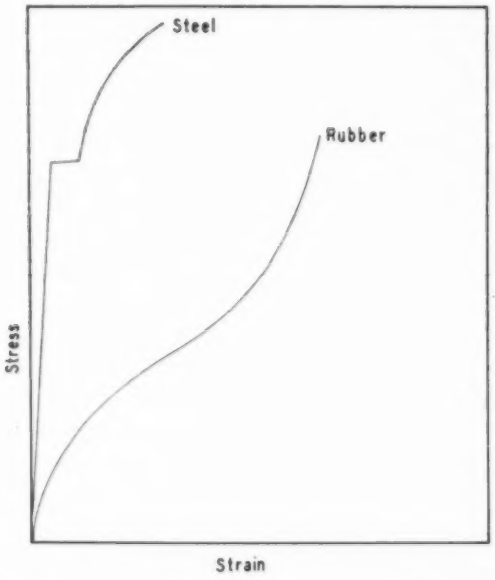

FIG. 1. Stress-strain curves for rubber and for steel. The curves were drawn to different scales for the purpose of comparison.

(6) the elastic and thermoelastic behavior of "normal" substances, (7) molecular structure of rubber, (8) free rotation, (9) intra- and intermolecular statistics, (10) synthetic rubbers, (11) experimental technique for obtaining stress-strain curves, (12) optical, electrical and other properties of rubber and finally (13) rubber elasticity and mechanism of muscular action.

STRESS-STRAIN RELATIONS OF RUBBER

Rubber is a representative of solids which is distinctly different from metals. No other solids can be made to undergo a large reversible elastic deformation by applying a comparatively small force. It is hard to say who was the discoverer of this fact. For simplicity we will confine ourselves mainly to the discussion of the best-known of these deformations, namely, the stretching of a rubber band (ring or filament).

Rubber is generally a plastoelastic solid, i.e., its strain is only partly pure elastic and partly plastic. The degree of plasticity of rubber depends largely upon its composition and treatment. Raw rubber shows this much more than vulcanized rubber. In the following, for the sake of simplicity, we will consider mainly elastic deformations. How to avoid plasticity, or better, how to suppress it, we will describe in section 11 dealing with the experimental technique of obtaining stress-strain curves.

The result of a stress-strain experiment is usually plotted in the so-called stress-strain diagram. It is instructive to compare the behavior of rubber with that of an elastically normal substance like a metal. Fig. 1 shows a typical form of a stress-strain curve for a rubber-sulfur vulcanizate together with a stress-strain curve for a metal. The curve for rubber was obtained at Notre Dame. The dotted line is a magnification for a metal curve, which facilitates its comparison with the rubber. A glance at these curves shows the uniqueness of the stress-strain behavior of rubber in contrast to that of an elastically normal material. Noteworthy features of it are: (1) the tremendous difference in extensibility. Therefore, Young's modulus has for rubber and only for rubber a very concrete sense: The doubling of the length of a piece of unit cross section can be realized. (2) Whereas, the metal has a breaking elongation of 30 percent or 40 percent, that of rubber is around 1000 percent. (3) Nevertheless, the tensile strength of rubber is of the same order of magnitude as that of a copper wire or of cellulose, for instance. Cf. Table I. (4) Rubber does not obey Hooke's law as do elastically normal substances, but it obeys that law for small extensions—5 percent to 20 percent. (5) Rubber does

TABLE I. *Tensile strength of different materials in kg/mm².*

Steel hardened	up to 170
Copper wire	up to 40
Wood	8–15
Silk	35
Cotton	28
Irish flax	over 100
Viscose, normal	25
Viscose, oriented	up to 80
Rubber, normal	15–20
Rubber, oriented	up to 60

not show a yield point after its plastic flow begins but rather shows the converse phenomenon of a "not yield" point at which its resistance increases. Note the S-shape of the curve. While the reality of this shape is much discussed[3] its appearance under definite conditions seems to be certain. It is plausible to consider it as an indication of at least three mechanisms acting to cause the retraction of rubber; (*a*) in the Hookian (straight line) part, probably a mechanism like that for elastically normal substances (*b*) in the middle, a mechanism peculiar to rubber, (*c*) at the end (almost straight line again) a mechanism combining (*a*) and (*b*). Other phenomena point in a more direct manner to this "trisection," more definitely than the indications here.

The stress-strain relation for rubber was first studied by Villari.[4] From his data the typical rubber stress-strain curve shown in Fig. 2 is obtained.

Let F be the actual force; l the actual length; σ, the actual cross section; l_0 the original unstretched length; σ_0, the original unstretched cross section.

$Z=F/\sigma_0=$ stress referred to the original cross section;
$\zeta=F/\sigma=$ stress referred to the actual cross section;
$L=l/l_0=$ relative length.

The relationship given by the stress-strain curve:

$$Z=Z(L) \qquad (1,1)$$

or

$$\zeta=\zeta(L)$$

represents an isotherm, i.e., an equation of state for rubber of a definite temperature similar to the isotherm of a gas or a fluid:

$$p=p(V)$$

where p denotes the pressure and V the volume.

The modulus of elasticity (Young's modulus) can be defined as:

$$E_1=\frac{dZ}{dL}=\frac{l_0}{\sigma_0}\cdot\frac{dF}{dL} \quad \text{or} \quad E_2=\frac{d\zeta}{dL}=\frac{l}{\sigma}\frac{dF}{dL}. \qquad (1,2)$$

Thus we are led to Hooke's law for a straight line stress-strain curve.

Villari, using the second definition, concluded that rubber, different from all other known bodies, has three elastic coefficients: The first or smallest, approximately constant; the third or largest approximately constant; and a middle or variable one which increases quickly and connects the first and third. Bouasse,[5] in the most accurate work hitherto done on the modulus, finds results which are like those of the much more primitive work of Villari. Bouasse, however, denies the possibility of a *unique* determination of the modulus.

As a second example of a stress-strain curve, one is reproduced for raw rubber prepared by evaporating latex poured on gelatine as given by Ornstein and collaborators[6] (cf. Fig. 3). The dependency of the modulus E upon the stress Z obtained from Fig. 3 by differentiation is shown in Fig. 4. More examples of stress-strain curves are given in Section 11, dealing with the technique of obtaining stress-strain curves, and in Section 3, dealing with the temperature dependency of stress and strain.

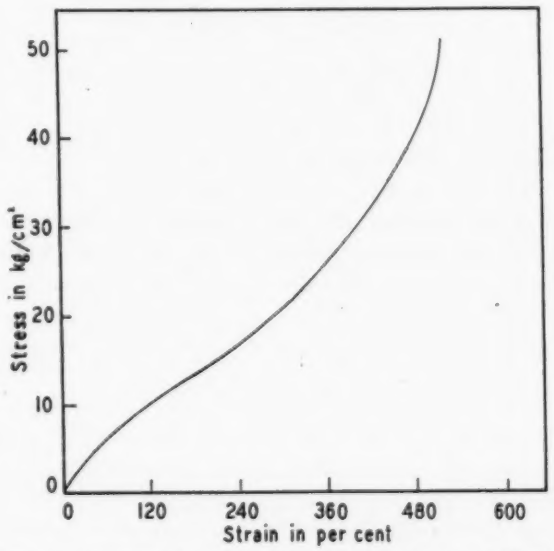

FIG. 2. Stress-strain curve according to data of Villari.[4] Material: Rubber cord.

Not much can be concluded from stress-strain data at a constant temperature alone. The introduction of a modulus is merely a matter of the definition and has physical significance only in connection with the elasticity theory of non-linear deformations.

2. POISSON'S RATIO

For gases and fluids one equation of state alone is sufficient for a characterization of state. The

simplest types of solids—the isotropic solids—can, however, be characterized only by two relationships: For small deformations, through two constants of the material (which depend, of

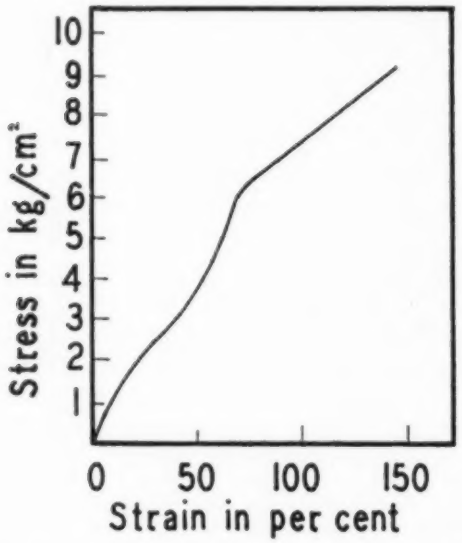

FIG. 3. Stress-strain curve for raw rubber according to Ornstein, Eymers and Wouda.[5]

course, on the temperature and the deformation). With increasing strain a change of the cross section of the sample takes place, and for finite deformations we have for the change of the cross section a relationship similar to equation (1, 2):

$$d\mu = -\frac{dB/B}{dL/L}, \qquad (2, 1)$$

where B = lateral dimension of the sample. Obviously if $\mu = 0.5$, there is no change in volume and the substance is incompressible. Such is the case for fluids. Poisson's ratio was first investigated by Wertheim.[7] However, the first exact determinations using the definition (2, 1) were carried out by Roentgen[8] and by G. F. Becker.[9] They found for μ a value around 0.5 which was confirmed by later investigators; probably the most accurate being the values given by Holt and McPherson.[10] According to these authors, Poisson's ratio is precisely 0.5 at low elongations where there is no change in volume on stretching and is slightly greater than 0.5 at elongations over 400 percent, where the volume decreases on stretching. This was found with a pure gum compound (that is, a compound which does not contain fillers like whiting or reinforcing agents like carbon black). For the same kind of raw rubber for which the stress-strain curves were given above, Ornstein and collaborators find a considerable decrease in μ with elongation until finally a value which tends to remain constant is reached (cf. Fig. 5).

From considerations of the crystallization of rubber one could expect that for high elongations μ will tend to assume a value between 0.25 and 0.5 as is the case for substances which show normal elasticity. It may be, however, that there is a difference between Poisson's ratio obtained from a curve which gives a continuous elongation, and a value which one gets when one first stretches rubber to a certain elongation and lets it stay there for a time before measuring Poisson's ratio for an infinitesimal elongation using the stretched state as the initial state. The same applies, of course, to Young's modulus. Unfortunately, no investigations have yet been made on that point. However, it is interesting to note that Roentgen remarked, "It seems to me probable that the high value of μ for only slightly extended rods—as a consequence of the possibility of the easy displacement of the particles

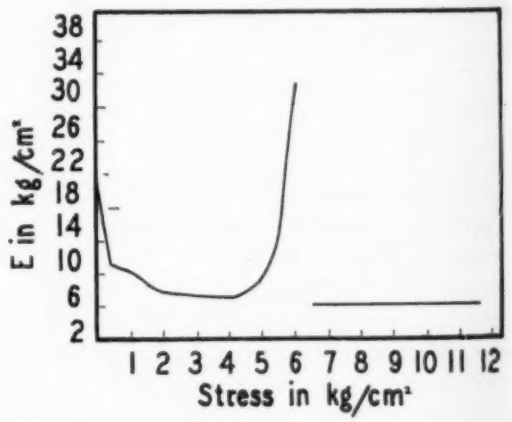

FIG. 4. Elasticity modulus: $E = dZ/d(l - l_0/l_0)$ *vs.* stress, derived by differentiation from stress-strain curve in Fig. 3.

(constituents of rubber)—will decrease with increasing extension, and that finally at very high extensions where the modulus is known to increase strongly, μ also will approach the value for more rigid bodies."

3. The Thermoelastic Behavior of Rubber

(A) *Heat development with adiabatic stress*

The most outstanding characteristic of rubber is undoubtedly its reversible long-range extensibility. Its next most characteristic property, however, is its anomalous thermoelastic behavior. Whereas, elastically normal substances, like copper, steel, wood, show a cooling effect, when stretched adiabatically (i.e., rather fast) rubber exhibits not only the opposite behavior, i.e., shows a heat development, but this heat effect is very much larger than that of copper, etc. In fact, this heat effect can be observed in a sensory manner, stretching a rubber band quickly and applying it to the lip. It was in this way that Gough[11] found the effect in 1805 which was rediscovered by Page and Joule[12] independently. Gough found, also, the converse phenomenon: Stretched rubber contracts when heated.

William Thomson[13] showed that this behavior follows from a combination of the first and second laws of thermodynamics, whose correct formulation and extension was largely his own work. Joule, unaware of Gough's work, verified Thomson's conjecture. Thomson also gave a quantitative formula, relating the temperature change at adiabatic stretching with other thermal quantities like the specific heat at a constant length, thermal expansion coefficient, etc.* In a remark-

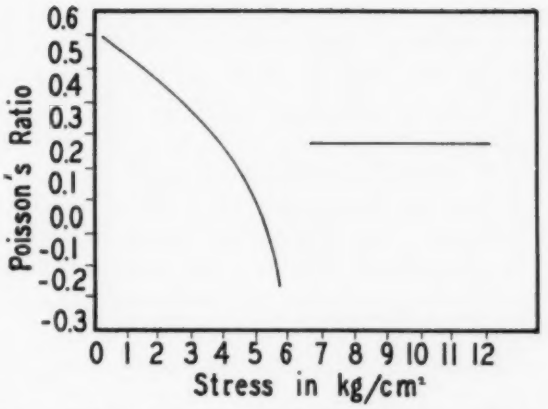

FIG. 5. Poisson's ratio: $\mu = -(dB/B)/(dl/l)$ *vs.* stress for raw rubber.[5]

* Thomson's formula:

$$H = \frac{t}{J} \times \frac{P}{1} \times \frac{e}{1} \times \frac{1}{S} \times \frac{1}{W}.$$

H = temperature change °C; t = temperature °K; J = mech. equiv. of heat; P = pressure applied in pounds; e = longitudinal expansion per degree C; S = specific heat; W = weight in pounds of a foot length of the bar.

TABLE II. *Joule's comparison of experiment and theory for temperature change when rubber is stretched adiabatically.*

Weight in pounds		$\frac{t}{J}$	P	e	$\frac{1}{S}$*	$\frac{1}{W}$	H theor.	H exp.	H exp. corrected
Permanent	Temporary								
0	7	$\frac{281}{1390}$	−7	$\frac{1}{+9009}$	$\frac{1}{0.415}$	$\frac{1}{0.1917}$	−0.002	−0.004	−0.004
7	14	"	"	$\frac{1}{-5003}$	"	$\frac{1}{0.1759}$	+0.004	+0.003	+0.003
14	21	"	"	$\frac{1}{-2435}$	"	$\frac{1}{0.1576}$	+0.009	+0.015	+0.016
21	28	"	"	$\frac{1}{-1360}$	"	$\frac{1}{0.1383}$	+0.018	+0.039	+0.043
28	35	"	"	$\frac{1}{-814}$	"	$\frac{1}{0.1194}$	+0.035	+0.042	+0.047
35	42	"	"	$\frac{1}{-656}$	"	$\frac{1}{0.1031}$	+0.050	+0.042	+0.050
0	42						+0.114	+0.137	+0.155

* Joule takes the same S value for all elongations.

able paper, Joule verified Thomson's relation as well as could be done with his relatively primitive tools (cf. Table II). Joule's work showed that the change in temperature ΔT is negative for small elongations, but goes through zero to positive values for larger elongations.

We can conclude again that rubber behaves with regard to its thermoelasticity normally for small elongations, but exhibits an anomalous behavior for large ones. This behavior was indicated, but in a less direct manner, through the stress-strain curves of rubber at a constant temperature.

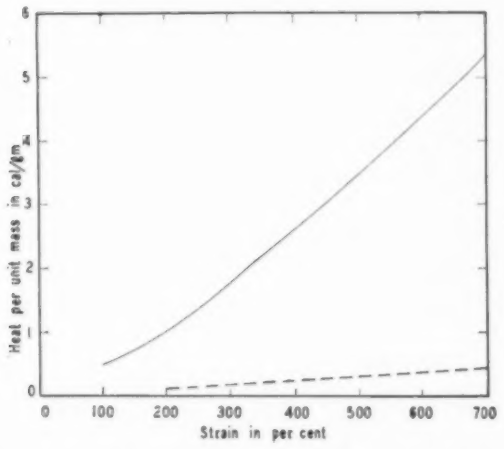

FIG. 6. Gough effect (heat developed during stretching) of raw rubber according to Hock and Bostroem.[16] Full curve: heat effect; dotted curve: mechanical work input.

Joule remarked also, that raw rubber, due to its plasticity, is not suitable for thermodynamic work and made use of vulcanized rubber. (The vulcanization of rubber was discovered in 1839 by Charles Goodyear (U. S. Patent 3,633 (1844).) The only investigation in which all the quantities occurring in Thomson's formula (cf. Table II) were measured directly, was carried through by Ornstein and collaborators[13] (cf. Section 5).

More light was thrown on the nature of the sensory heat effect through the work of Hock[14] and Katz.[15] Hock showed in 1924 that stretched raw rubber, when cooled down to the temperature of liquid air, and then struck with a hammer, shatters into fibrous fragments. Katz demonstrated in 1925 that stretched rubber gives a crystal pattern. He interpreted the heat evolved with adiabatic stress as a heat of crystallization, and Hock and Bostroem[16] then made a determination of the amount of heat evolved. They measured (using a calorimeter) the change of the heat content of raw rubber when it passes from the crystalline to the "liquid" phase. They observed a linear increase of the heat with elongation (cf. Fig. 6). For comparison the work done during the stretching as a function of elongation is plotted (dotted line).

The rather large heat effect observed by Hock cannot be related to the small effect reported by Joule. The latter is the analog of the minute effect observed for "normal" materials. The material was also different, in that raw rubber instead of vulcanized rubber was used. It is very hard to distinguish between these heats because the phase change mentioned is generally a rather unsharp one and the heat development begins long before a complete crystallization takes place. However, a separation of these effects will be attempted from the relation between stress and temperature by means of thermodynamics. For clarity we shall call the observed heat development due to crystallization the Gough effect and the much smaller heat effect mentioned above the Joule effect.

A direct measurement of the heat exchange when rubber was stretched in a calorimeter filled with mercury was begun under the author's direction. Preliminary results indicate, for a so-called latex vulcanizate containing two percent sulfur, the behavior shown in Fig. 7. We notice a small heat development, slowly increasing for smaller elongations, rising steeply,

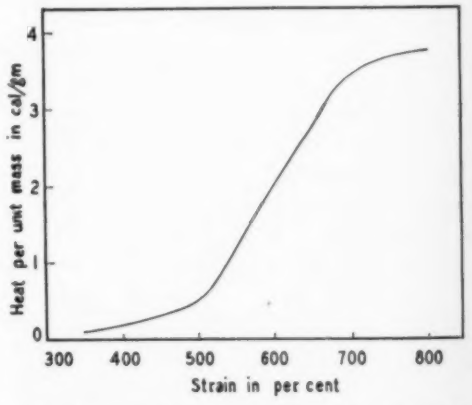

FIG. 7. Gough effect (heat developed during stretching) of vulcanized rubber.

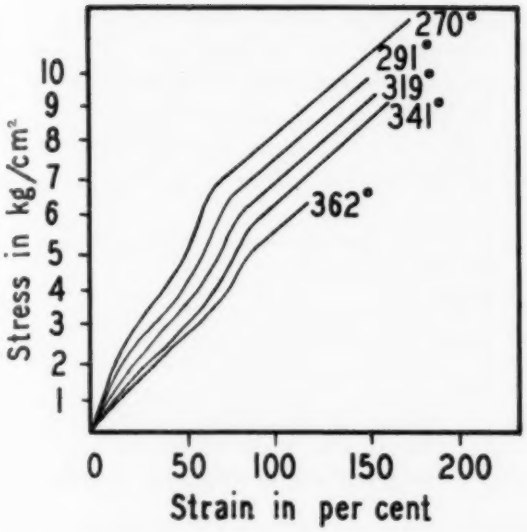

FIG. 8a. Stress-strain curves for raw rubber at various temperatures[6] (degrees Kelvin).

and then finally slowing down again. The first part is probably due to the heat development which is directly connected with the work done in stretching and corresponds to a continuation of the heat effect observed by Joule, to still higher elongations. The steep part is due to crystallization, and the decrease in slope due to the completion of the crystallization. Unfortunately, there are not very many investigations of these heat effects especially for large extensions.

(*B*) *Thermal expansion coefficient*

Another anomalous property of rubber which was exhibited by the work of Joule (cf. Table II), Lundal and others is the dependency of the linear thermal expansion coefficient upon stress. For small extension it is positive as for elastically normal bodies, and at stresses of the same order of magnitude for which a positive heat is developed, the coefficient becomes negative.

It is interesting to note that the coefficient of cubical expansion of rubber is also anomalous in that it is greater than that of almost any other solid body. This can be demonstrated in the following ways: Take a piece of rubber of a density a little above that of boiling water, throw it into the water and it sinks. However, in a short time the heat has expanded it sufficiently to bring it up to the surface. Again, take a piece of rubber which is lighter than cold water,

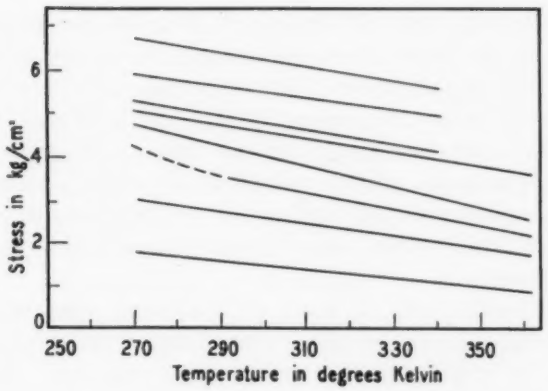

FIG. 8b. Effect of temperature upon stress at various elongations. This curve is derived from Fig. 8a.

weight it with pieces of iron to cause it to sink, then heat the water and the rubber rises to the surface as the temperature increases.

Despite its large value, the coefficient of cubical expansion of rubber is normal in that its value is the same under constant stress and under constant strain. One has to conclude from this fact that stretched rubber has a negative thermal expansion coefficient in the direction of the stress and a positive one perpendicular to that direction. That is really what observation shows. At the same time these facts exhibit the anisotropy of stretched rubber. This anisotropy manifests itself in the following ways: (*a*) strain double refraction, (*b*) dichromatism, (*c*) a kind of piezoelectricity, (*d*) different values for Poisson's ratio in different directions, (*e*) in the x-ray diagrams of stretched rubber, (*f*) in the fibrous structure of stretched rubber when frozen at temperatures of liquid air, and (*g*) in the semi-fibrous structure of stretched rubber as it appears in tear experiments.[17]

(*C*) *Equations of state*

Much controversy is contained in the older literature about the dependency of the stress-strain curves, i.e., the elasticity modulus, upon temperature. Some of the differences observed can be traced to the difference in the kind of rubber used; others to the technique applied, rate of extension, etc. Probably no one approached either the isothermal or the adiabatic case, but measured a polytrope lying between the isotherm and adiabate. In some instances some

plasticity too was measured because generally first extension curves were taken (cf. Section 11).

Summarizing the older and some of the newer experiments, we can state that the modulus of raw rubber appears to decrease with rising temperature. This is shown in Fig. 8, according to measurements of Ornstein and collaborators and was shown also through Hauser and collaborators.

Incidentally, it may be mentioned that raw rubber has a positive thermal expansion coefficient. We should expect, therefore, that for small elongations it would show a cooling effect. In reality, however, a heating effect is observed. This heating effect is partly caused by the plasticity of raw rubber which gives rise to a hysteresis loop and a permanent set, as Fig. 9 demonstrates. It is also probably caused in part by the starting of a crystallization phenomenon. In fact, Ornstein and collaborators demonstrated a sudden change in length at 70 percent elongation. They interpret this as a transition of the first kind and apply Clapeyron's equation to it. However, we wish to point out that the heating effect which one can derive from their data is

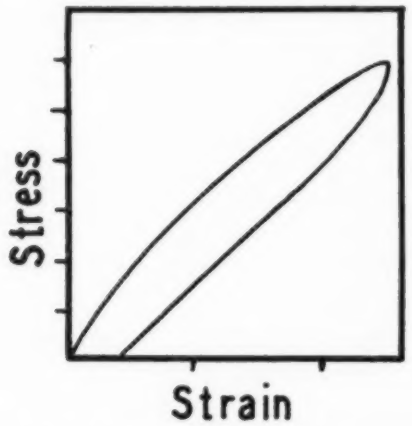

FIG. 9. Hysteresis loop for raw rubber.[6]

only 4×10^{-3} cal./gram. It has, therefore, nothing to do with the large heating effects about which we spoke at the beginning of this section and which one can observe only at much greater elongations (400 to 600 percent).

Slightly vulcanized samples show, at least for the first extension curves, qualitatively the same behavior as raw rubber. For greater elongations, however, there is practically no dependency upon temperature which makes it indicate the presence of two mechanisms, one which is like that for normal elastic substances, giving rise to a decrease of the modulus of elasticity with the temperature, and another which gives rise to the typical rubber elasticity and raises

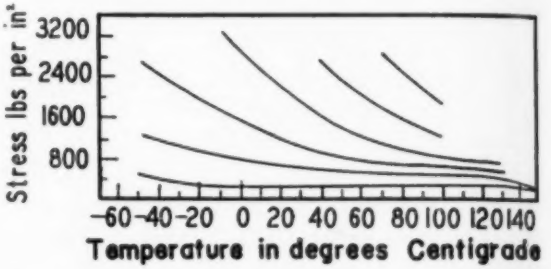

FIG. 10. Effect of temperature upon stress for rubber (vulcanized with 1.91 percent sulfur for 35 minutes at 125°C) at elongations from 300 (lowest curve) to 900 (highest curve) percent according to Tener, Kingsbury and Holt.[18]

the modulus with increasing temperature (cf. Fig. 10 according to Kingsbury, Tener and Holt.[18]) The same general behavior was also found by Somerville and collaborators[19] and Bouasse[4] who probably observed a polytrope or adiabate. The same was found for two types of rubber bands by Wiegand and Snyder.[20] Only two temperatures were considered in this work and more emphasis was placed on the dependency upon elongation. We will discuss this work in Section 5.

For vulcanizates containing more sulfur one gets a decrease for small elongations. For higher elongations, however, an increase of the modulus

TABLE III. *Effect of temperature on modulus of elasticity by oscillation method, according to Gerke*[21] *(material: "inner tube stock of high rubber content"; load: constant).*

Temperature °C	Distance Between Marks (Originally 2.50 cm Apart)				
	cm	cm	cm	cm	cm
36	7.7		8.0		8.0
10		8.3		8.3	

with rising temperature is obtained. It must be mentioned that when distinguishing between vulcanized samples containing less or more sulfur reference is made only to a definite time of vulcanization, use of same ingredients, etc. Exceptions are, therefore, likely. Furthermore,

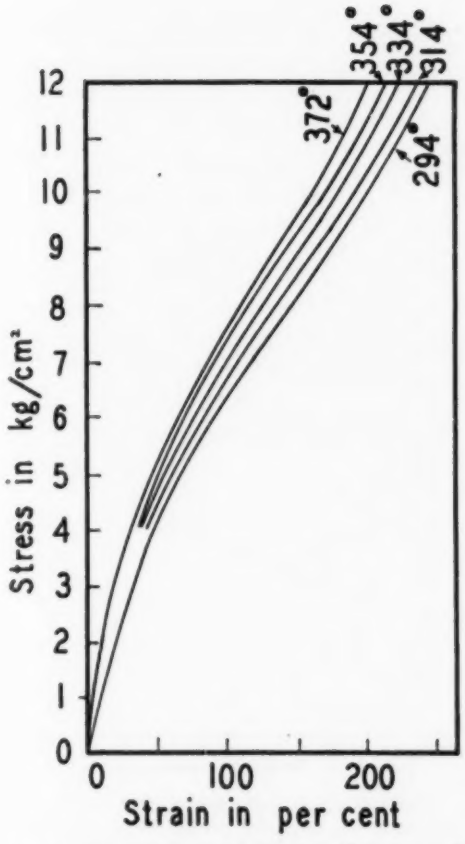

FIG. 11. Isotherms for vulcanized rubber according to Ornstein *et al.*[13]

some samples which show a decrease of modulus with temperature, if the first extension curve is taken according to the usual test technique, show an increase of the modulus with temperature, if certain techniques for reaching an equilibrium value for the stress are applied. An example given by Gerke[21] illustrates this statement (cf. Table III, about the technique applied; cf. Section 11).

With these reservations we are going to describe some more recent results in which composition of the samples and, also to a certain extent the technique is given in detail so that a reproduction of the results can be attempted.

Ornstein and collaborators[13] used a vulcanizate containing 100 parts of rubber, 3 parts of zinc oxide, 5 parts of sulfur and one of diphenylguanidine which was vulcanized for 30 minutes at 147°C. In the description of the work it is not clear whether or not purely elastic isotherms were obtained. From the stress-strain curves given in Fig. 11, we can derive a set of curves showing the stress as a function of the temperature at a constant length. We see that the stress appears as a linear function of the temperature (Fig. 12). Furthermore, we see that the inclination of the curves, which represents the temperature coefficient of stress, and which is dependent upon the temperature, rises with increasing elongation. Ornstein and collaborators themselves did not plot these curves and, therefore, overlooked the proportionality with absolute temperature. No doubt some of the older curves show also a linear behavior in a limited range of extension.

Direct measurement of the dependency of the stress upon temperature at a constant elongation by means of a Polanyi dynamometer was made by Meyer and Ferri.[22] They observed, for a sample of the same composition as used by Ornstein, the behavior shown in Fig. 13. The hysteresis loop they ascribe to crystallization effects. Over the whole range of extensions the stress is a linear function of temperature, the coefficient of the stress being first negative, as for bodies showing normal thermoelasticity, then zero, and finally, positive with increasing elongation. These curves do not give directly the thermal equation of state of rubber because in the method used the thermal expansion changes the length and, therefore, the stress also has to be corrected for.

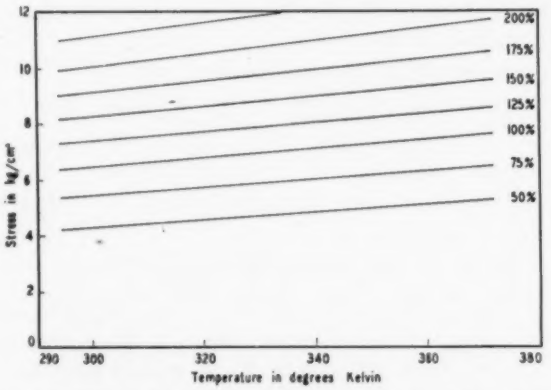

FIG. 12. Effect of temperature upon stress at various elongation derived from isotherms of Fig. 11.

Meyer and Ferri also used another vulcanizate with 8 percent sulfur vulcanized 90 minutes at 208°F. The dependency of stress upon temperature is shown in the curves in Fig. 15. Correcting

for the heat expansion in a more indirect way, Meyer and Ferri conclude that the stress at about 350 percent elongation is directly proportional to the absolute temperature.

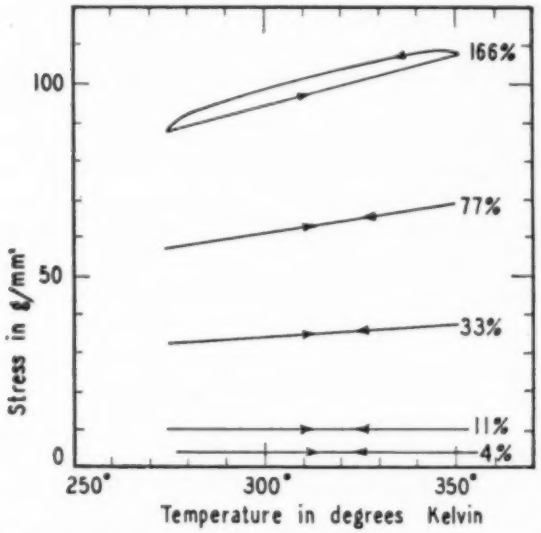

FIG. 13. Effect of temperature upon stress at various elongations for vulcanized rubber according to Meyer and Ferri.[21] Composition of rubber the same as that used by Ornstein *et al.*[12]

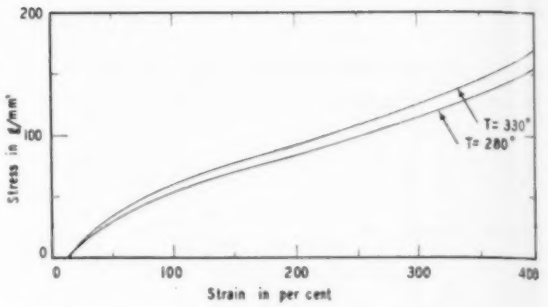

FIG. 14. Isotherms of rubber (vulcanized with 8 percent sulfur for 180 minutes at 420°K).[22]

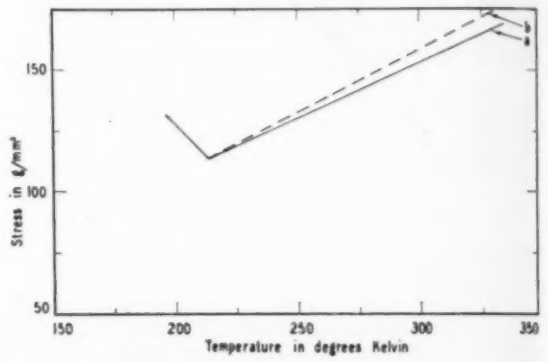

FIG. 15. Effect of temperature upon stress for 350 percent elongation for the same rubber as in Fig. 14. (a) uncorrected, (b) corrected for heat expansion.[22]

The method of correction used by Meyer and Ferri seems to contradict the data on temperature dependency which one obtains from their own stress-strain curves shown in Fig. 14.

The curves in Fig. 15 exhibit directly the two mechanisms which cause the retraction of stretched rubber.

The equation of state in the form $L = L(T, F)$, i.e., working at constant force (load) was investigated by Milton L. Braun.[23] Braun used a rubber sample containing $7\frac{1}{2}$ percent sulfur, i.e., of almost the same composition as that of sample 1 of Meyer and Ferri. In spite of this, a totally different but simple behavior was obtained: the length at constant force turned out to be a linear function of the temperature.

BIBLIOGRAPHY

1. Cf. W. F. Busse, J. App. Phys. **9**, 438 (1938).
2. *Intramolecular Statistics:* E. Guth and H. Mark, Monatsh. **65**, 93 (1934); Wien. Anz. (April, 1935); Naturwiss. **25**, 353 (1937); E. Guth, Kautschuk **13**, 201 (1937); cf. also W. Kuhn, Kolloid Zeits. **68**, 2 (1934) and forthcoming publications.
   Intermolecular Statistics: E. Guth, paper at the Detroit meeting Rubber Div. Am. Chem. Soc. (April, 1938); Bull. Am. Phys. Soc. Washington meeting, Christmas, 1938, and forthcoming publications.
3. Cf. I. Williams, Ind. Eng. Chem. **21**, 872 (1929); C. W. Shacklock, Trans. Inst. Rubber Ind. **8**, 568 (1933).
4. E. Villari, Cimento, **28**, 332, 361 (1869); Ann. d. Phys. **143**, 88, 290 (1871).
5. H. Bouasse, Annales de la Faculté des Sciences de Toulouse **6**, 177 (1904).
6. L. S. Ornstein, J. G. Eymers and J. Wouda, Proc. Acad. Amsterdam **32**, 1235 (1929).
7. G. Wertheim, Ann. de chim. phys. **23**, 52 (1848).
8. W. C. Roentgen, Ann. d. Phys. **159**, 601 (1876).
9. W. L. Holt and A. T. McPherson, Nat. Bur. Stand. J. Research **17**, 657 (1936).
10. J. Gough, Manchester Phil. Mem. **1**, 288 (1805); Nicholson's J. **13**, 305 (1806).

11. J. P. Joule, Phil. Mag. **14**, 226 (1857); Scient. paper I, p. 405; Phil. Trans. Roy. Soc. **149**, 91 (1859); Scient. paper I, p. 413.
12. W. Thomson (Lord Kelvin). Quarterly J. Math., April (1855); Math. and Phys. Papers, Vol. I, p. 291, pp. 309–310.
13. L. S. Ornstein, J. Wouda and J. G. Eymers, Proc. Acad. Amsterdam **33**, 273 (1930).
14. L. Hock, Kolloid Zeits. **35**, 40 (1924).
15. J. R. Katz, Naturwiss. **13**, 410 (1925); Kolloid Zeits. **36**, 300; **37**, 19 (1925).
16. S. Bostroem, Rubber Chem. and Tech. **2**, 259 (1929).
17. W. F. Busse, Ind. Eng. Chem. **26**, 1194 (1934).
18. R. F. Tener, S. S. Kingsbury and W. L. Holt, Nat. Bur. Standards Tech. Papers **22**, 367 (1927–28).
19. A. A. Somerville and W. H. Cope, Trans. Inst. Rubber Ind. **4**, 263 (1928); A. A. Somerville and W. F. Russell, Ind. Eng. Chem. **25**, 1096 (1933). Cf. also J. C. Shedd and R. L. Ingersol, Phys. Rev. **19**, 107 (1904); A. van Rossem and H. van der Meijden, Kolloid Zeits. **39**, 69 (1926).
20. W. B. Wiegand and H. Snyder, Trans. Inst. Rubber Ind. **10**, 234 (1934).
21. R. H. Gerke, Ind. Eng. Chem. **22**, 73 (1930).
22. K. H. Meyer and C. Ferri, Helv. chim. Acta **18**, 570 (1935).
23. M. L. Braun, J. App. Phys. **8**, 138 (1937).

No attempt was made to cover the whole literature. For further references cf. G. S. Whitby, *Plantation Rubber and Testing of Rubber* (London, 1920); T. R. Dawson and B. D. Porritt, *Rubber, Physical and Chemical Properties* (London, 1935); *The Chemistry and Technology of Rubber*, edited by C. C. Davis and J. T. Blake, Am. Chem. Soc. Monograph Series (New York, 1937).

. . . Since the time of Roger Bacon, the scientist has forged every sentence in the book of exploration "in the teeth of irreducible and stubborn facts." He has persuaded the world to adopt the same method in all departments of knowledge, no matter whether related to science or not. The historian, the sociologist, the psychologist, the theologian wrestle with stubborn and irreducible facts because the scientist has shown in his field of work that they must be faced and accounted for. There has grown up an attitude of intellectual honesty which has had a cathartic value in clearing away the unrealities which had worked themselves into the rationalism of the pre-Renaissance period.

Further, there has developed under the hand of the scientist a technique of obtaining the pertinent facts. Facts do not come of themselves. They must be sought for under controlled conditions, or under conditions which, if not controllable, are fully understood. The experimental sciences have provided the means wherewith to ascertain facts under controlled conditions. They have had their special sphere in the physical realm; but the biologist has used the experiment with amazing success in the less easily controllable field in which he operates. In the sciences which deal with man, and in social studies of all kinds, the experiment is less readily applicable, and the student is forced back on the study of the conditions under which the data accumulate. These conditions may be unplanned, but they must be known. The scientist has shown how to disentangle the significant conditions from the adventitious. He has placed facts in their setting in the flow of events.

—R. C. WALLACE, "The Changing Values of Science"
Science, September 23, 1938

The Operational Calculus. I

By Louis A. Pipes*

Electrical Engineering Department, The University of Wisconsin, Madison, Wisconsin

Physicists have long been interested and sometimes mystified by the methods of the Heaviside operational calculus. In this paper Professor Louis A. Pipes of the University of Wisconsin presents a clear and logical exposition of the modern points of view in use in this theory. It is hoped that this survey will prove useful not only to those who are interested in the Heaviside theory but also to those who would like to know what it is all about. Further installments of this paper will appear in forthcoming issues. They will include applications to linear lumped electrical networks, mechanical vibrations, wave filters, vibrating strings, transmission lines, heat conduction and electric circuit theory. A fine working bibliography will be included.—Editor.

I. Introduction

A. Purpose and General Plan

IT is the purpose of this discussion to present a unified account of the mathematical methods which are known under the name of "Heaviside's Operational Calculus." An attempt will be made to present the subject from the point of view of the modern development based on the Laplacian transformation. This modern treatment is more unified and general than the body of rules which are conventionally known as the "Heaviside Calculus." The modern Laplacian transformation point of view has placed the entire theory on a rigorous foundation and has removed the looseness which sometimes has led to erroneous conclusions in the past.

The Laplacian transformation development makes full use of the notion of contour integration and the theory of functions. Reference to standard texts on the theory of functions will be made for the necessary theorems.

B. Definition and Historical Background of Operational Methods

A rather comprehensive definition of an operator in mathematics is the following one:

"An operator is a symbol placed before a function to indicate the application of some process to the function to produce a new function."

In an operational analysis, the operators are divorced from the functions to which they apply and are manipulated as independent quantities in accordance to the various laws of algebra which they satisfy.

Under this definition of "Operational Analysis," the subject has a most extensive history. A most excellent and comprehensive account of the history of operational methods is given in two recent books.[A1, 2]

The reader interested in the historical phase and development of the subject is referred to these works. The historical development may be summarized briefly by stating that it can be divided into the following four main divisions.

1. The formal theory of operators.—This phase begins with the observation of G. W. Leibnitz (1646–1716) in which he noticed certain striking analogies between algebraic laws and the behavior of differential and integral operators. The work was further carried on by J. Lagrange (1736–1813) and his successors.

The formal theory of operators concerned itself with the following three problems: *a.* The interpretation of the formal inverses of well-known operators. *b.* Interpretation of symbolic products. *c.* The factorization of operators.

2. The second period.—This period was marked by the development of operational processes to the following fields: *a.* The theory of finite differences. *b.* The symbolic methods of fractional differentiation. *c.* The use of symbolic methods

* Now at Harvard University, Graduate School of Engineering, Pierce Hall, Cambridge, Massachusetts.

in the calculus of finite differences and differential equations.

The leaders during this period were: P. S. Laplace (1749–1827), George Boole (1815–1864), R. Murphy (1806–1843), R. Carmichael (1828–1861). Books embodying the theory were published by George Boole and Robert Carmichael and most of the theorems presented had their modern shape.

3. The Heaviside period.—This movement of the theory was initiated through the work of Oliver Heaviside (1850–1925). The first problem attacked by Heaviside was the solution of the system of integro-differential equations which express the behavior of a lumped electrical network subject to certain initial boundary conditions. The system of equations handled by Heaviside had been attacked by classical methods of great power before the time of Heaviside. As early as 1788 in the *Mécanique Analytique* of Lagrange[43] a method for the solution of the system of equations had been presented. The novel feature of the Heaviside treatment consists of the two innovations:

a. The functions $E_i(t)$ representing the known electromotive forces applied to the systems were considered by Heaviside to be of an impulsive type and equal to zero for negative values of the time parameter, t, and suddenly jumping to finite values for positive values of t. This type of function represented very well the actual physical system and enabled Heaviside to introduce several novel methods of treatment.

b. The formulation of a process by which a problem of this kind was solved by a single operational procedure which gave the solution of the problem subject to the initial conditions directly and without the usual laborious classical procedure of evaluating arbitrary constants.

Heaviside himself used heuristic reasoning and either was not aware of existing earlier work or at least makes no mention of it. Many electrical engineers hastened to explain certain of Heaviside's rules. Many papers of this explanatory character appeared during the period 1910–1925. Prominent workers of this period were John R. Carson, Louis Cohen, E. J. Berg, H. W. March, V. Bush, W. O. Pennell, and J. J. Smith.

4. The rigorous period.—In the last decade, mathematicians have entered the field in an attempt to clarify and put on a rigorous foundation the methods of Heaviside and his interpreters. Prominent workers are Bromwich, Jeffries, Paul Levy, Murnaghan, Wiener, Bateman, Carslaw, Davis, and many others.

Essentially four methods have been used in discussing the Heaviside Calculus. They are: *a.* Direct use of formal operators. *b.* Complex line integrals. *c.* The Laplacian transformati on. *d.* The Fourier integral.

In the development of the subject to be presented in this article, the method of the Laplacian transformation will be used because it appears to be the most general and natural method of approach.

C. Utility of Operational Processes in Engineering and Physics

The questions which naturally might arise in the mind of the reader are the following: *a.* What types of problems may be solved by the operational method? *b.* What advantages does this method possess that are not present in the older classical methods of approach?

The first question may be answered by stating that the operational method will solve the following problems:

1. Physical problems characterized by linear differential or integro-differential equations with constant coefficients or by systems of such equations subject to one-point boundary conditions. Problems leading to the solution of such equations are encountered in electrical circuit theory, mechanical vibrations, sound, etc.

2. Physical problems characterized by a linear partial differential equation with constant coefficients or a set of such equations involving a one-point boundary condition in one independent variable. Examples of this are found in problems of heat conduction, electrical transmission, sound, radiation, etc.

3. Evaluation of certain definite integrals.

4. The solution of integral equations of a certain type. Certain integral equations arising in mechanics and other branches of physics may be evaluated operationally.

5. The solution of certain difference equations may be effected operationally. These equations

arise in mechanical and electrical problems containing recurring elements.

The answer to the second question is that in many cases the operational methods are most direct. In a large class of cases the operational method will give the answer in a page where ordinary methods take several pages. In many other cases, where the nature of the solution by classical methods is most difficult to interpret, the operational method gives the general trend of the solution most simply. In short, by the use of the operational method, many problems that present insurmountable difficulties may be quickly and effectively solved and hence such methods are of great utility to the physicist and the engineer.

II. The Laplacian Transformation

A. The Modern Development

The modern theory of the Heaviside operational calculus is almost universally based on the Laplacian transformation. This basis places the operational method on a rigorous plane and extends the generality of the type of problems which may be solved by operational methods. Accordingly, in this discussion, a treatment of the Laplacian transformation will be presented. Modern workers employing this point of view are van der Pol, Dalzell, Kouziomi, and others.

B. Development of the Laplacian Transformation

We will begin our discussion with the Fourier-Mellin theorem which can be formulated in the following manner:

Consider the real function $f(t)$ which possesses the following properties: 1. $f(t)$ and its first derivatives are piecewise continuous in each finite interval. 2. $f(t)=\frac{1}{2}[f(t+0)+f(t-0)]$ at a point of discontinuity. 3. $\int_{-\infty}^{\infty}|f(t)|\,\epsilon^{-ct}dt$ exists when $\alpha_1<c<\alpha_2$.

Then $f(t)$ may be represented by the complex integral

$$f(t)=\frac{1}{2\pi i}\int_{c-i\infty}^{c+i\infty}\frac{F(p)e^{pt}dp}{p}, \qquad (1)$$

where $$F(p)=p\int_{-\infty}^{\infty}f(t)e^{-pt}dt. \qquad (2)$$

In (1) we assume the path of integration to be a straight line parallel to the imaginary axis of the p plane. This line, however, can be arbitrarily removed within the domain,

$$\alpha_1<Re(p)<\alpha_2,$$

without changing the value of the integral; it may also be replaced by any curve in this band between the extremities $c\pm i\infty$ (see Fig. 1). (The reader unfamiliar with the development of this basic formula will find an excellent discussion in Courant and Hilbert.[B1])

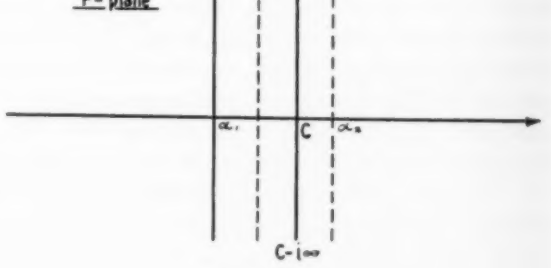

Fig. 1.

Without limiting the practical applicability of our methods we may assume that $f(t)=0$, when $t<0$. Accordingly, we may put the lower limit in (2) equal to zero. We may then write the above integral theorem in the form

$$f(t)=\frac{1}{2\pi i}\int_{c-i\infty}^{c+i\infty}\frac{F(p)e^{pt}dp}{p}, \qquad (3)$$

$$F(p)=p\int_{0}^{\infty}f(t)e^{-pt}dt. \qquad (4)$$

If a function $F(p)$ is related to a function $f(t)$ in the above manner, then the function $F(p)$ is called the direct Laplacian transform of $f(t)$, and $f(t)$ is the inverse Laplacian transform of $F(p)$.

To shorten the writing, we shall follow the notation of van der Pol, and express the above functional relation between $F(p)$ and $f(t)$ by the notation

$$F(p)\doteqdot f(t). \qquad (5)$$

C. The Fundamental Rules

Some very powerful and useful general theorems concerning operations on the transforms will now be established.

Theorem I.

If $g(p) \doteqdot h(t)$ then

$$\frac{d^n h(t)}{dt^n} \doteqdot p^n g - \sum_{k=0}^{n-1} h^{[k]}(0) p^{(n-k)}, \qquad (6)$$

where $h^{[k]}(0) = d^k h/dt^k$ at $t=0$.

This theorem is of great power in transforming and solving linear differential equations with constant coefficients

Proof:

Let $\Phi(p) \doteqdot d^n h/dt^n$

or $$\Phi(p) = p\int_0^\infty \epsilon^{-pt}\frac{d^n h}{dt^n}dt.$$

Integrating by parts, we obtain

$$p\int_0^\infty \epsilon^{-pt}\frac{d^n h}{dt^n}dt = p\epsilon^{-pt}\frac{d^{(n-1)}h}{dt^{(n-1)}}\Big]_0^\infty + p^2\int_0^\infty \epsilon^{-pt}\frac{d^{(n-1)}h}{dt^{(n-1)}}dt$$

$$= -ph^{[n-1]}(0) + p^2\int_0^\infty \epsilon^{-pt}\frac{d^{(n-1)}h}{dt^{(n-1)}}dt.$$

Repeating the procedure, we obtain

$$\frac{d^n h}{dt^n} \doteqdot p^n g - \sum_{k=0}^{n-1} h^{[k]}(0) p^{(n-k)},$$

where $h(t) \doteqdot g(p)$.

Theorem II.

If $g_1(p) \doteqdot h(t)$ and $g_2(p) \doteqdot \phi(t)$, where

$$h(t) = \int_{-\infty}^{t} \phi(u)du,$$

then

$$g_1(p) = g_2(p)/p + h(0). \qquad (7)$$

Proof:

$dh/dt = \phi(t) \doteqdot pg_1 - ph(0)$ by Theorem I. Hence

$$g_2(p) = pg_1 - ph(0)$$

or $$g_1(p) = g_2(p)/p + h(0).$$

This theorem is of great importance in transforming the integro-differential equations of circuit theory.

Theorem III.

If $g_1(p) \doteqdot h_1(t)$ and $g_2(p) \doteqdot h_2(t)$. Then

$$\frac{g_1(p)g_2(p)}{p} \doteqdot \int_0^t h_1(u)h_2(t-u)du \doteqdot \int_0^t h_2(u)h_1(t-u)du. \qquad (8a)$$

Proof:

Let us consider

$$h_3(t) \doteqdot g_1(p)g_2(p)/p.$$

Then by the Fourier-Mellin formula we have

$$h_3(t) = \frac{1}{2\pi i}\int_{c-i\infty}^{c+i\infty} \frac{g_1(p)g_2(p)dp}{p^2}. \qquad (3a)$$

However, by hypothesis

$$g_2(p) = p\int_0^\infty \epsilon^{-py}h_2(y)dy.$$

Therefore

$$h_3(t) = \frac{1}{2\pi i}\int_0^\infty h_2(y)dy\int_{c-i\infty}^{c+i\infty}\frac{g_1(p)}{p}\epsilon^{p(t-y)}dp$$

if we do not question the validity of reversing the order of integration. However,

$$\frac{1}{2\pi i}\int_{c-i\infty}^{c+i\infty}\frac{g_1(p)}{p}\epsilon^{p(t-y)}dp = h_1(t-y).$$

Hence $$h_3(t) = \int_0^t h_2(y)h_1(t-y)dy.$$

Now, by hypothesis, $h_1(t)=0$ if t is less than 0. Hence $h_1(t-y)=0$ if $y>t$. The infinite limit of integration may, consequently, be replaced by the limit t. Therefore,

$$h_3(t) = \int_0^t h_2(y)h_1(t-y)dy,$$

and by symmetry,

$$= \int_0^t h_1(y)h_2(t-y)dy.$$

Corollary to Theorem III.

By applying Theorem I letting

$$g(p) = \frac{g_1 g_2}{p} \doteqdot \int_0^t h_2(u)h_1(t-u)du$$

we obtain

$$pg(p) = g_1 g_2 \doteqdot \frac{d}{dt}\int_0^t h_1(t-u)h_2(u)du. \quad (8b)$$

Theorem IV.

If $g(p) \doteqdot h(t)$, then

$$\frac{p}{p+\alpha} g(p+\alpha) \doteqdot \epsilon^{-\alpha t}h(t). \quad (9)$$

Proof:

Let $\phi(p) \doteqdot \epsilon^{-\alpha t}h(t)$. Therefore,

$$\phi(p) = p\int_0^\infty \epsilon^{-pt}\epsilon^{-\alpha t}h(t)dt.$$

But

$$\phi(p) = p\int_0^\infty \epsilon^{-t(p+\alpha)}h(t)dt$$

and

$$(p/(p+\alpha))g(p+\alpha) = p\int_0^\infty \epsilon^{-t(p+\alpha)}h(t)dt.$$

Hence

$$(p/(p+\alpha))g(p+\alpha) \doteqdot \epsilon^{-\alpha t}h(t).$$

Theorem V.

If $g(p) \doteqdot h(t)$ then

$$\epsilon^{-kp}g(p) \doteqdot \begin{cases} 0 & t<k \\ h(t-k) & t>k \end{cases} \quad k>0. \quad (10)$$

Proof:

Let $\phi(t) \doteqdot \epsilon^{-kp}g(p)$.

Hence $$\phi(t) = \frac{1}{2\pi i}\int_{c-i\infty}^{c+i\infty} \frac{\epsilon^{pt}\epsilon^{-kp}g(p)dp}{p}.$$

Now

$$h(t) = \frac{1}{2\pi i}\int_{c-i\infty}^{c+i\infty} \frac{\epsilon^{pt}g(p)dp}{p}.$$

Therefore,

$$\phi(t) = h(t-k).$$

However, $h(t)=0$ if $t<0$. Hence $h(t-k)=0$ for $t<k$ and the theorem is proved.

Theorem VI.

If $g(p) \doteqdot h(t)$, then

$$\epsilon^{kp}g(p) \doteqdot h(t+k), \quad k>0, \quad (11)$$

provided $h(t)=0$ for $0<t<k$.

Proof:

Let

$$\phi(p) = p\int_0^\infty \epsilon^{-pt}h(t+k)dt.$$

Now let us make the change in variable, $t+k=y$. We then obtain:

$$\phi(p) = p\epsilon^{pk}\int_k^\infty \epsilon^{-py}h(y)dy,$$

$$\phi(p) = \epsilon^{pk}g(p) - p\epsilon^{pk}\int_0^k \epsilon^{-py}h(y)dy.$$

Now, if $h(y)=0$ for $0<y<k$, then

$$\phi(p) = \epsilon^{pk}g(p) \doteqdot h(t+k).$$

Other important theorems may be proved, but they will be deferred until they are required in the subsequent work.

D. Calculation of Direct Transforms

From our basic Eqs. (3) and (4) we have the relations that if, $g(p) \doteqdot h(t)$ then

$$h(t) = \frac{1}{2\pi i}\int_{c-i\infty}^{c+i\infty} \frac{g(p)e^{pt}dp}{p} \quad (3b)$$

or

$$g(p) = p\int_0^\infty h(t)e^{-pt}dt. \quad (4a)$$

Now if $h(t)$ is known, and the integral (4) can be computed, we may obtain the direct transform of $h(t)$. If, however, $g(p)$ is known, then the

inverse transform depends on the evaluation of the complex line integral. We shall defer the consideration of the complex line integral until later and compute some direct transforms.

1. Transformation of the "unit function."—Let us consider the function $h(t)=\begin{cases}1 & t>0\\ 0 & t<0\end{cases}$ and let such a function be denoted by $h(t)=l$. Then

$$g(p)=p\int_0^\infty e^{-pt}dt=p(-e^{-pt}/p)\rceil_0=1.$$

Hence $$l\doteqdot 1. \tag{12}$$

2. Transformation of integrals of the unit function.—From the result (12) $l\doteqdot 1$ and by the use of (7), Theorem II, we have that if, $g(p)\doteqdot h(t)$, then

$$\int_0^t ldt\doteqdot 1/p \quad \text{or} \quad t\doteqdot 1/p,$$

$$\int_0^t tdt\doteqdot 1/p^2 \quad \text{or} \quad t^2/2\doteqdot 1/p^2,$$

and, by repetition, we obtain the general formula

$$t^n/n!\doteqdot 1/p^n \tag{13}$$

valid for n a positive integer.

3. Fractional powers of p.—The integral $\int_0^\infty x^{n-1}e^{-x}dx$ converges and defines a function of n for positive values of n. This function is called the gamma-function and we have:

$$\Gamma(n)=\int_0^\infty x^{n-1}e^{-x}dx \text{ for } n \text{ greater than 0.} \tag{14}$$

Where, by direct evaluation, $\Gamma(1)=1$ and by an integration by parts, we can establish the recursion formula: $\Gamma(n+1)=n\Gamma(n)$. The integral, and the recursion formula taken together, define the gamma-function for all values of the argument n.

Now if we place $x=pt$, $dx=pdt$, we obtain

$$\Gamma(n)=p^n\int_0^\infty e^{-pt}t^{(n-1)}dt. \tag{15}$$

But by the basic Eq. (4) we have that if

$$g(p)=\int_0^\infty pe^{-pt}h(t)dt, \tag{4a}$$

then $g(p)\doteqdot h(t)$. Consequently, comparing the above integrals, we have

$$1/p^{(n-1)}\doteqdot t^{(n-1)}/\Gamma(n) \quad \text{for} \quad n>0. \tag{16}$$

If we now place $n-1=m$, then, for $m>-1$,

$$1/p^m\doteqdot t^m/\Gamma(m+1), \quad m>-1. \tag{17}$$

It will be shown in a later section that this formula also holds for any m except negative integers. We note that since $\Gamma(m+1)=m!$ when m is a positive integer, that the above transform reduces to that of the preceding section for such values of m. By the use of the above equation and a table of gamma-functions, the transforms of fractional powers of p may be computed readily.

As an example, since $\Gamma(1/2)=\sqrt{\pi}$, we infer that,

$$p^{(\frac{1}{2})}\doteqdot 1/(\pi t)^{\frac{1}{2}}, \text{ etc.} \tag{18}$$

E. List of Transforms

By the direct integration of the integral $g(p)=p\int_0^\infty e^{-pt}h(t)dt$ and the application of the basic theorems of Section II, *C*, many useful transforms may be obtained. These will be listed below for reference.

$$1/p^m\doteqdot t^m/\Gamma(m+1) \tag{19}$$

for all m's except negative integers,

$$1/p^n\doteqdot t^n/n! \tag{20}$$

for n, a positive integer,

$$1\doteqdot 1, \quad \text{where} \quad 1=\begin{cases}1 & t>0\\ 0 & t<0\end{cases}, \tag{21}$$

$$\frac{1}{p^{n-\frac{1}{2}}}\doteqdot\frac{(2t)^n}{1\cdot 3\cdot 5\cdots(2n-1)}\frac{1}{(\pi t)^{\frac{1}{2}}} \tag{22}$$

for n, a positive integer,

$$p/(p+\alpha)\doteqdot\epsilon^{-\alpha t} \tag{23}$$

α real or complex,

$$1/(p+\alpha)\doteqdot(1/\alpha)(1-\epsilon^{-\alpha t}), \tag{24}$$

$$\frac{1}{p(p+\alpha)}\doteqdot\frac{t}{\alpha}-\frac{1}{\alpha^2}+\frac{\epsilon^{-\alpha t}}{\alpha^2}, \tag{25}$$

$$\frac{p^2}{(p+\alpha)(p+\beta)} \doteqdot \frac{1}{(\alpha-\beta)}\left[\alpha\epsilon^{-\alpha t}-\beta\epsilon^{-\beta t}\right], \quad (26)$$

$$\frac{p}{(p+\alpha)(p+\beta)} \doteqdot \frac{1}{\alpha-\beta}\left[\epsilon^{-\beta t}-\epsilon^{-\alpha t}\right]. \quad (27)$$

If $\omega_0^2>\alpha^2$, $\omega^2=\omega_0^2-\alpha^2$, $\tan\phi=\omega/\alpha$,

$$\frac{p}{p^2+2\alpha p+\omega_0^2} \doteqdot \frac{\epsilon^{-\alpha t}}{\omega}\sin\omega t, \quad (28)$$

$$\frac{p^2}{p^2+2\alpha p+\omega_0^2} \doteqdot -\frac{\omega_0}{\omega}\epsilon^{-\alpha t}\sin(\omega t-\phi), \quad (29)$$

$$\frac{1}{p^2+2\alpha p+\omega_0^2} \doteqdot \frac{1}{\omega_0^2}\left[1-\frac{\omega_0}{\omega}\epsilon^{-\alpha t}\sin(\omega t+\phi)\right]. \quad (30)$$

If $\alpha^2>\omega_0^2$ and $(-m)$ and $(-n)$ are the roots of $p^2+2\alpha p+\omega_0^2=0$,

$$\frac{p^2}{p^2+2\alpha p+\omega_0^2} \doteqdot \frac{1}{n-m}\left[n\epsilon^{-nt}-m\epsilon^{-mt}\right], \quad (31)$$

$$\frac{p}{p^2+2\alpha p+\omega_0^2} \doteqdot \frac{1}{n-m}\left[\epsilon^{-mt}-\epsilon^{-nt}\right], \quad (32)$$

$$\frac{1}{p^2+2\alpha p+\omega_0^2} \doteqdot \left[\frac{1}{\omega_0^2}-\frac{1}{n-m}\left(\frac{\epsilon^{-mt}}{m}-\frac{\epsilon^{-nt}}{n}\right)\right]. \quad (33)$$

If $\alpha^2=\omega_0^2$, the case of equal roots of $p^2+2\alpha p+\omega_0^2=0$,

$$p^2/(p+\alpha)^2 \doteqdot \epsilon^{-\alpha t}(1-\alpha t), \quad (34)$$

$$p/(p+\alpha)^2 \doteqdot t\epsilon^{-\alpha t}, \quad (35)$$

$$1/(p+\alpha)^2 \doteqdot (1/\alpha^2)\left[1-\epsilon^{-\alpha t}(1+\alpha t)\right], \quad (36)$$

$$p/(p+\alpha)^n = \epsilon^{-\alpha t}t^{(n-1)}/(n-1)!, \quad (37)$$

$$\omega p/(p^2+\omega^2) \doteqdot \sin\omega t, \quad (38)$$

$$p^2/(p^2+\omega^2) \doteqdot \cos\omega t, \quad (39)$$

$$\omega p/(p^2-\omega^2) \doteqdot \sinh(\omega t), \quad (40)$$

$$p^2/(p^2-\omega^2) \doteqdot \cosh(\omega t), \quad (41)$$

$$\frac{p\omega}{(p+\beta)^2+\omega^2} \doteqdot \epsilon^{-\beta t}\sin\omega t, \quad (42)$$

$$\frac{p(p+\beta)}{(p+\beta)^2+\omega^2} \doteqdot \epsilon^{-\beta t}\cos\omega t, \quad (43)$$

$$\frac{p\omega\cos\phi \pm p^2\sin\phi}{p^2+\omega^2} \doteqdot \sin(\omega t\pm\phi), \quad (44)$$

$$\frac{p^2\cos\phi \mp \omega p\sin\phi}{p^2+\omega^2} \doteqdot \cos(\omega t\pm\phi), \quad (45)$$

$$\frac{p\omega\cos\phi \pm p(p+\beta)\sin\phi}{(p+\beta)^2+\omega^2} \doteqdot \epsilon^{-\beta t}\sin(\omega t\pm\phi), \quad (46)$$

$$\frac{p(p+\beta)\cos\phi \mp \omega p\sin\phi}{(p+\beta)^2+\omega^2} \doteqdot \epsilon^{-\beta t}\cos(\omega t\pm\phi), \quad (47)$$

$$p/(p^2+\alpha^2)^{\frac{1}{2}} \doteqdot J_0(\alpha t), \quad (48)$$

J_0 is Bessel function of zero order.

This list may be greatly added to by the application of some of the theorems of Section II, *C*, or by the integration or differentiation with respect to a parameter.

As a typical illustration of one of these devices, let us consider

$$p/(p^2+\omega^2) \doteqdot \sin\omega t/\omega, \quad (38a)$$

$$\frac{\partial}{\partial\omega}\frac{p}{(p^2+\omega^2)} \doteqdot \frac{\partial}{\partial\omega}\left\{\frac{1}{\omega}\sin\omega t\right\},$$

$$\frac{-2\omega p}{(p^2+\omega^2)^2} \doteqdot \frac{t\cos\omega t}{\omega}-\frac{1}{\omega^2}\sin\omega t,$$

$$\frac{\omega p}{(p^2+\omega^2)^2} \doteqdot \frac{\sin\omega t}{2\omega^2}-\frac{t\cos\omega t}{2\omega}. \quad (49)$$

Similarly, other results may be obtained.

F. Calculation of Inverse Transforms

We have considered the method of computing the direct transform of a function by the fundamental formula (2); now, the problem of finding the inverse transform by the formula:

$$h(t)=\frac{1}{2\pi i}\int_{c-i\infty}^{c+i\alpha}\frac{e^{pt}g(p)dp}{p} \quad (1a)$$

will be considered.

The evaluation of the contour integral (1) is greatly facilitated by the use of the following theorem known as Jordan's theorem.[B2] This theorem may be stated in the following manner:

Let $\Phi(p)$ be a function integrable in the region $Re(p)\geq c$ along any smooth curve, when $|p|\geq c$,

and such that $|\Phi(p)|$ tends uniformly to zero when $|p|\to\infty$. Let C denote a half-circle with radius r and center at $(c, 0)$ in the same region. Then

$$\underset{r\to\infty}{\text{Limit}}\int_C \Phi(p)\epsilon^{pt}dp=0 \qquad (50)$$

for all negative values of t.

A corresponding lemma exists for positive values of t and an infinite half-circle convex to the left if $\Phi(p)$ fulfills the same conditions in the region $Re(p)\leq c$.

The general method of computing an integral of the type (1) follows.

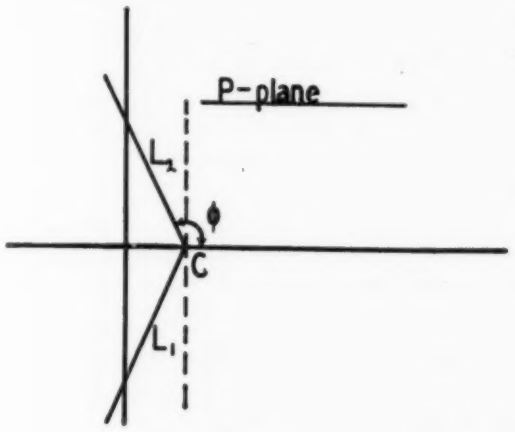

FIG. 2.

It is easy to verify that a function $g(p)$ defined in accordance with the equation,

$$g(p)=p\int_0^\infty h(t)e^{-pt}dt \qquad (2a)$$

has the following properties:

1. Within the half-plane $Re(p)>c$ the function $g(p)/p$ is holomorphic.

2. Within the half-plane $Re(p)>c$, the function $g(p)/p$ tends uniformly to zero when $|p|\to\infty$.

Now in accordance to these propositions, the function $g(p)/p$ fulfills the conditions for Jordan's lemma. Hence by Cauchy's integral theorem we are permitted to change the path of integration into an infinite half-circle convex to the right. Then by Jordan's lemma we are assured that $h(t)$ is zero for all negative values of t. The calculation of $h(t)$ when $t>0$ requires a more complete knowledge of the analytic properties of $g(p)/p$ on the left-hand side of the line $Re(p)=c$. In most cases $g(p)/p$ has such properties that Jordan's lemma is applicable also in this half-plane. Then the line of integration may be completed by an infinite semicircle convex to the left. We thus get a contour C, inside which the integrand possesses certain singularities as poles and branch-points. By means of suitable cuts we can make the integrand uniform inside C. By Cauchy's residue theorem we may compute the integral by means of calculating the residues of the integrand inside C.

G. The Modified Integral

Let us begin with our fundamental integral for the inverse transform,

$$h(t)=\frac{1}{2\pi i}\int_{c-i\infty}^{c+i\infty}\frac{g(p)e^{pt}dp}{p}, \qquad (1a)$$

and perform a formal differentiation under the integral sign. We then obtain

$$\frac{dh(t)}{dt}=\frac{1}{2\pi i}\int_{c-i\infty}^{c+i\infty}\frac{pg(p)e^{pt}dp}{p}, \qquad (51)$$

and we see that the differentiation introduces a factor of p before $g(p)$. In many cases, however, the new integral does not converge uniformly. In such cases, the process of differentiation cannot be performed in this manner since for the operation to be valid, the new integral must converge uniformly. It is possible, however, to modify the original integral in such a way that the procedure is correct. This may be done provided that $g(p)$ satisfies certain conditions. The conditions that are usually fulfilled in practice are the following:

1. $g(p)/p$ is analytic in the region to the right of the straight lines $p=c+re^{i\vartheta}$ and $p=c+re^{-i\vartheta}$, where $\pi\geq\theta>\pi/2$.

2. $|g(p)/p|$ tends uniformly to zero when $p\to\infty$ in this region (see Fig. 2).

It is possible, when these conditions hold, to complete the line integral by the way of an infinite semicircle convex to the left and with center at $(c, 0)$ as before. Then, since no singularities are traversed, the path of integration

may be changed into two straight lines L_1 and L_2 as shown in Fig. 2. This integral along L_1 and L_2 will be known as the modified integral. The modified integral is easily proved uniformly convergent for all positive t's and also integrals of the type

$$\frac{1}{2\pi i}\int_{L_1 L_2} \frac{Q(p)g(p)e^{pt}dp}{p}, \tag{52}$$

where $Q(p)$ is a function that in the region under consideration increases at most as a power of p when p becomes infinite may also be proved uniformly convergent.

H. Examples on Computation of Inverse Transforms

In Section II, *E*, a list of transforms which were calculated by direct evaluation of the integral (2) was given. In that case for a given $h(t)$, if we could compute this integral, then we obtained $g(p)$. Let us now use the theory of residues to compute $h(t)$ when $g(p)$ is given.

1. As a simple example, let us consider (38). We have then

$$g(p)=p/(p^2+a^2); \tag{38b}$$

hence,
$$h(t)=\frac{1}{2\pi i}\int_{c-i\infty}^{c+i\infty}\frac{e^{pt}dp}{p^2+a^2}$$

or hence $h(t)$ = sum of the residues of $e^{pt}/(p^2+a^2)$. The residues at the poles $p=\pm ia$ are, respectively, $\pm e^{iat}/2ia$. The sum of the residues is, therefore, $\sin(at)/a$ and hence,

$$p/(p^2+a^2)\doteqdot \sin(at)/a$$

as in (38).

2. Another example is (37). Here we have: $g(p)=p/(p-a)^n$. This function has a pole of the nth order at $p=a$. The residue at this pole is seen to be $e^{at}t^{(n-1)}/(n-1)!$ and we have

$$p/(p-a)^n \doteqdot t^{(n-1)}e^{at}/(n-1)!. \tag{37}$$

3. In Section II, *D*, a discussion of fractional powers of p was given and the formula

$$1/p^m \doteqdot t^m/\Gamma(m+1), \quad m>-1 \tag{19}$$

was obtained.

It is our purpose now to remove the above restriction on m and to obtain a general formula of the form

$$1/p^r \doteqdot t^r/\Gamma(r+1) \tag{53}$$

for all r's except negative integer values of r. If we begin with the restricted result above, we have the equality

$$t^m/\Gamma(m+1)=\frac{1}{2\pi i}\int_{c-i\infty}^{c+i\infty}e^{pt}dp/(p)^{m+1}\ m>-1, \tag{54}$$

the function $g(p)/p=1/p^{(m+1)}$ tends to zero uniformly in the manner prescribed in the above section on the modified integral as p tends to infinity. Hence we are permitted to differentiate with respect to t any number of times under the integral sign. Hence, differentiating s times, where s is an integer, we obtain

$$p^s/p^m \doteqdot \frac{m(m-1)\cdots(m-s+1)t^{(m-s)}}{\Gamma(m+1)}, \tag{55}$$

where $m>-1$.

Now from the fundamental recursion formula for the gamma-functions we have

$$m(m-1)\cdots(m-s+1)=\frac{\Gamma(m+1)}{\Gamma(m-s+1)} \tag{56}$$

and, therefore,

$$1/p^{(m-s)} \doteqdot \frac{\Gamma(m+1)t^{(m-s)}}{\Gamma(m+1)\Gamma(m-S+1)}. \tag{57}$$

If we let $m-s=r$, then we have for all r's except negative integers

$$1/p^r \doteqdot t^r/\Gamma(r+1). \tag{53}$$

If r is a negative integer, we place $r=-q$, and we have

$$h(t)=\frac{1}{2\pi i}\int_{c-i\infty}^{c+i\infty}e^{pt}p^{q-1}dp \tag{58}$$

and this equals zero since $q=1, 2, 3$, etc. and there are no poles of the function in the finite part of the p plane. Accordingly, we have thus found the transforms for all real powers of p. It may thus be seen that by using the theory of residues it is a simple matter to verify the formulas given in Section II, *E*.

Resumés of Recent Research

Recent advances in experimental and theoretical physics are described in these columns in nontechnical language. It is intended that sufficient background be given to introduce the reader to the subject.

Study of Beta-Brass in Single Crystal Form

Beta-brass is one of the simplest of certain binary alloys which exist in an ordered structure (superlattice) at low temperatures and a completely disordered one (random solid solution) above a "critical temperature." A recent paper by Wayne Webb[1] describes measurements of some properties of single crystal specimens of this alloy. The structure is body-centered cubic. In the orderly arrangement cube centers are occupied by one sort of atom, cube corners by the other. Compositions from 50.22 to 55.85 atomic percent copper were studied. Measurement of electrical resistivity at room temperature showed the phase boundaries to be at 51.3 and 55.5 atomic percent copper. The resistivity-composition relation is linear in this region. Extrapolated to 50 percent copper (the ideal copper-zinc alloy with complete order), the resistivity is a mean between that of copper and zinc. Thus the additional resistance due to the irregular placing of one kind of atom in a random solid solution disappears completely in the ordered state. The resistance of the crystals were measured as the temperature was raised to well above the critical temperature (465°C).[2] By assuming an increment of resistance proportional to disorder[3] it was possible to plot order as a function of temperature and to compare with theory. The agreement with the theory of Bragg and Williams is fairly good except for a distinct continuation of the order above the critical temperature. This is interpreted as being due to the breakdown of "local order." Thermoelectric properties were not appreciably affected by the ordering process; the only observed effect being a slight discontinuity in slope of the thermoelectric power-temperature curve near the critical temperature. Some preliminary results on elastic properties were obtained by measuring Young's modulus for ten crystals at room temperature. Up to the elastic limit (estimated to occur at about 35×10^6 dynes/cm^2 resolved shearing stress on the glide plane or planes) the stress strain relation was linear with no observable permanent set, hysteresis nor creep. For cubic crystals the reciprocal of Young's modulus should be linear when plotted against $(l^2m^2+m^2n^2+n^2l^2)$, in which m, l, n, are direction cosines of direction in which modulus is measured with respect to the crystallographic axes (cube edges). This was verified within experimental error. The maximum and minimum values of Young's modulus were found to be: 19.9×10^{11} dynes/cm^2 in the [111] direction and 2.23×10^{11} dynes/cm^2 in the [100] direction, respectively. The maximum/minimum ratio, 8.9, is unusually high. This large degree of anisotropy is possibly due to the ordered condition.

[1] W. Webb, Phys. Rev. **55**, 297 (1939).
[2] C. Sykes and H. Wilkinson, J. Inst. Met. **61**, 223 (1937).
[3] W. L. Bragg and E. J. Williams, Proc. Roy. Soc. A**144**, 340 (1934).

Capture of Neutrons by Atoms in a Crystal

According to present views on nuclear structure, the probability for the capture of slow neutrons by nuclei may become very large for certain quite definite values of the energy of the neutron corresponding to the formation of a compound nucleus of relatively long life. For a free atom at rest, this probability in its dependence on the energy of the neutron is

just that of the bell-shaped natural absorption line form known in spectroscopy. If the atoms are in a gas at a finite temperature, however, the effect of the relative motion of the gas atoms, or Doppler effect, must be taken into account for both types of absorption. The result is a marked broadening of the line dependent on the temperature of the gas.

The experiments with neutrons, however, have been performed with absorbers and detectors in the solid state, and a discussion of the expected line shape for this case has recently been given by W. E. Lamb, Jr.[1] In general, one would expect to obtain not a single absorption line, but a very large number of lines corresponding to the various amounts of the kinetic energy of the neutron which go into excitation of vibrations in the crystal, instead of into the formation of the compound nucleus. This fine structure is in many cases covered up by the natural width of the single lines due to the great number of the possible crystal vibrations. Then it turns out that the absorption line for neutron capture has just the Doppler effect *form*, except that it is somewhat broader than it would be in a gas at the same temperature. In fact, at absolute zero, the Doppler broadening is just that of a gas at a temperature essentially equal to the Debye temperature of the solid. In case the natural width of the level is small, however, the absorption line may show a marked rudimentary structure.

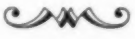

The Rotation of the Milky Way, the Earth's Magnetic Field and the Intensity of Cosmic Rays

Painstaking astronomical observations, which cannot be delved into here, have shown that the Milky Way, of which our solar system forms a very minute part, rotates in such a way that the sun together with the earth describes an immense circle, of several tens of thousands light years radius, with a velocity (at present) of about 300 km/sec. in the direction towards a point at declination 47° North and 20 hr. 55 min. right ascension.

A fundamental question, which must be solved before a true insight is gained into the nature of cosmic rays and the part they play in the general economy of the universe, is whether they come from beyond our own galaxy, or whether they are born within it, in either case by processes as yet not well understood. For if the former is true, they presumably exist throughout the universe, and an easy calculation then shows that a comparatively large fraction of the total energy contained in it is in the form of cosmic rays. If the latter is the case, however, then they are a relatively unimportant local phenomenon, and they lose a large part of their right to be called "cosmic."

In 1935 A. H. Compton and I. A. Getting[1] suggested a possible way of finding an answer to this question. They pointed out that, as a consequence of this motion of rotation of the Milky Way in which the earth takes part, if cosmic rays come from outside the galaxy there should be more rays received when a point of the earth is moving in the direction of the velocity vector due to the galactic rotation, and less when opposite to it. Because of the rotation of the earth a point on its surface is alternately, at twelve-hour intervals, either in the direction of the velocity vector or opposite it. Consequently there should be a diurnal variation of the intensity of cosmic rays (number of particles per unit area and unit time) as a function of sidereal time. This is not to be confused with the diurnal variation of intensity as a function of solar time, the origin of which is entirely different.

Compton and Getting developed their theory while neglecting the deflection of primary cosmic rays by the earth's magnetic field. But since it is now established beyond question that most, if not all, primaries are electrically charged, their conclusions must be taken only as a first approximation. In view of the importance of the question at issue, it seemed worth while to take into account the deflection by the earth's magnetic field and develop the more rigorous theory even if at present, because of mathematical difficulties having to do with the nonintegrability of the

[1] W. E. Lamb, Jr., Phys. Rev. **55**, 190 (1939).

[1] A. H. Compton and I. A. Getting, Phys. Rev. **47**, 817 (1935).

equations of motion, this can be done only in the particularly simple case of particles arriving in any direction in the east-west plane at the geomagnetic equator. The theory developed by M. S. Vallarta, C. Graef, and S. Kusaka[2] shows that the expected effect depends essentially on three factors: (a) How many primaries there are for each energy (i.e. their energy spectrum), (b) what is the ratio of positives to negatives, and (c) whether or not low energy primaries are filtered off before arriving at the measuring apparatus. Taking the vertical direction as typical, the theory leads one to expect, for instance, a diurnal variation of amplitude 0.17 percent with maximum at 13 hr. 20 min. sidereal time, if the distribution of primaries varies with the inverse cube of their energy, and all are positive. If there were as many positives as negatives, the amplitude should be 0.06 percent and the maximum should come at 8 hr. 40 min. sidereal time. If under the same conditions the apparatus were shielded in such a way that only electrons (or positrons) of energy above 17×10^9 ev could be measured the expected effect is zero, but if particles of energy below 25×10^9 ev were filtered off the effect would be 0.1 percent with maximum at 20 hr. 40 min. sidereal time. According to Compton and Getting's approximation the amplitude in the vertical direction should be always 0.3 percent irrespective of the energy spectrum and of course irrespective of the percentage of positives and negatives and should increase with the low energy cut off.

The present experimental evidence, which has been assiduously sought for, not only by Compton and Getting, but by others as well, seems to indicate that the effect, if it exists at all, is of very small amplitude. The possibility that there may be as many positive as negative primaries coming from beyond the galaxy does not seem to be ruled out by the present evidence. Thus the fundamental question whether or not cosmic rays come from beyond our galaxy is as yet largely open.

[2] M. S. Vallarta, C. Graef and S. Kusaka, Phys. Rev. 55, 1 (1939).

Aberrations in Electron Optics

Geometrical electron optics, as a discipline paralleling geometrical light optics, dates from the discovery by H. Busch, in 1926, that any axially symmetric electric and magnetic field possesses the property of forming a first-order, or "Gaussian," electron image of an object on the axis which gives off or is irradiated by electrons of uniform velocity. Later, particularly in view of the wide application of such "electron lenses" in television and electron microscopy, attention was directed toward the defects of these electron images, the problem of the Seidel or third-order aberrations being treated theoretically by Glaser, Scherzer and Rogowski. Experimentally the individual aberrations were demonstrated by Diels, Knoll and Wendt. In a paper entitled "A Simplified Derivation of the General Properties of an Electron-Optical Image," E. G. Ramberg[1] derives the image properties of an electron image including the third-order aberrations anew, making use of symmetry conditions and Larmor's theorem to determine the form of the latter. The "iconal"—or the existence of the electron wave surfaces—is introduced only as a final step to determine fully the shape of the coma figure and, in the presence of a magnetic field, the astigmatic ellipse as well.

[1] E. G. Ramberg, J. Opt. Soc. Am. **29**, 79 (1939).

A Temperature Symposium

TEMPERATURE—its measurement certainly and its control probably—comes under the head of physics. It is appropriate, therefore, that plans are now being made by the American Institute of Physics to hold a symposium on *Temperature, Its Measurement and Control in Science and Industry*. It is hoped that preparations can be completed in time to hold the meeting in the Fall of this year.

Just twenty years ago a Symposium on Pyrometry was held and there were other meetings in the field of temperature before that. Although phenomena related to temperature are often assigned to "classical physics," our fundamental ideas of these phenomena have changed in the last twenty years as much as most of our other viewpoints. The techniques associated with temperature have also undergone marked development in many directions.

These and other considerations led the Institute last April to call an informal conference of men interested in temperature. It was held at the National Bureau of Standards in Washington. This preliminary conference brought out so much interest and so many suggestions that a decision to hold the symposium was quickly made. At the suggestion of the conference, an advisory committee has been formed to consider general questions of time and place and the important matter of cooperation by the industries and allied sciences principally concerned with the measurement and control of temperature. This Advisory Committee consists of the Chairman, C. O. Fairchild, Director of Research, C. J. Tagliabue Mfg. Co.; Dr. E. F. DuBois, Medical Director, Russell Sage Institute of Pathology, and Professor of Medicine, Cornell University Medical College; Dr. Gustav Egloff, Director of Research, Universal Oil Products Company; Dr. John Johnston, Director of Research, U. S. Steel Corporation; Dr. Walter G. Whitman, Head, Department of Chemical Engineering, Massachusetts Institute of Technology; and Dr. H. A. Barton, Director, American Institute of Physics.

This note refers to an important symposium to be sponsored by the American Institute of Physics. The Institute is very anxious to receive suggestions regarding the proper content of such a symposium. Correspondence should be addressed to the Director of the Institute.

The symposium itself will be organized by a committee of authorities in the various aspects of temperature. This committee will shortly be appointed and its membership announced.

Among the purposes now contemplated for the symposium are: (1) Coordination of the treatment of the subject of temperature in the several branches of science and engineering, (2) review of principles and recording of recent work, (3) accumulation, if possible, of contributions for a comprehensive text to be published after the symposium, (4) emphasis on the importance of temperature as a branch of physics, (5) improvement of technical curricula through making available up-to-date information.

Mr. C. O. Fairchild, Chairman of the Advisory Committee, has prepared a list of topics and topic groupings under the heading of "temperature." His list is appended to this note not as a design for the symposium—which will be determined by the Symposium Program Committee—but to indicate the variety and breadth of the subject. The list is published first, to invite and suggest papers to be contributed and second, to afford an opportunity for general advice and criticism of plans for the symposium.

Suggested Topics for a Temperature Symposium

Principles and Elementary Theory

Syllabus of definitions
Thermodynamic temperature scale
The international temperature scale in practice
Psychology of temperature or the thermal sense
Thermoelectric theory
Heat transfer
Optical and radiation pyrometry
"Temperature" in contemporary physics
Electrical measurements
Thermohygrometry

Teaching

Heat and radiation
Thermodynamics
Thermochemistry
Thermoelectricity
Laboratory courses and equipment
"Instrumentation" for engineers

Laboratory Methods

Standardization method of the National Bureau of Standards
Measurement of
Critical temperatures
Equilibrium relations
Thermal expansion
Heat of reactions
chemical, biological, medical
Heat transfer
Temperature in the air-conditioning laboratory
Temperature of tungsten lamps
Temperatures in vacuum
Temperatures under the microscope
Temperature by spectroscopic methods
Temperature of flame
Temperature of the arc
Temperatures near absolute zero
Pyrometric cone equivalents
Electrical measurements
Laboratory equipment: Instruments, ovens, baths, high boiling point liquids, stills, furnaces, refractory materials, controllers and thermostats.

Methods and Technique Peculiar to Various Sciences

The thermal sense of man and other living creatures
The thermal sense of plants
Temperature regulation in man
Temperature coefficient of root pressures
Temperature distribution of life
Temperature effect on life cycles
Work of the U. S. Weather Bureau
Temperature of the sun
Earth temperatures: Soil, ocean, deep mine, glacier, desert, volcano, stratosphere
Detection of icebergs
Temperature phenomena for museum display
Clinical thermometry
Measurements in febritherapy

Methods and Technique Peculiar to Various Industries and Processes

Classification of industrial temperature instruments
Theories of instrument design
Theories of temperature regulation
Heat transmission: Resumé, methods of calculation
Temperature measurements in:
Air-conditioning
Burning (of lime, sulphur, etc.)
Brewing
Carburizing
Casting (of metals, glass, ceramics, etc.)
Coking
Cooking, domestic and industrial
Crystallizing
Digesting
Distilling, fractionating
Drying
Dyeing
Electroplating
Electrolyzing
Enameling
Evaporating (as in vacuum pans)
Expressing (fats, oils, etc.)
Fermenting
Firing (e.g. clay ware, e.g. regenerative, recuperative)
Forging
Generating power, steam, dynamoelectric, internal combustion
Grain storing
Heating and ventilating
Heat treating (of metals and alloys, glass, etc.) (annealing, hardening, tempering, etc., etc.)
Ironing (industrial laundering)
Liquefying of gases
Melting (metals, glass, varnish, etc.)
Mixing (rubber, etc.)
Molding (glass, synthetic plastics, etc.)
Nitriding
Pasteurizing
"Processing" (miscellaneous operations, e.g. scouring, mercerizing, calorizing, etc.)
Refining (metals, oils, etc.)
Refrigerating
Roasting (ores, coffee, etc.)
Rolling, hot (metals, glass)
Seasoning (aging)
Sintering (cement, powdered metals)
Soldering
Steaming
Sterilizing
Teeming
Thermo-chemical processing: Cracking, catalyzing, polymerizing, synthesizing
Use or performance testing (e.g. of tires, brakes, bearings, etc.)
Vaporizing and sublimating
Vulcanizing
Washing (laundering)
Welding

Miscellaneous Thermometric Methods, Devices, Phenomena

Pyrometric cones: The Edward Orton, Jr. Ceramic Foundation
Low-melting alloys and eutectic mixtures
Thermostatic metal
Surface temperature measurements

Special Thermal Phenomena of Broad Interest

Cooling of earth, sun
Cooling of Boulder Dam
Icing of airplanes
Formation of anchor ice
Thermal distortion of large structures: Empire State Building, George Washington Bridge
Thermal history of 200-inch telescope reflector
Volcanology

Industrial Temperature Instruments, Modern Designs and Features

Thermoelectrical, thermomechanical

Standard Tables for Thermometry and Pyrometry

Critical temperatures of the chemical elements
Emergent stem corrections for mercury thermometers, various glasses
E.m.f. temperature data for standard thermocouples
Humidity tables, wet and dry-bulb temperatures

List of American Manufacturers of Temperature Instruments

Condensed Bibliography

Index

New Books

Physik fur Studierende un Technischen Hochschule und Universitat. DR. PAUL WESSEL. Edited by Dr. V. Riederer von Paar. Verlag von Ernst Reinhardt, Munchen.

As the title states this typical German text in physics is intended for college use. But it clearly illustrates the difference between continental and American college courses. The American texts, with their pains-taking efforts towards complete and persuasive lucidity are intended for those who have not studied physics seriously before. Wessel's *Physik* is more of a compendium of physics for those who are consolidating their knowledge, gained in earlier courses, by a final comprehensive general course. Though short and pithy and mathematical, the explanations are nevertheless clear and well illustrated. The material differs little from a standard American college course except for a very comprehensive and up-to-date section of modern physics including such items as relativity, quanta, material waves, nuclear physics in outline and the uncertainty principle.

There is a concise resumé of physical formulae in a special section for reference. There is a section on questions of a suggestive nature, some 1450 of them, which probably serves as classroom quiz material. But the typical American drill problems are conspicuously absent.

One could scarcely judge the book pedagogically, outside its own sphere, with fairness. Its interest to an American is mostly due to the rare opportunity which it gives to compare vastly different educational systems.

M. H. TRYTTEN
Johnstown Center
University of Pittsburgh

Magnetische und Elektrische Eigenschaften des Eisens und seiner Legierungen. O. V. AUWERS, Pp. 828, Figs. 628. Verlag-Chemie, Berlin, 1938. Price 84 M.

This book contains a very complete summary of the now known magnetic and electric properties of iron and its alloys. In spite of the enormous amount of detailed information that it contains, one can find any particular item quite easily by means of a comprehensive index which is not the usual alphabetically arranged list of every item mentioned in the text, but a list arranged in a very sensible way according to major and minor categories of subject matter. The book should be especially useful to those seeking complete and up to date information, and is a most valuable addition to the less exhaustive summaries and tables now available.

The following condensation of the table of contents may give the reader some idea of the scope and character of the work:

Part I. Magnetic and electric properties of pure iron and iron containing carbon
Theories of ferromagnetism. 17 pages.
The magnetic properties of atoms. 3 pages.
The magnetic properties of iron and iron+carbon. 107 pages. (This includes information on magnetization, permeabilities, hysteresis, Barkhausen effect, magnetostriction, and all the various gyromagnetic, thermomagnetic, and magneto-electric effects.)
The electric properties of atoms. 1 page.
The electric properties of iron and iron+carbon. 60 pages. (This includes electrical resistance, thermoelectric properties, contact potentials, the behavior of electrodes in vacuum tubes, and even such up-to-date matters as the absorption of neutrons.)
Additional references on the above. 15 pages.

Part II. Magnetic and electric properties of alloys. 420 pages.
The arrangement of subject matter is similar to that in Part I. The list of alloys discussed in the text takes up about 25 pages of the index. Part II ends with a very good brief discussion (9 pages) of the theoretical and practical achievements in this field, and a collection of data, patents, and trade names in tables.

Part III. An appendix bringing all the above right up to date.

F. BITTER
Massachusetts Institute of Technology

Standards on Electroacoustics, 1938. Pp. 37+vi. Figs. 8, 15×23 cm. The Institute of Radio Engineers, Inc., 330 West 42nd Street, New York, N. Y., 1938. Index. Price 50¢ postpaid.

This carefully prepared and authoritative document now appears for the first time as a separate work. In earlier issues it was a part of the much more comprehensive report upon standards in radio engineering and allied arts and sciences, published every few years by the Institute of Radio Engineers.

The three main divisions of the report are concerned with definitions, symbols, and methods of testing loudspeakers. Physicists who are not professional acousticians will be interested chiefly in the general definitions with which the report begins. Two recommendations deserve careful consideration; the first, that the term "cycles per second" replace the equivalent terms "double vibrations," "periods per second," "Hertz," etc.; the second, that the terms "bar" and "barye," which have been used to mean both 1 dyne/cm^2 and 10^6 dynes/cm^2, be abandoned in electroacoustic literature, pressures being stated instead in c.g.s. units.

It is always difficult to decide what should be included in a list of definitions. The reviewer feels that the logarithmic cent should not be mentioned (definition 1A9, p. 2) without explanation, and that if it is mentioned and explained the just scale and the tempered scale should also be defined. Many engineers would welcome the inclusion of the decibel and perhaps also the dyne! A footnote should be added to definition 1A7, p. 1, to the effect that a good many writers—and speakers too—still call the first overtone the first harmonic.

The general reader will be interested to learn how difficult it is to make reliable readings of the response curves of loudspeakers, and how highly developed the technique has become. He will perhaps wonder more than ever why the obvious competence of the sound engineer so seldom appears in commercial products!

There are a few minor errors. In the Table on p. 13 ϕ_e, ϕ_M, and ϕ_A are printed as ϕe, ϕM, and ϕA. It is stated on p. 15 that methods of securing the sound pressure of a sound source will be discussed; however, methods of securing the relative sound pressure characteristic are presented. The absolute measurement of sound pressure is quite another matter.

Occasional blemishes of style are noted, but in only one place do they produce obscurity. On p. 23 the writer seeks to describe an arrangement of microphone and loudspeaker in an acoustically deadened room. Only a person having previous knowledge of the art could hope to understand the set-up from this description.

Despite these small things, the report as a whole is highly praiseworthy. The committees named therein have evidently labored long and faithfully. They deserve the hearty thanks of the profession.

CHAS. WILLIAMSON
Carnegie Institute of Technology

Contributors to This Issue

Chauncey Guy Suits received his B.A. degree from the University of Wisconsin in 1927 and his Sc.D. degree from Eid. Technische Hochschule, Zürich, in 1929. He has been employed in the research laboratories of the General Electric Company since 1930 where he has made scientific contributions in the fields of nonlinear circuits and high pressure electric arcs.

Louis A. Pipes was born in Mexico City in 1912. He received his B.S., M.S., and Ph.D. from the California Institute of Technology in 1933, 1934, and 1936, respectively. During 1936–1937 he was an Instructor in Electrical Engineering at the Rice Institute; from 1937–1938 he was Research Associate at the University of Wisconsin, and since 1938 he has been Faculty Instructor at the Graduate School of Engineering at Harvard University.

Willi M. Cohn received the degree of Doctor of Engineering from the Berlin Institute of Technology, Germany, in 1923. He came to this country in 1931 and has been engaged in commercial consulting work since that time. He went to the Pacific Coast in 1933 with a Grant-in-Aid of the American Academy of Arts and Sciences in order to measure, at the Lick Observatory of the University of California, plates obtained during the 1932 eclipse of the sun.

C. G. Suits

L. A. Pipes

W. M. Cohn

Here and There

Conference on Industrial Physics

The Department of Physics of the University of Pittsburgh announces a Third Conference on Industrial Physics to be held March 24, 1939. The scheduled program is as follows:

Morning Session 9:30 A.M.
Mellon Institute Auditorium

1. **Industrial Applications of Extremely High Pressures.** Thomas C. Poulter, *Director of Research, Armour Institute of Technology*
2. **The Mass Spectrograph and Its Industrial Possibilities.** John Hipple, *Westinghouse Electric and Manufacturing Company*
3. **Physics of Flames and Explosions in Gases.** Bernard Lewis, **U. S. Bureau of Mines,** and Guenther von Elbe, **Coal Research Laboratory, Carnegie Institute of Technology**

Lunch 12:30 P.M.
University Club

The Future of Microfilm as a Record of Research. Watson Davis, *Director of Science Service*

Afternoon Session 2:30 P.M.
Mellon Institute Auditorium

1. **Measurement and Specification of Color in Industry.** Carl E. Foss, *Interchemical Corporation*
2. **A Metallurgist Looks at the Recent Progress in the Physics of Metals.** A. Allan Bates, *Westinghouse Electric and Manufacturing Company*
3. **Measurement and Analysis of Sound in Industry.** Ernest J. Abbott, *President, Physicists Research Corporation*

Anyone interested is cordially invited to attend. Further information may be obtained from Professor E. Hutchisson, University of Pittsburgh.

★

Physics Club of Chicago

The officers for the Physics Club of Chicago for the 1938–39 term are: Professor B. J. Spence of Northwestern University, President; Professor J. S. Thompson of Armour Institute of Technology, Vice President; Mr. A. J. Klapperich, Peoples Gas Light & Coke Company, Treasurer; and Mr. B. J. Barmack of the Commonwealth Edison Company, Secretary. Professor W. S. Huxford of Northwestern University is Chairman of the Program Committee.

Organized in 1931 by Professor Arthur H. Compton and Dean H. G. Gale of the University of Chicago, the Club now has 204 members. The membership is made up mainly of teachers, engineers, and patent lawyers.

The October meeting was opened by Professor Ralph A. Sawyer with a talk on "The Spectrograph in the Iron and Steel Industry." In November the Club acted as host to the American Physical Society, and the joint meeting, attended by about 350 members and guests, was addressed by Bertrand Russell on "Determinism in Physics." On December 20, Dr. Thomas C. Poulter addressed the Club on "Extreme Pressures and the Investigation of Engineering Problems," while on January 17, 1939, Professor J. W. Beams of the University of Virginia spoke on "High Speed Centrifuging and Some of its Applications."

★

A. I. P. Placement Service

Interested readers are reminded that the American Institute of Physics conducts a placement service for physicists. The Institute will be glad to register students receiving their degrees next June and others who are seeking employment as physicists, either with academic institutions or industrial laboratories. The Institute has found that employers welcome this service, a number of personnel needs having been satisfied through it in the past two years. Inquiries from employers or from registrants should be addressed to the American Institute of Physics, 175 Fifth Avenue, New York City.

★

Calendar of Meetings

March	
2–3	Conference on Instrumentation in Process Industries, Pittsburgh, Pa.
24	Metropolitan Section, American Physical Society, New York, N. Y.
31–April 1	Pennsylvania Conference of College Physics Teachers, Gettysburg, Pa.
31–April 1	Southeastern Section, American Physical Society, Athens, Ga.
April	
1	New York State Section, American Physical Society, Clinton, N. Y.
3–7	American Chemical Society, Baltimore, Md.
16–22	American Ceramic Society, Chicago, Ill.
26–29	Electrochemical Society, Columbus, Ohio.
27–29	American Physical Society, Washington, D.C.
May	
16–17	Acoustical Society of America, New York, N. Y.
22–June 8	World Automotive Engineering Congress, New York, Indianapolis, Detroit, San Francisco.
June	
19–24	American Association for the Advancement of Science, Milwaukee, Wis.
26–30	American Society of Testing Materials, Atlantic City, N. J.
28–30	American Physical Society, Stanford University, Cal.
July	
6–8	Sixteenth Colloid Symposium, Stanford University, Calif.
September	
4–12	International Congress of Mathematicians, Cambridge, Mass.
4–15	International Union of Geodesy and Geophysics, Washington, D. C.
11–15	American Chemical Society, Boston, Mass.
December	
27–Jan. 2	American Association for the Advancement of Science, Columbus, Ohio.

Contributed Original Research

On Resonators Suitable for Klystron Oscillators

W. W. Hansen and R. D. Richtmyer
Physics Department, Stanford University, California
(Received December 3, 1938)

Various resonators, of the *hohlraum* type, suitable for driving by the klystron method, are described and their leading properties computed. Various mathematical techniques are used, including the application, for the first time in this field, of Stevenson's method of determining a lower bound for the frequency.

Introduction

By the use of the bunching principle as discovered by Varian[1] it is now possible to excite electrical resonators with good efficiency at very high frequencies. There are, however, certain requirements on the resonators which give rise to interesting problems and it is the purpose of the present paper to study some of these.

The first of these requirements arises from the fact that, at wave-lengths of the order of ten cm, the apparatus is usually small and the electron beams must be likewise so that the beam currents are in the order of milliamperes. As convenient voltages are of the order of 1000 volts the voltage/current ratio for the beam is of the order of megohms. It follows that the resonators used should have an equivalent shunt impedance of some megohms. The above remarks are not to be taken too literally as far as numbers go, for it is often easy to get satisfactory operation with lower voltage/current ratios; nevertheless the general conclusion as to desirable impedance of resonators holds. Now it has been shown[2] that simple shapes of conducting enclosures, for example the sphere, show a shunt impedance of the order of $(\lambda/\delta)c$ where λ is the wave-length, δ the skin depth and c the velocity of light. Putting numbers into the above, or corresponding exact formulae, one finds that because λ/δ is large ($(\lambda/\delta)=5.88\times10^4$ for Cu, at $\lambda=10$ cm) and c is 30 ohms, it is quite possible to get shunt impedances of the desired order. This suggests the use of this general type of resonator. But here a second requirement enters which arises from the fact that if full use is to be made of the high shunt impedance the driving electrons must be able to traverse the electric field in about $\frac{1}{2}$ cycle. This means that in the regions of strong electric field the distance between boundaries of the resonator must be of the order of $\beta\lambda/2$ with $\beta=v/c$ ($v=$ velocity of electron) and therefore in general rather smaller than λ.

The above leads us to examine the properties of conducting enclosures of the general form shown in Fig. 1(A). This may be considered as a distortion of the sphere which is shown dotted. Alternatively, it could be considered as derived by distorting the "concentric line" type of resonator, also shown dotted. The point of view is immaterial as far as the mathematics is concerned, for it is known that any closed conductor

[1] R. H. Varian and S. F. Varian, article soon to be published.
[2] W. W. Hansen, J. App. Phys. 9, 654 (1938).

can act as a resonator and the only unusual ones from this point of view are those few, among the multiply infinite possible numbers, for which exact solutions are known.

In any case we consider, in this paper, resonators of the general form shown in Fig. 1, (B) and (C), and also resonators of similar cross-sections but of cylindrical form instead of the figures of revolution shown in Fig. 1.

In a second paper, we will give various approximate treatments of shapes such as Fig. 1, (A) and (D), and also a few mathematical results here used without proof.

Definition of Problem

As to what quantities should be computed we obviously want λ, the resonant wave-length, and something corresponding to shunt impedance. Although usually not of such direct importance, a knowledge of Q is also useful. Of these quantities, λ and Q are uniquely defined and no more need be said, but this is not so of the shunt impedance.

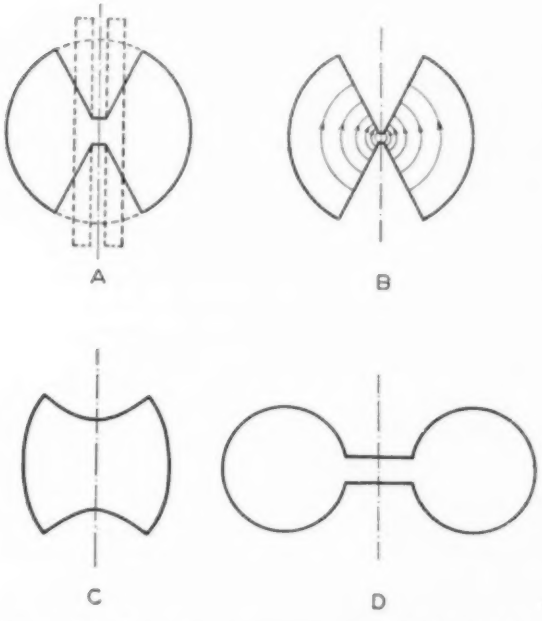

FIG. 1. Various shapes of resonators suitable for driving by the klystron method. In all cases a cross section is shown; the actual resonator is generated by rotating this about the center line or axis. The driving electrons would run in a stream parallel to this axis. (A) is a shape well suited for practical use, but not too simple to compute. Shown dotted in this figure are a sphere and a resonator of the concentric line type; (A) could be considered as a distortion of either. (B) is a shape that is very easy to compute. (C) is harder but quite possible. Also shown in (B) is an approximate picture of the lines of electric field. (D), like (A), is a useful shape in practice but cannot be computed exactly.

In a previous paper the shunt impedance was defined as Q times $L\omega$ with the inductance L defined as ($2x$ energy stored)/(current squared). As was pointed out at the time, such a definition is to a considerable extent arbitrary, for in addition to questions as to exactly what is to be taken as the current it is plain that one might equally well define the shunt impedance as Q times $(1/\omega C)$ with the capacity C defined as ($2x$ energy stored)/(voltage squared). Or, one might define L in terms of flux linkages per ampere and get still a third shunt impedance (the corresponding thing for C leads to the same result). Such ambiguities necessarily arise when one tries to use lumped constants to describe resonators of dimensions comparable to λ and one must choose that consistent scheme which is best adapted to the problem in hand. In the present case the choice is easy: If one takes the second definition, then (voltage)^2/shunt impedance gives the power loss, which is the quantity of interest, in terms of the "voltage," which is also of interest and sure to be known.

To make the above perfectly definite we write down formulae corresponding to the three possible definitions. The first mentioned is the one used previously, i.e.,

$$R=4\pi Q\frac{k\int \mathbf{B}^2 d\tau}{[\int \mathbf{B}\cdot d\mathbf{s}_1]^2}c=4\pi Q\frac{\int \mathbf{E}^2 d\tau}{k[\int \mathbf{E}\cdot d\boldsymbol{\sigma}_2]^2}c,$$

$$k=2\pi/\lambda. \quad (1)$$

The above gives the correct losses when used in the formula $P=(iL\omega)^2/R$ with i the total current crossing the closed path lying on the surface of the resonator and of which $d\mathbf{s}_1$ is a part. This path is to some extent arbitrary, but it seems natural to take it in such a way as to maximize the integral of $\mathbf{B}\cdot d\mathbf{s}_1$ subject to the condition that the path be a simple closed curve lying wholly on the surface of the resonator. Also, in the right-hand part of this equation, where standard transformations have been used to write the result in terms of $\mathbf{E}$ instead of $\mathbf{B}$, the integral $\mathbf{E}\cdot d\boldsymbol{\sigma}_2$ is over a surface bounded by a path s_2.

Finally, in Fig. 2 we have shown the paths for the case of the sphere and also represented other notations to appear presently.

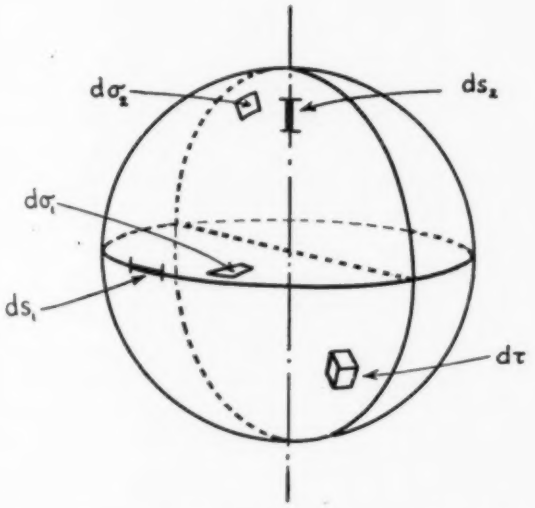

FIG. 2. This illustrates, for the special case of the sphere, various integration paths and surfaces occurring in Eqs. (1) to (3). The field is supposed like that of Fig. 1, reference 2, i.e., with **E** substantially vertical and with **B** running only in the φ direction. Then $d\tau$ is an element of volume lying inside the resonator, $d\mathbf{s}_1$ is an element of the equatorial great circle and $d\boldsymbol{\sigma}_1$ is an element of the surface bounded by s_1. Likewise, $d\mathbf{s}_2$ is an element of a path along the polar axis, and $d\boldsymbol{\sigma}_2$ is an element of the area bounded by s_2 and the surface of the resonator. Finally $d\boldsymbol{\sigma}$ whose absolute value appears in the expression for Q, is an element of the area of the sphere itself.

We now propose to use, instead of the above

$$R=4\pi Q\frac{[\int \mathbf{E}\cdot d\mathbf{s}_2]^2}{k\int \mathbf{E}^2 d\tau}c=4\pi Q\frac{k[\int \mathbf{B}\cdot d\boldsymbol{\sigma}_1]^2}{\int \mathbf{B}^2 d\tau}c, \quad (2)$$

where again the result is given in terms of both **E** and B. Here the line integral of **E** is taken along a path $\mathbf{s}_2$ such that integral $\mathbf{E}\cdot d\mathbf{s}_2$ is a maximum, subject to the condition that the paths terminate on the resonator surface; this path will ordinarily be taken to be the path of the driving electrons. According to this definition the losses are given by (voltage)$^2/R$, with the "voltage" taken to mean integral $\mathbf{E}\cdot d\mathbf{s}_2$. We may note that, using this definition, R may be computed without finding Q as an intermediate step. This is because of the cancellation of the integral $\mathbf{E}^2 d\tau$ in (2) with a similar integral in the definition of Q. The result is

$$R=4\sqrt{2}\frac{[\int \mathbf{E}\cdot d\mathbf{s}_2]^2}{\int \mathbf{B}^2|d\boldsymbol{\sigma}|}(\lambda/\delta)c. \quad (2.1)$$

There is a third definition possible which is really more symmetrical than either of the above, in fact the result is just the geometrical mean of the previous two. According to this scheme one defines L in terms of (flux linkages)/(current) or C in terms of (lines of force)/(volt) and then sets $R=QL\omega\equiv Q/C\omega$. The result is

$$R=4\pi Q\frac{\int \mathbf{E}\cdot d\mathbf{s}_2}{\int \mathbf{B}\cdot d\mathbf{s}_1}c=4\pi Q\frac{\int \mathbf{B}\cdot d\boldsymbol{\sigma}_2}{\int \mathbf{E}\cdot d\boldsymbol{\sigma}_1}c. \quad (3)$$

However, in cases we have met in practice so far, this is not as useful as either of the above because one can usually get at either a current or a voltage whereas (3) would need both.

Needless to say, the above possible definitions of R coalesce when λ becomes large compared to all dimensions of the resonator, in which case the fields **E** and **B** are fairly well separated and one part of the resonator can really be considered a lumped inductance and another a lumped capacity. For efficient resonators, however, one wants the size to be as large as possible by comparison with λ and in cases of this type the differences may be considerable. For example, for a sphere we find the results to be, in order, $4\pi Qc$ times 0.214, 0.863 and 0.429.

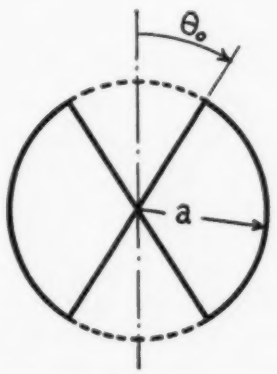

FIG. 3. Cross section of a resonator consisting of part of a sphere of radius a, and two cones whose semi-angle, measured from the polar axis, is θ_0.

§1. Calculations on certain mathematically simple shapes with axial symmetry

We begin by considering the shape shown in Fig. 3, which consists of a sphere $r=a$ and the cone $\theta=\theta_0$, $\theta=\pi-\theta_0$. The two halves of the cone are joined to the sphere, but their apices do not touch. Of course this shape is not strictly realizable in practice, but close approximations can be used and, even were this not so, the results would be valuable because they are all simple closed formulae for which the ratio (information)/(labor) is large.

General solutions of the vector wave equation, suitable for this boundary, can be written down and will be found to involve associated Legendre functions of the second kind (Q functions)

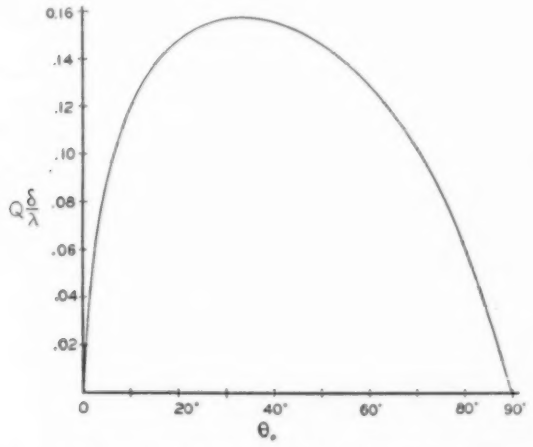

FIG. 4. Plot showing the variation of Q for the resonator of Fig. 3 with the angle θ_0. Instead of plotting Q we have plotted $Q(\delta/\lambda)$ which is independent of wave-length or resonator material and depends only on the shape of the resonator.

instead of the P functions encountered when the cones are not present. When the simplest of these solutions, corresponding to the ground state, is written out, it is found that the logarithmic terms ordinarily associated with Q functions disappear because of a differentiation; in fact the proper functions[3] for the field are, neglecting time

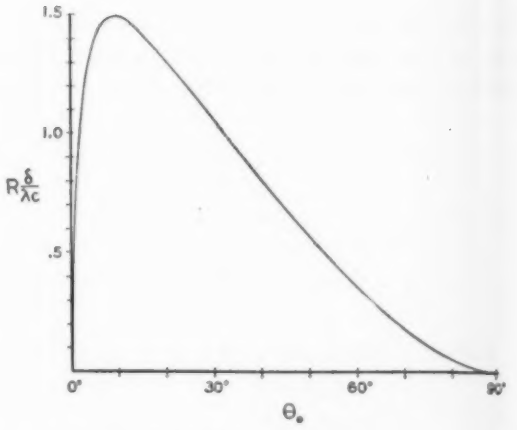

FIG. 5. Plot showing the variation of shunt impedance for the resonator of Fig. 3 as a function of the semi-angle of the cones. Here the quantity which depends only on resonator geometry is $R(\delta/\lambda c)$: this has been plotted instead of R itself.

factors,

$$E_\theta=\frac{1}{\sin\theta}\frac{\cos kr}{kr},\quad B_\varphi=\frac{1}{\sin\theta}\frac{\sin kr}{kr}. \tag{4}$$

Thus if the radius of the sphere is a, then since E_θ must vanish there, we find $ka=\pi/2$ and so

$$\lambda=4a \tag{5}$$

independent of the cone angle. Moreover, it is worthy of note that λ is not greatly increased over its values of $\lambda=2.28a$ for a sphere without cones.

From the above functions we find directly

$$Q=\frac{\sqrt{2}}{4}\frac{-\log\tan(\theta_0/2)}{1-\dfrac{0.825}{\sin\theta_0\log\tan(\theta_0/2)}}\frac{\lambda}{\delta} \tag{6}$$

and

$$R=\frac{4\sqrt{2}}{\pi}\frac{-\log\tan(\theta_0/2)}{1-\dfrac{0.825}{\sin\theta_0\log\tan(\theta_0/2)}}\frac{\lambda}{\delta}c. \tag{7}$$

[3] This function, because it has no nodes in E corresponds to what in spectroscopy might be called the ground state, or in sound the fundamental vibration. But here we must remember that we are dealing with vector waves so that, in addition to three numbers associated with the three dimensions of space and specifying the number of nodal surfaces, we also need to specify which of three directions of polarization is being considered. Thus there are in general three "ground states" if by this we mean states with no nodes in **E**. In general, this seems best as which of the three lies lowest depends on the exact shape of the resonator and may be altered by continuous changes thereof. In what follows we consider only one polarization.

One notes that, in the possible range of θ_0, $\log \tan (\theta_0/2)$ is negative. These formulae are represented graphically in Figs. 4 and 5. From this we observe that the cone angle giving the highest shunt impedance is about $\theta_0=9°$, that giving the highest Q is $\theta_0=34°$. From these graphs we note that neither Q nor the shunt impedance is greatly reduced from their values for a sphere without cones provided one uses, in each case, the optimum cone angle. Specifically Q goes from $0.45\lambda/\delta$ for a sphere to $0.155\lambda/\delta$ when the cones are added; R changes from $4.92(\lambda/\delta)c$ to $1.51\ (\lambda/\delta)c$. Putting numbers in the last we find a shunt impedance of 2.66×10^6 ohms at $\lambda=10$ cm for a copper resonator of 9° cone angle.

This verifies the assertion made in the introduction: It is indeed possible to obtain shunt impedances in the megohm range at 10 cm and with the walls of the resonator close together in the region of high field. On the other hand, this shape is not well suited for practical use because the available grid area is quite small. The same remark applies in some degree to the other resonators treated in this paper. Nevertheless results such as the above and those to follow are of great practical value because they are simple and exact. In the following paper various shapes more suited for actual use are considered, but owing to mathematical difficulties these must be treated by approximate methods.

We next note that the cylindrical counterpart of resonator and field of Fig. 3 is not simple. To be more specific, if ϵ is the distance between the apices of the wedges replacing the cones of Fig. 3 the solution for which integral $\mathbf{E}\cdot d\mathbf{s}_2$ is not zero in the limit $\epsilon\rightarrow0$ has also $\lambda\rightarrow\infty$. This is related to the fact that, while the capacity between two cones point to point is finite, the capacity between two wedges similarly placed is (logarithmically) infinite.

As the next shape consider the figure of revolution whose cross section is shown in Fig. 6. Here the bounding surfaces are sections of confocal ellipsoids and hyperboloids, so that they are simply described in prolate spheroidal coordinates. Since the wave equation separates in these coordinates we can obtain exact solutions, though unfortunately the needed functions are not tabulated and numerical integration must be resorted to.

To do this, we first define our coordinates by the equations

$$\begin{aligned} x&=(a/2)\sinh\mu\sin\vartheta\cos\varphi\\ y&=(a/2)\sinh\mu\sin\vartheta\sin\varphi\\ z&=(a/2)\cosh\mu\cos\vartheta \end{aligned} \tag{8}$$

with a the interfocal distance. For distances from the origin large compared to a, $(a/2)\cosh\mu$ or $(a/2)\sinh\mu$ approaches spherical r, and ϑ approaches spherical θ. Now the scalar wave equation, satisfied by any cartesian component of the fields, can be written down and separated. If we choose, for example, the x component of $\mathbf{B}$, and let this be proportional to $\sin\varphi$ (and $B_y\sim-\cos\varphi$) so that there are no nodes in $\mathbf{B}$, then we find, after sundry changes of variable designed to facilitate numerical integration,

$$(\rho^2-1)(d^2R/d\rho^2)+(\alpha^2(\rho^2-1)+A)R=0, \tag{9a}$$

$$(1-w^2)(d^2T/dw^2)+(\alpha^2(1-w^2)-A)T=0, \tag{9b}$$

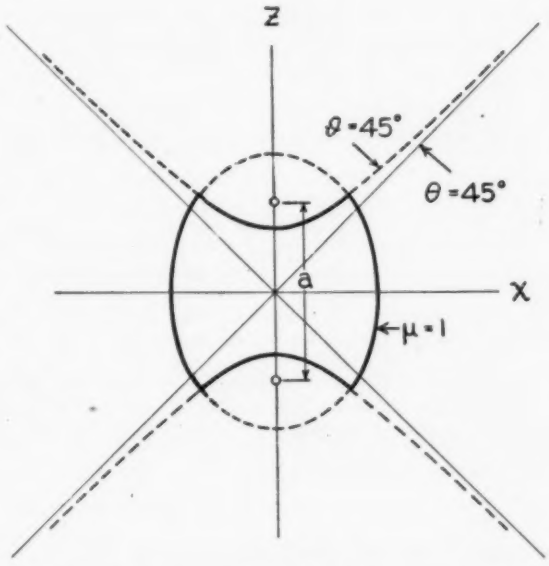

FIG. 6. This illustrates the prolate spheroidal coordinates defined in Eq. (8) and also shows a section of a typical resonator computable in these coordinates. The hyperboloids shown are obtained by holding ϑ constant at 45° and 135° and allowing μ to vary. At large distances these approach the cones described in spherical coordinates by $\theta=45°$, 135°. The ellipsoid shown corresponds to $\mu=1$. Similar ellipsoids for large values of μ would be almost spherical.

where

$$B_z = \frac{1}{\sinh \mu} R(\cosh \mu) \frac{1}{\sin \vartheta} T(\cos \vartheta) \sin \varphi$$

$$\alpha = ka/2 = \pi a/\lambda$$

$$\rho = \cosh \mu \to 2r/a \text{ for large } r/a, \tag{10}$$

$$w = \cos \vartheta,$$

A = separation constant.

The boundary conditions are that $T'(0)$ and $R(1) = 0$ and that T' and R' vanish on the surface of the resonator. Values of variables corresponding to boundaries are designated with a subscript nought. Now because numerical integration must be used, one can expect to compute

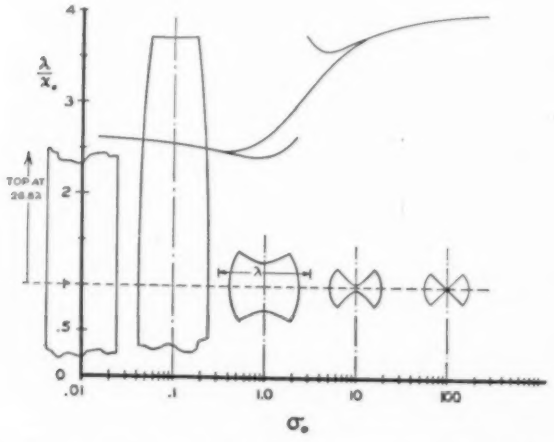

FIG. 7. Plot of λ/x_0 *vs.* σ_0 for resonators with shape of the type shown in Fig. 6. Here x_0 is the equatorial radius and $\sigma_0 = \sinh \mu_0 = 2x_0/a$ with a the interfocal distance. To show the effect of varying σ_0 on the shape we have shown, below the curve, cross sections for five values of σ_0. These little drawings are scaled so all would give the same wave-length. The shape corresponding to $\sigma_0 = 0.01$ is so long and slender that it cannot be got into the figure, likewise only the upper half of that for $\sigma_0 = 0.1$ is shown. Also shown are wave-lengths computed from the approximate formulae (13), valid for small σ_0, and from (26), valid for large σ_0.

a limited sequence of shapes only. Having in mind that some idea of the effect of varying the angle of the asymptotes can be obtained from the case of Fig. 3, it seemed to us most useful to calculate a sequence having always the same hyperboloids but with the ellipsoid varying from very large, in which case the shape approaches Fig. 3, to very small when the shape crudely approximates a circular cylinder with plane ends. As determining the asymptote angle we took $w_0 = \cos \vartheta_0 = 0.7$ so that $\vartheta_0 \leqq 45°$.

With the choice of ϑ_0 the integrations were carried out, the procedure being as follows: A value of α^2 was chosen and various values of A were tried in (9b) until a value was found for which starting with $T' = 0$ at $w = 0$ and integrating step by step one arrives at $T' = 0$ at $w = 0.7$. Thus, for given α^2, the separation constant A is determined so that the boundary conditions are satisfied over the hyperboloids. Then, with this value of A, Eq. (9a) is integrated step by step from $\rho = 1$ until one comes to a place where $R' = 0$; this determines the value of ρ, call it ρ_0, on the surface of the ellipsoid. In doing this one must start the function off by means of a power series, since the equation is singular near $\rho = 1$.

By successive applications of the above process we found λ for various shapes, and further integrations have been made to find the values of Q and shunt impedance. The results are shown graphically in Figs. 7, 8 and 9.

Now the above operations are rather time consuming and so we are led to search for approximate answers which one could expect to be good, at least in the two limiting cases.

Consider first the case in which λ is much smaller than the interfocal distance, i.e., $1 \ll \alpha^2$. Then the ellipsoid becomes long and slender and it is easy to guess, on physical grounds, that in any short length of this ellipsoid the field B will vary like J_1, of the cylindrical radius, for this is the correct solution for a circular cylinder. Thus λ will be determined by some average (cylindrical) radius of the ellipsoid. Going up and down the z axis the field will vary slowly and will have $(\partial^2 B/\partial z^2) < 0$ where the ellipsoid is larger than this average radius and vice versa, and the field will nearly vanish near the ends.

The above is easily verified analytically. First, we solve (9b) approximately by the Ritz variation method, using as a trial function $T = e^{-\alpha w^3/2}$ which approaches an exact solution as $\alpha \to \infty$. It will be observed that this does not exactly satisfy the boundary conditions since its derivative does not vanish at w_0. This is not serious, however, as we are considering α as large so that

the function practically vanishes at the end points. Not correcting for the derivatives at the boundary, then, and considering all the needed integrals as well approximated by integrating to infinity on w we easily find $A \cong \alpha^2 - \alpha - \frac{1}{4}$.

Now we take this value of A and endeavor to solve (9a), at least approximately. Before doing this, it is useful to change the independent variable from ρ to $\sigma = (\rho^2-1)^{\frac{1}{2}} = \sinh \mu$ and the dependent variable from R to $J = R/\sigma$. We note that, when $1 \ll \alpha^2$, σ is always small. Making the variable changes, we find

$$\frac{1}{\sigma}\left(\frac{d^2J}{d\sigma^2} - \frac{1}{\sigma}\frac{dJ}{d\sigma} + \left(A' - \frac{1}{\sigma^2}\right)J\right) + \sigma\left(\frac{d^2J}{d\sigma^2} + \frac{2}{\sigma}\frac{dJ}{d\sigma} + \alpha^2 J + \frac{A-A'}{\sigma^2}J\right) = 0 \quad (11)$$

with A' a constant as yet undetermined but nearly equal to A.

Now we solve this by the Ritz method, using for trial function $J_1(\sqrt{A'}\sigma)$ which reduces the first bracket identically to zero. Also, the second derivative in the right bracket can be reduced by recursion formulae, after which we find the approximate formula

$$\int J_1(x)J_1'(x)dx - (1-\alpha^2/A')\int J_1^2(x)dx = (A'-A-1)\int J_1^2(x)d(\log x), \quad (12)$$

where the limits of integration are zero and $x = 2.405$ where the derivative of $xJ_1(x)$ vanishes. Carrying out the integrations we find

$$A' \cong A + 2.13(\alpha^2/A') - 0.138. \quad (13)$$

Thus A' can be found from α and A. This determines σ_0, the value of σ on the boundary, since $(A')^{\frac{1}{2}}\sigma_0 = 2.405$. In this way we computed approximate values of λ, valid when $\lambda \ll a$ and these have been plotted in Fig. 7 along with the results of the numerical integration.

Plainly Q using the above functions will not differ appreciably from its value for a long circular cylinder, but there is some point in computing the shunt impedance because this depends on the effective length of said cylinder and we are in a position to determine this.

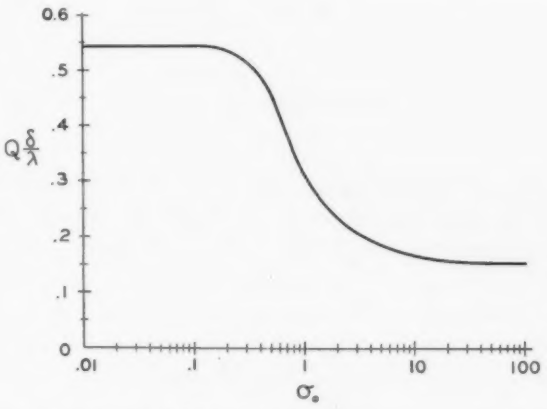

FIG. 8. Plot of $Q(\delta/\lambda)$ against σ_0 for resonators with shape of the type shown in Fig. 6.

Running through the calculation we find

$$R = 5.40(\lambda/\delta)(a/x_0)^{\frac{1}{2}}c. \quad (14)$$

This is plotted in Fig. 9 along with the exact results.

We now investigate approximations valid when $\alpha^2 \to 0$, i.e., when the interfocal distance becomes small and the shape approximates the sphere and cones of the first problem treated. Here we are able to do rather better than when $\alpha^2 \to \infty$ for we partially overcome the usual difficulty with approximate calculations, namely we are able to make some statement as to the limits of error.

This is made possible by certain developments of Stevenson's variational method. The needed new results are proved and explained in Part II; we will use these results without comment.

It is there shown that if we want to solve the equation $\nabla^2\psi_0 = -k_0^2\psi_0$ by the variation method then, for certain classes of trial function, it is useful to write

$$\nabla^2\psi = -\gamma k'^2\psi, \quad (15)$$

where k' is a constant, approximately equal to the unknown k_0 and γ is variable. Of course, if the trial function were the correct solution, we would have $k' = k_0$, $\gamma = 1$. Ordinarily γ will be approximately unity. Next we define certain

mean values, and the differences of these means from unity. Thus we write

$$\bar{\gamma}=1-\epsilon_1=\frac{\int\gamma\psi^2 d\tau}{\int\psi^2 d\tau}, \tag{16}$$

$$\bar{\gamma}^2=1-\epsilon_2=\frac{\int\gamma^2\psi^2 d\tau}{\int\psi^2 d\tau}. \tag{17}$$

Also we need a quantity $\beta=(k_0^2+k_1^2)/2k_0^2$ where k_1^2 is the first eigenvalue above k_0^2 having an eigenfunction with the same symmetry as ψ_0: this symmetry is supposed to be correctly reproduced in the trial function. Then it may be shown that the true eigenvalue, called k_0^2 above, is partially determined by the inequality

$$k'^2\left(\beta-(\beta-1)\left(1+\frac{2\beta\epsilon_1-\epsilon_2}{(\beta-1)^2}\right)^{\frac{1}{2}}\right)<k_0^2 <k'^2(1-\epsilon_1). \tag{18}$$

If ϵ_1 and ϵ_2 are small, the above can be much simplified by expanding when we find approximately

$$k'^2\left(1-\frac{\beta\epsilon_1-\epsilon_2/2}{\beta-1}\right)<k_0^2<k'^2(1-\epsilon_1). \tag{19}$$

Now we have found a trial function for which ϵ_1 and ϵ_2 are small and computable to a definite order in α: Moreover to this order $\epsilon_2=2\epsilon_1$ so that the two limits of (19) become equal and k_0^2 is determined to this order.

The trial function which does this is quite simple: it is

$$B_z\leqq\frac{1}{\sin\vartheta}\cos\varphi\frac{1}{(\rho^2-1)^{\frac{1}{2}}}\sin\alpha'(\rho-1). \tag{20}$$

Here $\alpha'(\rho_0-1)=\pi/2$, thus all the boundary conditions are satisfied. It will be observed that, for large ρ, this approaches the exact solution for the sphere with cones. Moreover, near the z axis, where $\mu\to 0$, the function (20) is linear in μ, as it should be.

Now on operating on this with ∇^2 it is found, after some manipulation, that

$$\nabla^2 B_z=\frac{-4\alpha'^2}{a^2}\frac{\rho^2-1}{\rho^2-w^2}B_z=-\gamma k'^2 B_z, \tag{21}$$

where

$$\gamma=\frac{\rho^2-1}{\rho^2-w^2},\quad k'^2=\frac{4\alpha'^2}{a^2}. \tag{22}$$

Moreover, if this be multiplied by $B_z^2 d\tau$ it will be found that all the integrations are elementary so that integral $\gamma B_z^2 d\tau$ is easily obtained.

To complete the determination of $\bar{\gamma}$ one needs also the integral of $B_z^2 d\tau$ and this turns out to be not quite so easy. In fact we find

$$\int B_z^2 d\tau=\frac{a^3\pi}{4}\left(\tfrac{1}{2}(\rho_0-1)\tanh^{-1}w_0 +w_0\int_1^{\rho_0}\frac{\sin^2\alpha'(\rho-1)}{\rho^2-1}d\rho\right). \tag{23}$$

It can easily be shown, however, that if the ρ^2-1 in the denominator be replaced by $(\rho-1)^2$ the integral will be changed by a fractional amount α'. We neglect this after which the integration is easily performed in terms of *Si* integrals and so we find integral $B_z^2 d\tau$ correct to α'^2. An exactly similar approximation must be made when computing the integral of $\gamma^2 B_z^2$. Making these approximations we find

$$\bar{\gamma}=\frac{1}{1+\dfrac{1.216\pi w_0}{(\rho_0-1)^2\tanh^{-1}w_0}}, \tag{24}$$

$$\bar{\gamma}_2=\frac{1-\dfrac{1.216\pi w_0}{(\rho_0-1)^2\tanh^{-1}w_0}}{1+\dfrac{1.216\pi w_0}{(\rho_0-1)^2\tanh^{-1}w_0}} \tag{25}$$

and these are both correct to terms in $1/\rho_0^2$, but not higher.

Now, to this order, $\epsilon_2=2\epsilon_1$, so that the upper and lower bounds for k_0^2 are the same. Thus we can write an approximate formula, good to $1/\rho_0^2$,

$$(\alpha\sigma_0)^2\leqq\left(\frac{2\pi x_0}{\lambda}\right)^2 =\left(\frac{\pi}{2}\right)^2\frac{\rho_0+1}{\rho_0-1}\frac{1}{1+\dfrac{1.216\pi w_0}{(\rho_0-1)^2\tanh^{-1}w_0}}, \tag{26}$$

where x_0 is the equatorial radius. This formula

also has been plotted in Fig. 7 and it will be seen to be amazingly good.

As to Q and the shunt impedance, it is felt not worth while to compute them using this approximate wave function. However a rather general remark on approximate formulae for Q may be of interest. We observe from the formula

$$\frac{\delta}{\lambda}Q=2\sqrt{2}\frac{\int \mathbf{B}^2 d\tau}{\lambda\int \mathbf{B}^2|d\boldsymbol{\sigma}|}, \tag{27}$$

that $Q(\delta/\lambda)$ depends on $(1/\lambda)$ times the ratio of a volume to a surface integral. Now the ratio of the volume to the surface integral will involve some dimension of the resonator (x_0 in the present case) and a numerical factor depending on the geometry of the resonator and the function B. Now it often happens that this numerical factor can be shown to be relatively constant, in which case $Q(\delta/\lambda)$ depends principally on the ratio of resonator size to λ. In the present case, for example, a fairly good, and very simple, approximation is obtained by altering the Q value for a sphere with cones in accordance with changes in x_0/λ: the formula so obtained is

$$Q(\delta/\lambda) \leqq 4x - x(x_0/\lambda).$$

Similar remarks may be made about the shunt impedance, the formula for which may be put in the form

$$\frac{\delta}{\lambda c}R=16\pi^2\sqrt{2}\frac{[\int \mathbf{B}\cdot d\boldsymbol{\sigma}_2]^2}{\lambda^2\int \mathbf{B}^2|d\boldsymbol{\sigma}|}, \tag{28}$$

where we recall that $d\sigma_2$ is an element of the cross-sectional area and $|d\sigma|$ is part of the surface of the resonator. Now the ratio of these two integrals will involve some two lengths of the resonator (or the square of one) and numerical factors depending on B and the resonator shape. Sometimes this numerical factor is relatively constant in which case changes in R can be estimated by estimating the change of the ratio of the above-mentioned two lengths to λ^2.

§2. Calculations on cylinders with cross sections similar to those of the figures of revolution of Section 1

We now set out to repeat for infinitely long cylinders the work of the preceding section on figures of revolution. We note first that such calculations are of more practical interest than might appear from the words "infinitely long" as such a cylinder can be fairly well approximated in practice by bending a straight cylinder of

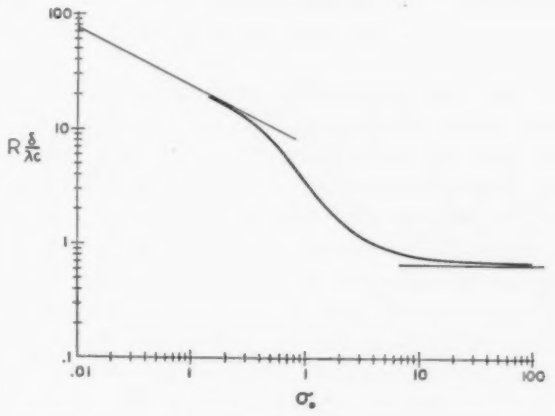

FIG. 9. Plot of $R(\delta/\lambda c)$ against σ_0 for resonators with shape of the type shown in Fig. 6. Also plotted is the approximate Eq. (14).

length large compared to its transverse extent into a ring with the same cross section. Also, we remark that, in general outline, the mathematics follows the same course as that of Section 1 so that we do not go into great detail in this section.

We start by repeating a previous observation, namely, no simple cylindrical counterpart of the sphere with two cones and a strong field between the cone points is possible.

Next, we describe the exact solution by numerical integration. For coordinates we took

$$\begin{aligned} z &= (a/2)\cosh\mu\cos\vartheta \\ x &= (a/2)\sinh\mu\sin\vartheta. \end{aligned} \tag{29}$$

So that a diagram of the coordinates would look like Fig. 6 except that we must remember that the ellipses and hyperbolae shown there are now to be considered as translated along the y axis to generate cylindrical coordinate surfaces, instead of being rotated about the z axis, as before. Now if one uses variables ρ and w like those used before one finds that the separated equations are exactly like (9a) and (9b) except that to (9a) there is added a term $\rho dR/d\rho$ and to (9b) a term $-wdT/dw$. Because of these terms it is easier to do the numerical integrations in terms of the

variables μ, ϑ, when the equations become

$$(d^2R/d\mu^2)+(\alpha^2\sinh^2\mu+A)R=0 \qquad (30)$$
$$(d^2T/d\vartheta^2)+(\alpha^2\sin^2\vartheta-A)T=0$$

with

$$B_y=R(\mu)T(\vartheta) \qquad (31)$$
$$\alpha=ka/2=\pi a/\lambda.$$

Then the numerical integration proceeds in the same way as before and after a sufficient amount of labor one finds corresponding values of α and μ_0. This time we used for ϑ_0 the value $0.8\sim46°$. The results are plotted in Fig. 10.

Then further integrations are made which give Q and the shunt impedance; these are plotted in Figs. 11 and 12. As to the shunt impedance, we note that, according to any of the definitions given, this is inversely proportional to the length l of the cylinder, in the limit of large l. This is of course because the losses are proportional to the length. We have therefore plotted shunt impedance times l/λ.

We next consider the problem of finding useful approximations, valid in the limiting cases of

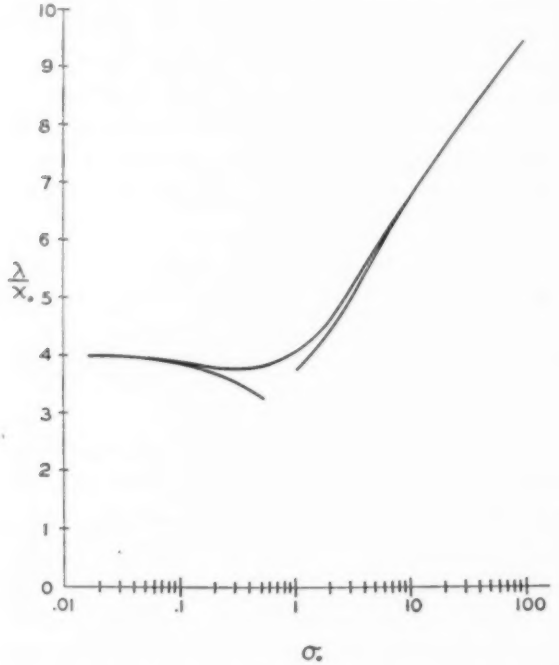

FIG. 10. Plot like that of Fig. 7 but for a resonator of cylindrical form instead of the previous figure of revolution. Cross sections for various values of σ_0 are not shown but would be similar to those of Fig. 7 except that as σ_0 is increased, the cylindrical resonators continue to shrink in width, whereas those of Fig. 7 approached a constant width (diameter).

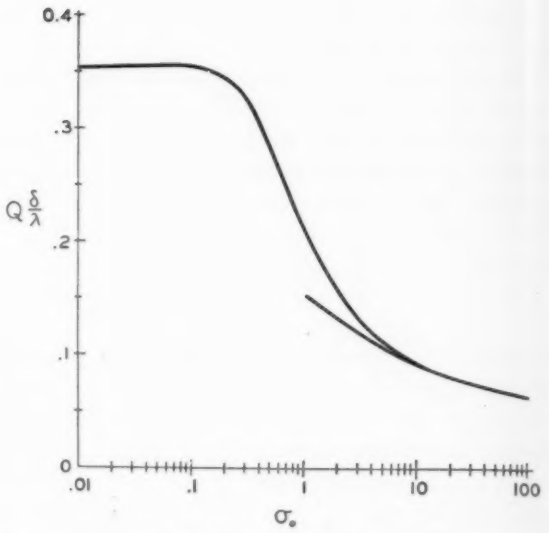

FIG. 11. Plot of $Q(\delta/\lambda)$ *vs.* σ_0 for cylindrical resonators. Also plotted is approximate formula (42).

large and small α. Proceeding much as before in the case of large α we take as an approximate solution the expression $e^{-\alpha w^2/2}$ and using this by the Ritz method find that A is given approximately by $A\leqq\alpha(\alpha-1)-1$. Then, we transform the μ equation to the dependent variable $\sigma=\sinh\mu$ and solve by the Ritz method, with trial function $\sin\sqrt{A'}\sigma$. The integrations are elementary and combining the result with the previous one relating σ_0 and A we find

$$\alpha(\alpha-1)+1.32(\alpha^2/A')-1.82\leqq A', \qquad (32)$$

to determine A' and from this $\sigma_0=\pi/(2(A')^{\frac{1}{2}})$. Using this method we have computed one of the approximate curves shown in Fig. 10. Also we have developed a formula for shunt impedance which is plotted in Fig. 12.

The approximation for small α is also done much as before though the details and the difficulties are slightly different. It seems best to use as independent variable $u=e^{\mu}/2$ and as trial function

$$B_y\leqq Z_0(\alpha' u), \qquad (33)$$

where Z_0 is a combination of Bessel and Neumann functions satisfying the boundary conditions

$$Z_0(\alpha'/2)=0, \quad Z_0'(\alpha' u_0)=0. \qquad (34)$$

Then one computes integral B^2 and integral $B\nabla^2 B$ as before. The latter reduces without

difficulty to the simple form

$$\int \mathbf{B}\cdot\nabla^2\mathbf{B}\,|d\boldsymbol{\sigma}| \leqq \int d\vartheta \int_1^{u_0} Z_0^2(\alpha' u)\alpha' u\, d(\alpha' u), \quad (35)$$

where, in the left integral, $d\boldsymbol{\sigma}$ is an element of area in the cross section of the cylinder. The integral of $\mathbf{B}^2$ is rather more complex, because the surface element is not simple in terms of u. The result is

$$\int \mathbf{B}^2\,|d\boldsymbol{\sigma}| \leqq \frac{a^2}{4\alpha'^2}\Big[\int d\vartheta\Big(\int Z_0^2(\alpha' u)\alpha' u\, d(\alpha' u) + 2\alpha'^2\int Z_0^2(\alpha' u)\, d(\log u) + \alpha'^4\int \frac{Z_0^2(\alpha' u)}{(\alpha' u)^3}\, d(\alpha' u)\Big) - \int \cos^2\vartheta\, d\vartheta \int Z_0^2(\alpha' u)\, d(\log u)\Big]. \quad (36)$$

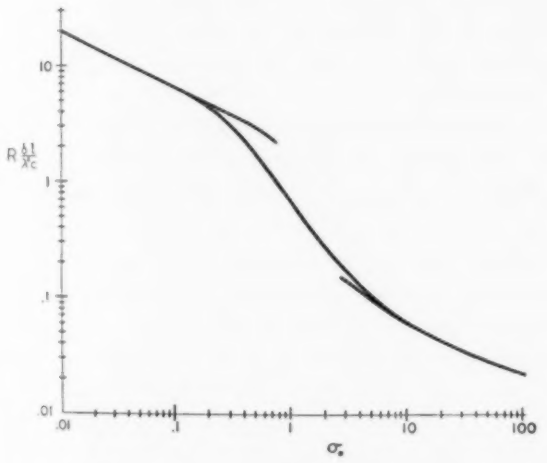

FIG. 12. Plot of $R(\delta/\lambda c)(l/\lambda)$ *vs.* σ_0 for cylindrical resonators. Also plotted are approximate formulae for same.

Now we neglect the third integral in (36) both because it isn't a known form, and because it is small of order α'^4. But even the second integral gives trouble because, though a simple formula for such integrals for integral orders of cylinder functions exists, this formula fails when the order is zero. We have therefore approximated the integral, and this is justified since it is only a correction term, by replacing $Z_0(\alpha' u)$ by $\log(2u)$. A little reflection will show that, for small α', this should be very close. Then all the integrations can be done and we find the formula, valid for small α, i.e., large u_0,

$$(\alpha\sigma_0)^2 = \left(\frac{2\pi x_0}{\lambda}\right)^2 \leqq (\alpha' u_0)^2\left(1-\frac{1}{4u_0^2}\right) \times \frac{1}{1+\dfrac{1}{6u_0^2}\dfrac{\log^3(2u_0)}{(\log(2u_0)-\frac{1}{2})^2}}. \quad (37)$$

Here u_0 is determined by the conditions (34) which may be reduced to

$$\frac{N_0(\alpha'/2)}{J_0(\alpha'/2)} = \frac{N_1(\alpha' u_0)}{J_1(\alpha' u_0)}. \quad (38)$$

Thus, for a chosen value of α' one uses (38) to find u_0, and then (37) to find $\alpha\sigma_0$. In this way a curve has been constructed which is reproduced in Fig. 10.

In general (38) is most easily solved graphically, but in the extreme limit when α' is so small that $1 \ll -\log\alpha'$ we can find the following approximate formulae

$$u_0^2 \leqq -2/\alpha'^2 \log\alpha' \quad (39)$$

and from this

$$(\alpha\sigma_0)^2 \leqq -2/\log\alpha, \quad (40)$$

so that the wave-length goes infinite logarithmically as the interfocal distance is decreased.

Finally, we have used the remarks made in connection with (27) and (28) and computed Q and R using very crude wave functions in the integrals but taking the wave-lengths from the curve of Fig. 10. In fact, we simply took B as constant over the cross section of the resonator and so found

$$Q\delta/\lambda \leqq 0.63(x_0/\lambda) \quad (41)$$

and

$$R(\delta/\lambda c)(l/\lambda) \leqq 79.3(x_0/\lambda)^3. \quad (42)$$

These are plotted in Figs. 11 and 12.

A Note on the Quantitative Spectrographic Analysis of Small Amounts of Rubidium and Potassium in Biological Materials

WILLI M. COHN
Berkeley, California

(Received August 20, 1938)

The sample is placed into the capillary of a gas discharge tube operated under standardized conditions. The emission spectrum is investigated from 3500 to 8500A. Intensity marks are printed on each plate. The blackening of the Rb and K lines is measured. Equivalent amounts of RbCl and KCl in the sample are obtained graphically from curves derived from standard samples. The method seems of special interest in cases where small samples only are available.

I. INTRODUCTION

THE determination of rubidium and potassium in biological materials is desirable in connection with work regarding the accumulation of ions, etc. Chemical determinations and ordinary spectrographic methods are difficult, particularly if only small amounts of a sample are available, see for instance Brooks.[1] The following note on the quantitative spectrographic analysis of Rb and K seems of interest, since I was unable to find a prior application of this method to biological materials. It should be mentioned that several investigators studied the spectra of alkalies in discharge tubes, for instance Filippov,[2] Cs and K; Kopfermann and Krüger,[3] Rb; and others. All these investigations were carried out, however, with highly purified alkalies and were not used for quantitative determinations as discussed here.

II. METHOD

The sample to be tested is dried and powdered to pass a 20 mesh sieve. The sample is placed into the small bulb *d* of tube *c* which is three inches long (see Fig. 1). Tube *c* is blown to the gas discharge tube *a–a'* of *V* shape equipped with capillary *b*. The length of the straight part of *b* equals 25 mm, its inside diameter amounts to 1.7 mm. The discharge tube is pumped and processed as usual, care being taken, however, to keep *d* at a low temperature while preparing the tube. I found it most advisable, after a series of experiments, to fill the tube with purified helium gas of eight mm pressure. The tube is sealed off from the exhaust system. The sample is moved by shaking into *b*; this can be achieved quantitatively with a little care, provided the sample is finely powdered and free of moisture as mentioned above. The V-shape of the discharge tube permits a uniform distribution of the powdered material along the straight part of the capillary tube *b*. An image of *b*, preferably in a horizontal position, is projected on the slit of the spectrograph.

Passing a discharge through the tube will result in the excitation of emission lines of Rb, K, etc., present in the sample. The emission of lines from the sample seems to be caused by a combination of heat and electric excitation. It was found that passing a rather high current through the tube will cause an attack of the inner wall of the capillary tube resulting in the eventual breakage of the tube. The heavy current will also cause a condensation of vapor on the coldest parts of the tube. Cooling the tube in a water jacket improved the operation of the tube, but difficulties in handling this set-up did not seem to justify the extra expense of the water jacket. We cut down, therefore, the current passing through the tube, although the time of exposure was increased. The most satisfactory results were obtained, for the tube of Fig. 1, with 30 ma and 7500 volts (a rheostat in the primary circuit of the transformer was used to compensate, as far as possible, for voltage fluctuations). The temperature of the surface of the capillary tube will not exceed, under these conditions, 50°C.

[1] S. C. Brooks, J. Cell. and Comp. Physiol. **2**, 221 (1932); **6**, 169–180 (1935).
[2] A. Filippov, Zeits. f. Physik **42**, 495–498 (1927).
[3] H. Kopfermann and H. Krüger, Zeits. f. Physik **103**, 485–490 (1936).

The spectra were taken with the first order of my Hilger grating spectrograph (dispersion 49.4A/mm). Since Rb and K show spectral lines in the visible and near infra-red regions of the spectrum, both Wratten and Wainwright Hypersensitive Panchromatic and pre-exposed Eastman 144-P or I-P plates were used to cover the range from 3500 to 8500A. A rather wide slit (0.8 mm) gave best results in the photometric reduction. The grating was preferred here to the prism spectrograph because of the uniform dispersion in the red and infra-red regions of the spectrum. This permits an accurate identification and measurement of the near infra-red Rb and K lines. With 30 ma and 7500 volts the time of exposure amounts to one minute for hypersensitive panchromatic plates, and to four minutes for I-P plates.

Each plate was standardized with a set of intensity marks by means of my neutral Zeiss wedge illuminated by a two-volt lamp which was fed from a storage battery with voltage control. Data for the wedge has been given previously.[4] The spectra and intensity marks were measured with the Zeiss recording microphotometer of the Physics Department, University of California,

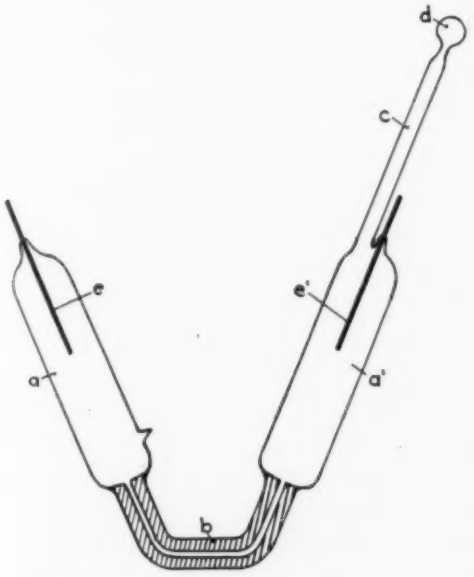

FIG. 1. Gas discharge tube. a–a'=tube; b=capillary; c=extension tube for container of sample, d; e, e'=tungsten electrodes.

[4] W. M. Cohn, Astrophys. J. 87, 284–334 (1938).

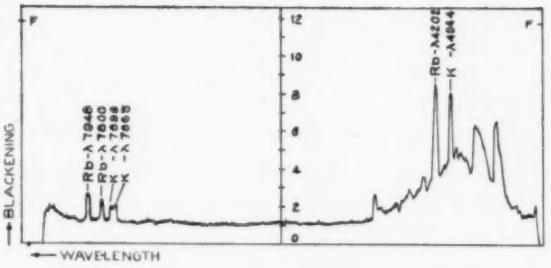

FIG. 2. Microphotometer record of spectrum from standard sample containing 20.0 mg RbCl+20.0 mg KCl; I-P Eastman Kodak plate, time of exposure 4 min.; F–F=full blackening marks.

care being taken to work always under the same standardized conditions.

III. RESULTS

Standard samples were prepared from C.P. rubidium chloride and potassium chloride in various ratios. The substances were dried and powdered to pass a 20 mesh sieve before weighing. All samples had a total weight of 40.0 mg. Several sets of spectra were taken from each of several samples. Fig. 2 presents a microphotometer record of a spectrum from a standard sample containing 20.0 mg RbCl and 20.0 mg KCl. The following persistent lines were used in this work:

Rb—λ4201.8, 7800.3, 7947.6A;
K—λ4044.2, 7664.9, 7699.0A.

The characteristic (blackening) curve of each plate was determined from the intensity marks; Fig. 3 presents a microphotometer record through one series of intensity marks (two series being printed on each plate). The blackening of the Rb and K lines in the microphotometer record was determined and converted into relative intensity.[4] (The continuous background of the spectra was kept down as much as possible; the blackening of the lines being measured above the background.) "Standard curves" were determined for blackening against concentration for the above-mentioned spectral lines of each element. It was found desirable to cover, with standard samples, the entire range of RbCl and KCl occurring in the unknown samples, in order to avoid an extrapolation of the standard curves. The original set of standards extended from 3.6 to 20.0

mg RbCl in the samples of 40.0 mg (RbCl+KCl). The results of the determinations were found to be reproducible; the average accuracy of a determination deviates from the amount of the element present in the sample by not more than ± one percent. The very small amount of gas liberated from the walls of *c–d*, Fig. 1, was found

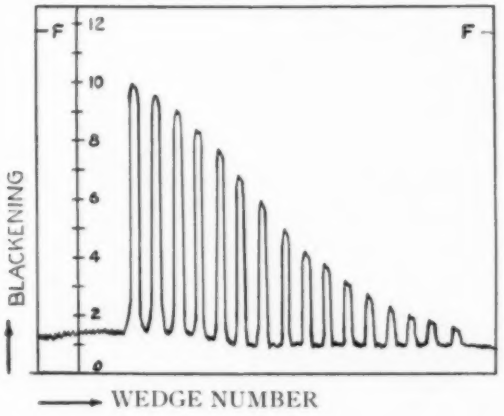

FIG. 3. Microphotometer record of one set of intensity marks on same plate as Fig. 2; time of exposure 4 min.; *F–F*=full blackening marks.

not to interfere with the accuracy of the results keeping the pressure in the discharge tube practically constant during excitation (8 mm).

The unknown samples were converted into chlorides, dried, and powdered in exactly the same manner as the standard samples. The blackening of the lines obtained from the sample gave, by using the standard curves, the equivalent amounts of RbCl and KCl in the sample.

It should be emphasized that the success of this method depends, like that of any other method of quantitative spectral analysis, on the most careful reproduction of all the details mentioned above, both while preparing the sample and while obtaining the spectra. Samples developing large amounts of gas during excitation cannot be tested in the sealed off tube of Fig. 1. Some preliminary tests indicate that such samples may be handled in a tube connected permanently to a pumping system equipped with a fine needle valve. The use of open tubes will also reduce the costs of this method, in which new tubes were prepared for individual samples of sap, etc.

IV. SUMMARY

A gas discharge tube was developed which permits processing without injury to the sample. The sample is placed into a capillary tube. Emission spectra are obtained by a combination of thermal and electrical excitation. Each plate is standardized by means of intensity marks from a neutral wedge. The blackening of the lines permits, by means of standard curves, the computation of equivalent amounts of RbCl and KCl in the sample.

ACKNOWLEDGMENTS

This work was carried out in connection with the research work of Dr. S. C. Brooks of the Zoology Department, University of California. Dr. M. M. Brooks prepared the samples. Dr. R. T. Birge permitted the use of the microphotometer of the Physics Department. Messrs. W. J. Cummings and E. H. Guyon of Berkeley, California, helped prepare the gas discharge tubes.

Measurement of Some Arc Characteristics at 1000 Atmospheres Pressure

C. G. SUITS
General Electric Company, Schenectady, New York
(Received December 5, 1938)

By an oscillographic method the total arc voltage e is measured as a function of arc current i at high pressure in a 1500-volt d.c. circuit in which i (in the 1–7 ampere range) is independent of changes in e. The e-i characteristics are taken for copper electrodes in nitrogen up to 1275 atmospheres pressure, with the result that e increases two times at $p=100$ atmos. and five times for $p=1000$ atmos. The pressure effect in helium is similar to nitrogen. Attempts to obtain measurements in hydrogen showed a striking instability of the hydrogen arc at high pressure.

INTRODUCTION

SOME measurements of the electrical constants of carbon arcs at a pressure of ten atmospheres were made by Duncan, Rowland and Todd[1] in 1893, and at a pressure of three atmospheres by Mathiesen[2] in 1918. Humphreys,[3] in 1907, studied the carbon arc spectra at pressures up to 100 atmospheres, observing the pressure shifts in the metallic lines and cyanogen bands. More recently the quartz capillary mercury lamps have been studied[4] at pressures in the range from 10 to 100 atmospheres.

It is the purpose of the present paper and some others in preparation to report on a series of measurements of the electrical characteristics of arcs in various gases in the pressure range above atmospheric. In the present paper are described some exploratory measurements in the 1–1000-atmosphere pressure range in several gases. In a paper to follow a more comprehensive study of the 1–100-atmosphere range in argon, nitrogen, helium and hydrogen will be described.

EXPERIMENTAL METHODS AND RESULTS

In initial experiments a cylindrical steel chamber with a 1″ bore and 2″ wall, equipped with a thick glass window, was used for measurements of the e–i (volt-ampere) characteristic. Starting of the arc was accomplished by means of a fine metallic wire which served as a fuse. Current was varied in definite steps by a motor-driven commutator by a method previously described.[5] This method was applied to arcs between copper electrodes through the following ranges: current 1–20 amp., arc length 1–10 mm, nitrogen gas 1–220 atmospheres. It was found that the arc drop increases slowly with pressure, that the spread in the measurements becomes serious at great arc lengths, high currents and high pressures, and that the total light intensity increases with pressure.

As a result of this experiment, two new chambers were built, one to cover the same pressure range with more convenience, and a second, hydraulically operated, to explore the pressure range above 220 atmospheres. The experiments with this hydraulic chamber will now be described in some detail. The arc chamber is shown disassembled in Fig. 1.

The construction employs a 1″ inside diameter high pressure cylinder, 1, made from a tempered and ground nickel steel inner member, over which a mild steel outer shell has been shrunk. The 1″ diameter high pressure piston, 2, is driven by a 5″ diameter piston, 3, from a water supply of 2500 lb. in.$^{-2}$ pressure. The high pressure bushing, 4, carrying a $\frac{1}{4}$″ diameter electrode, 5, together with a quartz disk, 6, for protecting the bushing from hot gas, is shown at the right in the photograph.

Following the teaching of Bridgman, we used gaskets of the unsupported area type on both the piston head and the bushing. "Sandwich" gaskets made from Glyptals of two degrees of softness served very well.

The chief design problem in this chamber is in the bushing, since the other parts can be

[1] L. Duncan, A. J. Rowland and R. J. Todd, Elektrot. Zeits. **14**, 602 (1893).
[2] W. Mathiesen, Electrician **81**, 451 (1918).
[3] W. J. Humphreys, Astrophys. J. **26**, 18 (1907).
[4] W. Elenbaas, Physica **4**, 279 (1937); W. Elenbaas and W. DeGroot, *ibid.* **2**, 807 (1935).
[5] C. G. Suits, Phys. Rev. **46**, 252 (1934).

built for whatever strength the bushing will allow. The bushing, however, must stand moderately high voltages in the presence of hot arc gas, which imposes a limit on the insulation creepage path. The best solution of this problem was found in a glass-to-metal seal, hot pressed. These seals, which have long been used in a commercial process, are made by fusing a glass bead to a central conductor of Dumet and an outer steel tube with tapered bore. The materials are so chosen that when pressed and cooled the glass is under compressional strain. In the size used in this experiment the bushing will stand a high potential test (in air at N.T.P.) of 4 kv. They have been used repeatedly at 3600 atmospheres without a failure of any kind. The compressional strain is important; a series of strain-free bushings of the same size failed uniformly at approximately 2000 atmospheres. This means is an important addition to high pressure technique.

To allow maximum arc stability the current is supplied from a 1500-volt d.c. source through a 10-kw pliotron, operated as an emission-limited two-element tube. In this way the arc current i is maintained at a value which is entirely

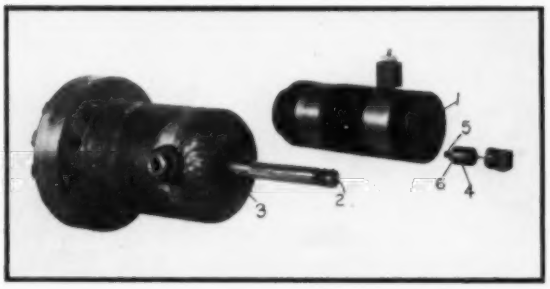

FIG. 1.

independent of the arc potential drop e, provided the latter does not exceed approximately 1000 volts.

Up to 1360 atmospheres the pressures are read directly by gauge. Up to 3600 atmospheres the pressure can be calculated from the average pressure on the low pressure piston for up and down strokes. Tests at 1000 atmospheres, however, showed that the latter method is susceptible to large uncertainties, so that the data reported all lie in the range of pressures readable by gauge.

In this chamber the observable quantities are the arc current, i, total arc voltage, e, and e as $f(i)$ for various gases, pressures and electrode materials. Some light is transmitted through the glass seal, so that changes in the spectrum might be studied. It is possible that the glass surfaces at the seal could be ground sufficiently plane to allow the transmission of an image of the arc, or that an auxiliary pressed glass window could be mounted in the bushing.

The e–i characteristic of the arc was recorded as follows: The arc chamber was filled with gas of 99 percent purity from high pressure cylinders at pressures up to a maximum of 200 atmospheres. By slowly forcing the small piston, which carried one electrode, into the cylinder the pressure was raised until the volume of the arc space was approximately 15 cc. The upper electrode, supported by the glass bushing, carried a three-mm length of fine wire of the electrode material. The establishment of contact between this fuse wire and the lower electrode determines the arc length, starts the arc, opens the filament circuit of the pliotron, and starts the oscillograph. The pliotron filament current is initially adjusted for a saturation current (arc current) of approximately ten amperes, and when this circuit is opened, the filament temperature drops, causing the arc current to decrease from ten amperes to zero in about one second. Subsequently a saturable core reactor was inserted in the filament circuit, so that this decay rate could be varied between one and ten seconds. The oscillograph thus records the volt-ampere characteristic at a known arc length and pressure. The time required to establish the steady state in the high pressure arc is very small,[6] so that the data obtained by this method can be regarded as steady-state values. Since the rate of increase and the rate of decrease of arc current varied considerably in a given record, a comparison of e and E at the same current at two different points of an oscillogram would show differences if steady-state properties were not fully developed. No systematic differences of this kind were found under the conditions of our experiments.

The arc characteristic may be expected to depend upon the gas and its pressure if metal

[6] C. G. Suits, Gen. Elec. Rev. **39**, 194 (1936).

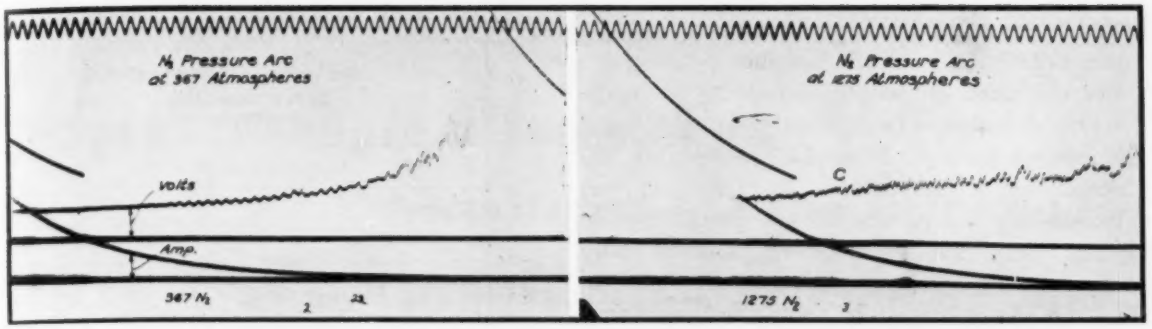

(a) (b)

FIG. 2.

vapor from the electrodes is not a contaminant in the arc atmosphere. Favorable experimental conditions for obtaining an arc characteristic which does depend upon the gas and its pressure are obtained by the use of tungsten, pure carbon, or polished copper electrodes,[7] over limited ranges of current and pressure. In the case of the copper electrodes the high conductivity acts to limit the temperature and vapor pressure, while with tungsten and carbon the high boiling point performs this function. In the case of the experiments at the highest pressures (*ca.* 1000 atmos.), polished copper electrodes were chosen as the most satisfactory from the above standpoint. The effect of metal vapor on the reported results must, however, remain open to some question. Indirect evidence indicates that a good deal of copper vapor was present in the arcs at highest pressures and especially in hydrogen.

Oscillographic records showing the character of the data obtained by the method described appear in Fig. 2, (a) and (b) for nitrogen at pressures of 367 atmospheres and 1275 atmospheres. From a set of approximately 60 records, the e–i characteristics have been plotted with pressure p as parameter, and from this set the curves of Fig. 3 are obtained, where e is shown as $f(p)$ with i as parameter, for an arc length of 3 mm. The arc voltage e is seen to increase slowly with pressure; thus e increases approximately two times at $p=100$ atmos., and five times at $p=1000$ atmos. The detailed results show an increasing spread as p increases, so that an uncertainty of ± 15 percent in e is present at $p=1000$ atmos. The relative value of e for changes in p are more accurate, however.

The causes for the spread in the measurements at high pressures are to be found partly in movements of the arc column due to convection currents. These movements cause a lengthening of the arc and a corresponding increase in arc voltage; the effect has since been studied in some detail at lower pressures. Instability of other types, not entirely explained, arises at pressures above one atmosphere in nitrogen. At a pressure of one atmosphere the arc between polished copper electrodes in air or nitrogen shows a regular arc voltage, nearly free from fluctuations.[7] At pressures above 30 atmospheres, however, a periodic fluctuation in e and I occurs. This is shown in Fig. 2(a) particularly well. The effect is not associated with changes in arc length. The frequency of this fluctuation is nearly independent of current and varies with pressure, being 70 periods per second at $p=300$ atmos. and 180 periods per second at $p=1000$ atmos. for copper electrodes. At the same pressure the frequency is higher with tungsten electrodes. Other causes of instability seem to be definitely associated with cathode phenomena. A discussion of this case will be deferred to a later paper.

ARCS IN HELIUM AND HYDROGEN AT HIGH PRESSURE

Under otherwise identical conditions e as $f(i)$ characteristics were taken in helium (99 percent purity) at 1, 81 and 200 atmospheres. The oscillograms show that the volt-ampere characteristics and the change with pressure in

[7] C. G. Suits, Physics **5**, 380 (1934).

helium are comparable to nitrogen but lie somewhat higher in absolute value.

For the same arc length and electrode conditions the experiments were extended to hydrogen (99 percent purity). After 12 attempts at 100 atmospheres it was found that the arc was extinguishing by virtue of its instability so rapidly that the oscillograms showed only vertical traces where the current decreased to zero and the voltage rose to the full generator value. At this pressure the arc duration was less than 0.01 sec. Positive evidence that the arc started was available, however, from the appearance of the electrodes. These electrodes, of copper, were initially brightly polished;[7] after each attempt to strike the arc, in spite of the very short duration of the arc, the entire surfaces of both electrodes were eroded so that they had the appearance of having been sandblasted. To increase arc stability the electrode separation was decreased to one mm; the pressure range between 220 atmos. and 20 atmos. was further explored without discovering sufficient stability to permit oscillographic data. The great instability of the hydrogen arc at high pressure is a striking effect, particularly when the stable circuit conditions are considered.

Discussion

From these explorative measurements the general character of the change in the electrical characteristics of the arc with pressure in various gases was determined. The arc properties which are of the most importance for the interpretation and theory are the electric gradient E (volts cm^{-1}) and current density I (amp. cm^{-2}). The preliminary results pointed to the necessity for developing a new measurement method for E at high pressure, if this quantity was to be determined with any pretense of precision. The conventional method is to calculate E from the volt-ampere characteristic at several arc lengths. At a pressure of one atmosphere in air and with stable electrode conditions (e.g., with a thermionic cathode) this can be done with fair accuracy. It can be done with good accuracy if air-stream stabilizing methods of fixing the position of the arc column are used. As pressure increases, however, the various types of instability cause

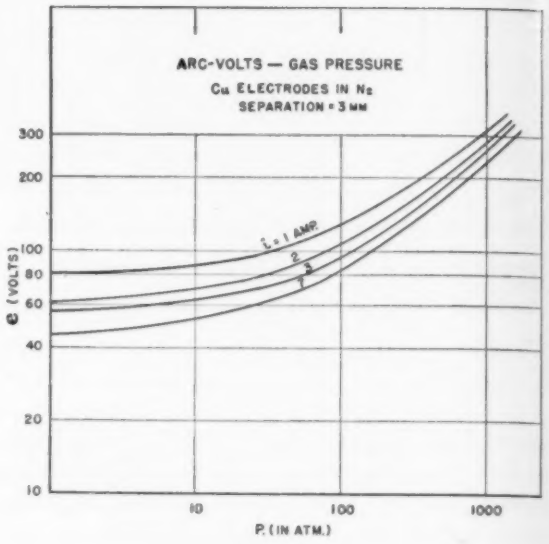

Fig. 3.

the spread in the measurements to be so great that the accuracy in determining E by this method is negligibly small.

In an arc in nitrogen at one atmosphere, five amperes, and ten mm length the total arc voltage e is approximately 80. If the length is reduced to three mm, the voltage e is reduced to 48,[8] so that the change in voltage produced in the positive column is relatively small. It is precisely this small quantity which must be measured in the presence of a large spread in e. At the highest pressures the available range of arc lengths is too limited to permit an accurate measurement of E even if other causes of instability were eliminated. A new method for measuring E which provides a satisfactory solution for these problems will be described in a separate paper.

It is clear that the development of high gradients and instability with pressure for such practical purposes as circuit interruption are possibilities; but that in general substantial pressures must be accommodated by the structure. In small devices, however, almost any structure that will support itself will tolerate sufficient pressure to show the arc pressure effect.

Acknowledgment is gratefully given to Mr. S. O. Evans, who assisted in the design of the chamber.

[8] See reference 7, Fig. 7.

Spectroscopic Plates, Type V

Sensitized for the Infrared

EASTMAN SPECTROSCOPIC PLATES, TYPE V, are now available with Classes N, R, P, and U infrared sensitizing. These plates are of high contrast, high resolving power, and very fine grain structure . . . they are especially adapted for use in spectrographs of high aperture and low dispersion.

When ordering, specify "Eastman Spectroscopic Plates, Type V-N, V-R, V-P, or V-U." These plates are not as yet listed in the booklet, *Photographic Plates for use in Spectroscopy and Astronomy*, but the information therein concerning sizes, prices, etc., applies.

EASTMAN KODAK COMPANY

Research Laboratories **ROCHESTER, N. Y.**

TWO IMPORTANT NEW BOOKS

Sutton—**DEMONSTRATION EXPERIMENTS IN PHYSICS**

Edited by RICHARD M. SUTTON, Haverford College. 545 pages, 6 x 9. $4.50

This collection of nearly twelve hundred lecture experiments in physics was prepared under the auspices of the American Association of Physics Teachers, with contributions from two hundred physicists in one hundred thirty institutions. Descriptions of experiments are direct; every demonstrable principle of physics has been illustrated by one or more experiments; in many cases, experiments are described for which published accounts have not hitherto been available.

Burington and Torrance — **HIGHER MATHEMATICS. With Applications to Science and Engineering**

By RICHARD S. BURINGTON and CHARLES C. TORRANCE, Case School of Applied Science. 838 pages, 6 x 9. $5.00

Designed primarily to meet the growing needs of students interested in the applications of mathematics to physics and engineering, this new book emphasizes physical meanings of the various notations and relationships encountered in the subject. The precise mathematical interpretations of the concepts studied here have also been stressed. Emphasis has been placed on the conditions which must be met for a given theorem or formula to be valid, and no pains have been spared to make every proof complete.

Send for copies on approval

McGRAW-HILL BOOK COMPANY, Inc.

330 West 42nd Street **New York, N. Y.**

Please mention this journal when writing to advertisers

REPORTS ON PROGRESS IN PHYSICS

VOLUME V (1938)

445 pages: Illustrated *$5.00 post free* *Bound in cloth*

A COMPREHENSIVE REVIEW

by leading physicists and under the general editorship of Prof. Allan Ferguson

THE CONTENTS INCLUDE CHAPTERS ON

ABSOLUTE ELECTRICAL MEASUREMENTS
PLASTICS IN INDUSTRIAL PHYSICS
AIDS FOR DEFECTIVE HEARING
TEACHING OF PHYSICS IN SCHOOLS
X-RAYS AND γ-RAYS IN MEDICINE
ELECTRIC WAVE FILTERS
THE GEIGER COUNTER
QUANTUM MECHANICS
THE LIQUID STATE
SOFT X-RAY SPECTROSCOPY OF THE SOLID STATE
ATOMIC PHYSICS
SOUND
ASTRONOMY
METEOROLOGY
HEAT
OPTICS
SPECTROSCOPY
ELASTICITY
SURFACE TENSION
VISCOSITY

Orders, with remittance, to

The Physical Society, 1 Lowther Gardens, Exhibition Road, London, S.W.7, England.

NUCLEAR PHYSICS

DR. H. A. BETHE and his associates, Drs. R. F. Bacher and M. S. Livingston, have written a thorough and comprehensive review of the developments in the field of nuclear physics for the American Physical Society's quarterly publication, *Reviews of Modern Physics.*

•

Part A. Stationary States of Nuclei by H. A. BETHE AND R. F. BACHER. 148 journal pages (222 book pages). April, 1936 issue. The original edition has been sold out.
Price of reprinted edition, per copy **$1.75**

•

Part B. Nuclear Dynamics, Theoretical by H. A. BETHE. 176 journal pages (264 book pages). April, 1937 issue. Price per copy **$1.20**

•

Part C. Nuclear Dynamics, Experimental by M. S. LIVINGSTON AND H. A. BETHE. 146 pages (230 book pages). July, 1937 issue. Price per copy **$1.20**

•

As their titles indicate these three timely reviews cover every aspect of what is today known about the nuclei of atoms. In a field of knowledge which is growing at such an unprecedented rate they perform the invaluable service of integrating in an unbiased but critical manner the information contained in the thousands of nuclear research papers written during the past few years.

REVIEWS OF MODERN PHYSICS is available on subscription as follows:

	Domestic	Foreign
To members	$3.00	$3.40
To all others	4.00	4.40

Send orders for separate copies or for subscriptions with remittance to

American Institute of Physics
175 Fifth Avenue, New York, New York

A LUMMER-BRODHUN PHOTOMETER

of Improved Design

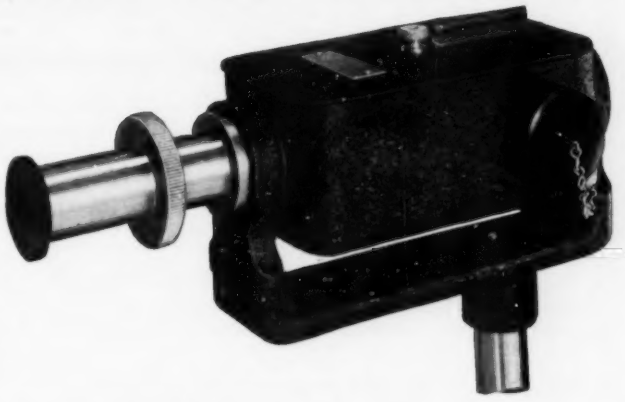

This instrument serves either as a Contrast or as an Equality-of-Brightness Photometer.

The eyepiece is concentric with the axis of rotation of the box, increasing the convenience in use. The conversion to an Equality-of-Brightness Photometer is accomplished by swinging the contrast glasses (which are mounted on a pivoted frame) out of the field. The entrance holes have dust proof caps. The reflecting surfaces are on opposite sides of a reversible screen. The box is rotable through 180°; stops are provided. Construction is precise and durable throughout.

PHOTOMETER BENCHES

Photometer benches can be furnished to any desired specifications. A standard model consisting of a double rail bench 320 cm long, three carriages, a universal mounting for the specimen lamp with horizontal and vertical angular scales, a fixed mounting for the standard lamp, a photometer box as described above, and a standard lamp, is priced at $265.00.

THE GAERTNER SCIENTIFIC CORPORATION
1212 WRIGHTWOOD AVENUE, CHICAGO, ILLINOIS

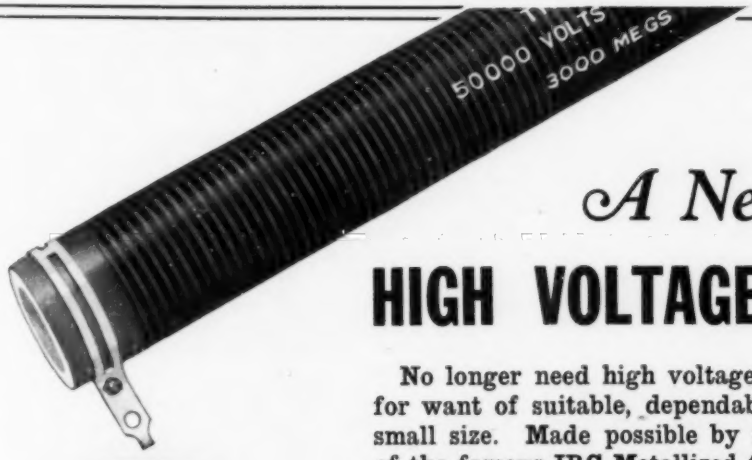

A New Tool for
HIGH VOLTAGE RESEARCH

No longer need high voltage research be handicapped for want of suitable, dependable resistors in convenient small size. Made possible by a unique spiral formation of the famous IRC Metallized type resistance element on a ceramic base, IRC Type MV Resistors pave the way for new engineering conceptions in the handling of difficult high voltage protection and measurement problems. Made in 5 standard sizes from 1 to 150 watts and from 150 to 10,000 meg. Many special units also available for experimental use. Write for IRC Resistance Engineering Data Booklet, Section 2.

IRC

TYPE MV METALLIZED HIGH VOLTAGE RESISTORS

INTERNATIONAL RESISTANCE CO., 419 N. Broad St., Philadelphia, Pa.

RECENT BOOKLETS ON INSTRUMENTS AND MATERIALS

For the convenience of our readers we list these booklets with a key number for each publication. A coupon is supplied at the bottom of the page. If you wish several booklets, jot down the key numbers on the coupon or a postcard, together with your full business address, and mail to this journal and we will have them sent to you.

61. **Elmometer and Precision Apparatus for the Measurement of Dielectric Constants.** P. J. KIPP & ZONEN, *Delft, Holland.* Leaflet. Pp. 14, illustrated, 19½×26½ cm.

62. **Science Textbooks and Reference Works.** LONGMANS, GREEN AND COMPANY, *114 Fifth Avenue, New York, N. Y.* Catalog. Pp. 100, 13½×20½ cm.

63. **Catalog of McGraw-Hill Books.** MCGRAW-HILL BOOK PUBLISHING COMPANY, *330 West 42 Street, New York, N. Y.* Pp. 292, 15×22½ cm.

64. **Keep In Touch With Developments.** REINHOLD PUBLISHING CORPORATION, *330 West 42 Street, New York, N. Y.* List of ACS Books. Pp. 8, 23×30 cm.

65. **G-M Comments.** G-M LABORATORIES, INC., *1733 Belmont Avenue, Chicago, Ill.* House organ with news on electrical instruments. Pp. 8, illustrated, 21½×28 cm.

66. **Auditorium Color Slide Delineascope.** SPENCER LENS COMPANY, *19 Doat Street, Buffalo, N. Y.* Booklet. Pp. 4, illustrated in full color, 18×25½ cm.

67. **Save Money by *p*H Control.** W. A. TAYLOR & CO., INC., *872 Linden Avenue, Baltimore, Md.* Folder on new slide Comparator. Pp. 4, illustrated, 21×28 cm.

68. **The Testing of Finished Pieces of Plastic and Moulded Insulating Materials for Physical Properties.** TESTING MACHINES, INC., *460 West 34 Street, New York, N. Y.*. Reprint (Bulletin No. 20584). Pp. 12, illustrated, 21×29½ cm.

69. **Operation of Rotary Oil and Condensation Pumps and General Vacuum Technique.** W. M. WELCH MANUFACTURING COMPANY, *1515 Sedgwick Street, Chicago, Ill.* Booklet. Pp. 20, illustrated, 18×26 cm.

70. **Whiting Filters.** WHITING FILTERLITE CORPORATION, *1674 Broadway, New York, N. Y.* (Transmitting "White Light" to Produce Color Effects.) Booklet. Pp. 4, illustrated, 19½×26 cm.

71. **Spectrometric Equipment.** BAUSCH & LOMB OPTICAL COMPANY, *Rochester, N. Y.* Catalog D-221. Pp. 24, illustrated, 21½×28 cm.

72. **New and Improved Equipment for Type 333⅜" Coaxial Transmission Line.** COMMUNICATION PRODUCTS, INC., *245 Custer Avenue, Jersey City, N. J.* Catalog Supplement No. 1. Pp. 6, illustrated, 21½×28 cm.

73. **Du Mont Oscillographer.** ALLEN B. DU MONT LABORATORIES, INC., *2 Main Avenue, Passaic, N. J.* Bi-monthly publication devoted to cathode-ray tubes and their applications. Pp. 4, illustrated, 15×28½ cm.

74. (a) **Synchrometer.** (b) **Photo-Electric Colorimeter.** (c) **Bio-photometer.** FROBER-FAYBOR COMPANY, *4610-12 Prospect Avenue, Cleveland, Ohio.* Leaflets. Pp. 4, illustrated, 21½×28 cm.

75. **The General Radio Experimenter.** THE GENERAL RADIO COMPANY, *30 State Street, Cambridge, Mass.* Issued ten times a year and contains descriptions of recent developments in the field of electrical instruments. Illustrated, 15½×28 cm.

76. **Mechanical Topics.** THE INTERNATIONAL NICKEL COMPANY, INC., *67 Wall Street, New York, N. Y.* Quarterly publication devoted to mechanical problems with alloys. Pp. 8, illustrated, 21½×28 cm.

77. **Manually-Operated Indicators for Thermocouple Temperatures.** LEEDS & NORTHRUP COMPANY, *4907 Stenton Avenue, Philadelphia, Pa.* Catalog N-33a(5). Pp. 4, illustrated, 19½×27 cm.

78. **Fold-O-Leg Laboratory and Work Tables.** MITCHELL MANUFACTURING COMPANY, *Milwaukee, Wis.* Folder. Pp. 4, illustrated, 21½×28 cm.

79. **Sigma Relays, Enclosed Switch—Sensitive—Acoustical Switch and Audio Frequency.** SIGMA INSTRUMENTS, INC., *Belmont, Mass.* Leaflets. Pp. 4, illustrated, 21½×28 cm.

80. **Current and Potential Transformers.** R. E. UPTEGRAFF MANUFACTURING COMPANY, *7522 Meade Street, Pittsburgh, Pa.* Folder. Pp. 4, illustrated, 21½×28 cm.

JOURNAL OF APPLIED PHYSICS
175 FIFTH AVENUE, NEW YORK, N. Y.

Please send me the booklets listed by key numbers below:

....

Name..... **Title**.....

Business connection.....

Address..... **Place**.....

Two Outstanding Physics Texts

DUFF
Physics
8th EDITION

(For Students in Science and Engineering)

This text presents a sound and substantial treatment of the fundamentals of general physics for students of science and engineering. Now in its eighth edition, it is the mature work of experienced teachers.

627 Illus. *715 Pages.*
Washable Fabric $4.00.

By A. W. Duff (Editor), Worcester Polytechnic; E. P. Lewis, Revised by F. A. Jenkins (Calif.); Chas. E. Mendenhall, Revised by L. R. Ingersoll (Wisc.) and R. J. Stephenson (Chicago).

FOLEY
College Physics
2d EDITION

(For Students in Liberal Arts)

This book is giving exceptional satisfaction in over 350 colleges. It is characterized by clarity and forcefulness of presentation, an abundance of original illustrations and a fortunate choice of problems. There is a teacher's handbook.

466 Illus. *777 Pages.*
Washable Fabric $3.75.

By Arthur L. Foley, Ph.D., Indiana University.

P. Blakiston's Son & Co., Inc., Philadelphia

SPECTROMETER

An outstanding **WELCH SPECIALTY.**

R. W. WOOD Design.

An outstanding design of an inexpensive, yet precise and practical Replica Grating Spectrometer.

THE LATEST SPECTROMETER
Mounted on a separable base so that the spectrometer may be removed from the base and held by the convenient handle in any desired position.

"Brightline" type replica grating, 15 times more brilliant than all other commercially available replicas.

Spectrometric measurements can be made on a moment's notice—assured accuracy of less than 50 Angstroms. Quick observations possible in complicated laboratory set-ups. Brilliant brightline spectra easily observed from vacuum tubes or by ordinary flame method without darkening the room.

The scale is graduated in Angstroms from 4000 to 7500 and mounted on a ground glass plate giving a brilliant easily read scale. An adjustable slit is provided and on the same bracket is a holder for filters for studying absorption lines.

Write for complete circular.

W. M. Welch Scientific Company
Established 1880

1515 Sedgwick Street Chicago, Illinois, U.S.A.

WELCH

Scientific Instruments—Laboratory Apparatus. Catalog lists more than 10,000 items covering all the sciences.

New **SENSITIVE ELECTRONIC AC VOLTMETER**

Ideal for Research and Teaching

10 to 100,000 cycles

Range .001 to 100 volts

Logarithmic scale

AC or DC operated models

Stable calibration

Accurate and compact

Operating on a new principle—capable of reading down to one millivolt and up to 100 volts (or 1,000 volts with multiplier) over an extremely wide frequency range with an overall accuracy of 2 percent—single (logarithmic) scale to read for all ranges—unaffected by changes in line voltage or tubes—can also be used as an amplifier (70 DB gain), flat to 100,000 cycles.

Send for Bulletin 2H

Ballantine Laboratories, Inc.

BOONTON NEW JERSEY

SYNTHETIC CRYSTAL OPTICS

The Harshaw Chemical Company is producing optical crystals of:

LITHIUM FLUORIDE
ROCK SALT
POTASSIUM BROMIDE
SODIUM NITRATE

Prices and specifications will be furnished on request.

THE HARSHAW CHEMICAL CO.

SPECIAL PRODUCTS DIVISION

CLEVELAND, OHIO

NEW SHALLCROSS

Single Decade Resistances mounted on a ceramic switch with engraved bakelite panel and ceramic binding posts.

No. 544—10 x		1	ohm	accuracy	0.25	of	1%
No. 545—10 x		10	"	"	0.1	"	"
No. 546—10 x		100	"	"	"	"	"
No. 547—10 x		1,000	"	"	"	"	"
No. 548—10 x		10,000	"	"	"	"	"
No. 549—10 x		100,000	"	"	"	"	"
No. 550—10 x	1,000,000		"	"	"	"	"

Send for Bulletin No. 2405A

SHALLCROSS MFG. COMPANY

Resistors . Switches . Instruments

Collingdale, Pa.

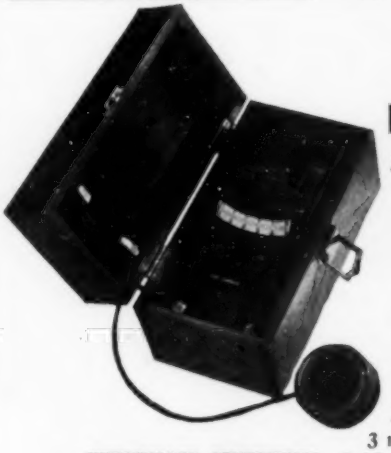

PHOTRIX UNIVERSAL PHOTOMETER

MODEL A:
4 measuring ranges
With single cell:
0-2.5, 0-10, 0-50, 0-250 ft. cdl.
$57.00

With double cell:
0-0.25, 0-1, 0-5, 0-25 ft. cdl.
$100.00

MODEL B:
3 measuring ranges
0-12, 0-60, 0-1000 ft. cdl.
$37.50

UNEQUALLED SENSITIVITY
PERMANENT STABILITY

ALSO INDIVIDUAL PHOTOCELLS:

ELECTROCELL

SELF-GENERATING PHOTO-ELECTRIC ELEMENTS
(Barrier Layer Cells)

Great variety of sizes and shapes.
Round cells from ½" to 2½" diam.
Unmounted or mounted.

DR. F. LOEWENBERG

10 East 40th St. New York City

IMPROVED "SPOTLIGHT" GALVANOMETERS

Rubicon **MULTIPLE REFLECTION** galvanometers have recently been improved through a redesign of the optical system. The definition of the line-image is now so sharp that readings can be estimated to .1 of a millimeter division.

These sturdy, self-contained galvanometers are available with sensitivities as high as .0006 microampere per millimeter. The scales, which are 100 mm. long, are remarkably proportional. Send for Bulletin 320.

RUBICON COMPANY

ELECTRICAL INSTRUMENT MAKERS

29 North Sixth Street Philadelphia, Pa.

2½" Portable Type A. C. or D. C.

FERRANTI ELECTROSTATIC VOLTMETERS

FEATURES

- Zero Consumption
- Magnetic Damping
- Self-Contained Over-voltage Protection
- Reading 20 to 25,000 Volts
- A. C. or D. C. up to 3,500 Volts
- Flush, Projecting and Portable Types
- 2½-inch, 3¼-inch and 4-inch Dials
- Single, Dual and Triple Ranges

WHERE accurate voltage measurements are required in high impedance circuits, the Ferranti Electrostatic Voltmeter has a multitude of applications. Up to 3500 volts these instruments can be directly connected to either A. C. or D. C., and are absolutely independent of wave form, frequency and temperature.

Send for New Illustrated Bulletin

FERRANTI ELECTRIC, INC. 30 Rockefeller Plaza New York City

An Unusual Type of PORTABLE OHMMETER

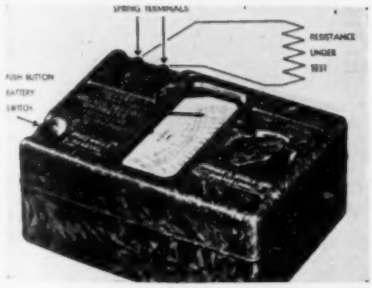

MIDGET "MEGGER" CIRCUIT TESTING OHMMETER

Quite **different from a voltmeter calibrated in ohms,** this direct-indicating "Megger" Ohmmeter requires no adjustment for the voltage of the battery that supplies current for the test. The instrument is a *true* ohmmeter of the "Megger" cross-coil type, having great flexibility as to range, and is remarkably accurate and reliable. Well adapted for laboratory, shop and portable use for checking coils, resistors, contacts, windings, circuits, relays, etc. down to .1 ohm, and even insulation resistance up to 200,000 ohms. Mounted in molded case, mottled green in color. Write for descriptive Bulletin 1495-R.

JAMES G. BIDDLE CO.

ELECTRICAL INSTRUMENTS

1211-13 ARCH STREET PHILADELPHIA, PA.

A

GEORGE C. WYLAND

PRODUCT

X-Ray Non-Symmetrical Focusing Identification Camera. Mounted on full universal stand. Completely adjustable. Camera is detachable without changing adjustments.

GEORGE C. WYLAND

RAMSEY, NEW JERSEY

INDEX TO ADVERTISERS

Name	Page
BALLANTINE LABORATORIES, INC. — Sensitive Electronic AC Voltmeter, 10 to 100,000 cycles, range .001 to 100 volts.	xii
BAUSCH & LOMB OPTICAL CO. — Makers of Microscopes, Microtomes, Colorimeters, Refractometers, Spectrometers, Balopticons, Photomicrographic and Microprojection Apparatus and related instruments. Also makers of Orthogon Eyeglass Lenses for Better Vision.	v
JAMES G. BIDDLE COMPANY — "Jagabi" Rheostats; Adam Hilger and Kipp & Zonen Optical Instruments; "Pointolite" Lamps; Electrical Testing and Speed-measuring Instruments.	xiii
P. BLAKISTON'S SON & CO., INC.	xi
CAMBRIDGE UNIVERSITY PRESS	iii
CENTRAL SCIENTIFIC COMPANY — Manufacturers of Cenco Physical Apparatus and Instruments to meet all requirements of University, College and High School Physics Laboratories—Educational Distributors of Leeds and Northrup Electrical Measuring Instruments, Weston Electric Meters, Paulin Barometers, etc.	Cover 4
EASTMAN KODAK COMPANY — Purified Organic Chemicals for research purposes; Plates for Photography, Photomicrography, Spectroscopy, Photometry, Astronomy; Wratten Light Filters; Cameras and Films.	vii
THE EPPLEY LABORATORY, INC. — Standards of e.m.f. (standard cells). Precision electrical instruments; potentiometers, bridges, temperature bridges, volt boxes. Thermopiles and pyrheliometers.	iv
FERRANTI ELECTRIC, INC.	xiii
GAERTNER SCIENTIFIC CORP. — Spectroscopes, Spectrometers, Spectrographs, Spectrophotometers, Heliostats, Measuring Microscopes, Comparators, Cathetometers, Reading Telescopes, Interferometers, Chronographs, Dividing Machines, etc.	ix
GENERAL RADIO COMPANY — Manufacturers of electronic measuring instruments; vacuum-tube voltmeters, amplifiers and oscillators; wave analyzers, noise meters and analyzers, stroboscopes; laboratory standards of capacitance, inductance and frequency; impedance bridges, decade resistors and condensers; air condensers and variable inductors; rheostats, Variacs, transformers; other laboratory accessories.	Cover 3
G–M LABORATORIES — Photoelectric Cells; Photoelectric Relays; Slide Wire Rheostats; Galvanometers; Galvanometer Suspensions; Laboratory Stands and Clamps.	vi
HARSHAW CHEMICAL CO. — Optical Lithium Fluoride grown in single crystal to predetermined size. Industrial Chemicals.	xii
INTERNATIONAL RESISTANCE COMPANY — Manufacturers of metallized and wirewound fixed and variable Resistors including high voltage and high frequency types.	ix
LEEDS & NORTHRUP COMPANY — Manufacturers of Galvanometers, Resistors, Bridges, Condensers, Inductances, Potentiometers, Testing Sets; Temperature Measuring, Recording and Controlling Apparatus; Instruments for Measuring and Controlling Conductivity of Electrolytes and Hydrogen Ion Concentrations.	i
LOEWENBERG, DR. F. — Light measuring instruments, single and double cell types. Self-generating photo-electric elements, wide variety of electrocells.	xii
MACMILLAN COMPANY	ii
MCGRAW-HILL BOOK CO., INC.	vii
OHMITE MANUFACTURING CO.	xiv
PHYSICAL SOCIETY (LONDON)	viii
REINHOLD PUBLISHING CORP.	iv
RUBICON COMPANY — Galvanometers, electrometers, potentiometers, Wheatstone and Kelvin bridges, resistance boxes, hydrogen ion and conductivity apparatus.	xiii

INDEX—*Continued*

Name	Page
SHALLCROSS MFG. COMPANY — Taylor High Voltage Resistors for Voltmeter Multipliers. High resistance and high Wattage Decade Boxes and other laboratory instruments. Super Akra Ohm wire wound, non-inductive and accurate resistors. Special resistors for special purposes.	xii
W. M. WELCH SCIENTIFIC CO. — Scientific instruments—laboratory apparatus. Catalog lists 10,000 items.	xi
GEORGE C. WYLAND — X-Ray Symmetrical Focusing Precision Cameras, Non-Symmetrical Focusing Identification Cameras, Gas Type X-Ray Tubes and complete X-Ray equipment.	xiii

Situations Open & Wanted

Physicist Wanted

For Physical Research Department of large manufacturing company in Middle West. Man with graduate work preferred. State age, education, experience, and salary desired. Address Box M3–5, Rm. 1502, 175 Fifth Ave., New York, N. Y.

Technical Physicist

High Frequency, electronics, short wave diathermy, lab. and factory experience, trained in Physical Chemistry and Chemistry. Address Box M3–4, Rm. 1502, 175 Fifth Ave., New York, N. Y.